MODELING DENSITY EFFECTS IN CO_2 INJECTION IN OIL RESERVOIRS

AND

A CASE STUDY OF CO_2 SEQUESTRATION IN A QATARI SALINE AQUIFER

A Thesis

by

TAUSIF KHIZAR AHMED

Submitted to the Office of Graduate Studies of
Texas A&M University
in partial fulfillment of the requirements for the degree of

MASTER OF SCIENCE

August 2011

Major Subject: Petroleum Engineering

Modeling Density Effects in CO_2 Injection in Oil Reservoirs and a Case Study of CO_2

Sequestration in a Qatari Saline Aquifer

MODELING DENSITY EFFECTS IN CO_2 INJECTION IN OIL RESERVOIRS

AND

A CASE STUDY OF CO_2 SEQUESTRATION IN A QATARI SALINE AQUIFER

A Thesis

by

TAUSIF KHIZAR AHMED

Submitted to the Office of Graduate Studies of
Texas A&M University
in partial fulfillment of the requirements for the degree of

MASTER OF SCIENCE

Approved by:

Co-Chairs of Committee,	Steve Holditch
	Hadi Nasrabadi
Committee Members,	Maria Barrufet
Head of Department,	Steve Holditch

August 2011

Major Subject: Petroleum Engineering

ABSTRACT

Modeling Density Effects in CO_2 Injection in Oil Reservoirs and a Case Study of CO_2 Sequestration in a Qatari Saline Aquifer. (August 2011)

Tausif Khizar Ahmed, B.S., Texas A&M University at Qatar

Co-Chair of Advisory Committee: Dr. Steve Holditch
Dr. Hadi Nasrabadi

CO_2 injection has been used to improve oil recovery for several decades. In recent years, CO_2 injection has become even more attractive because of a dual effect; injection in the subsurface 1) allows reduction of CO_2 concentration in the atmosphere to reduce global warming, and 2) improves the oil recovery.

In this study**,** the density effect from CO_2 dissolution in modeling of CO_2 injection is examined. A method to model the increase in oil density with CO_2 dissolution using the Peng-Robinson equation of state and the Pedersen viscosity correlation is presented. This method is applied to model the observed increase in oil density with CO_2 dissolution in a West Texas crude oil. Compositional simulation of CO_2 injection was performed in a 2D vertical cross section and a 3D reservoir with the density effect. The results show that the density increase from CO_2 dissolution may have a drastic effect on CO_2 flow path and recovery performance. One main conclusion from this work is that there is a need to have accurate density data for CO_2/oil mixtures at different CO_2 concentrations to ensure successful CO_2 injection projects.

While CO_2 enhanced oil recovery (EOR) is part of the solution, saline aquifers have the largest potential for CO_2 sequestration. A literature review of the CO_2 sequestration in saline aquifers is performed. The dominant trapping mechanisms and transport processes and the methods used to model them are discussed in detail. The Aruma aquifer, a shallow saline aquifer in southwest Qatar is used as a case study for CO_2 sequestration. A compositional simulation model is prepared for the Aruma aquifer using the available log data and flow test data. It was found that the grid size is a key parameter in modeling CO_2 sequestration accurately. It affects the propagation of the CO_2 plume and amount of CO_2 dissolved in brine.

DEDICATION

To my family, teachers and friends

ACKNOWLEDGEMENTS

I would like to thank my supervisor, Dr. Hadi Nasrabadi, for his guidance and support throughout the course of this research. His constant support, advice and timelines streamlined my research and made it more efficient. I would also like to thank Dr. Steve Holditch and Dr. Maria Barrufet for serving on my committee.

I am also grateful to the Qatar National Research Fund for financially supporting this research and my studies at Texas A&M University. Thanks also go to my friends, colleagues and the department faculty and staff, both at College Station and at the Qatar campus, for making my time at Texas A&M University a great experience. I also want to extend my gratitude to the Computer Modeling Group (CMG) for providing the research license and technical support. I also want to thank Dr. Kamel Mustafa from the Qatar Department of Agriculture and Water Research for providing data on the Aruma aquifer.

Finally, thanks to my family for their unconditional love and support.

TABLE OF CONTENTS

LIST OF FIGURES

Page

Page

LIST OF TABLES

1. INTRODUCTION: THE PROBLEMS ADDRESSED

1.1 Introduction

The combustion and flaring of fossil fuels produces large quantities of CO_2. The Intergovernmental Panel on Climate Change (IPCC 2007) stress the need to control anthropogenic greenhouse gases in order to mitigate the climate change that is adversely affecting the planet. They report that over the last three decades CO_2 emissions have been growing at a rate of 1.9% per year . Atmospheric CO_2 concentrations have increased by 100 ppm in comparison to its preindustrial level, reaching 379 ppm in 2005. Geologic storage of CO_2 would be to sequester CO_2 captured from anthropogenic sources, such as power plants, oil refineries and chemical plants. Value added geologic sequestration would include injecting CO_2 for enhanced oil recovery. However it is important to understand the dynamics of CO_2/ crude oil at reservoir conditions and predict fluid properties accurately. The impact of modeling this behavior will be discussed in this study.

The largest, but least defined sources of geologic storage possibilities lies in saline aquifers (Beecy and Kuuskraa 2001). Firoozabadi and Cheng (2010) estimate that about 2×10^4 gigatons can be stored in saline aquifers in the United States and Canada alone.These formations have the advantage of being close to many CO_2 emission sources.

This thesis follows the style and format of *SPE Reservoir Evaluation and Engineering.*

This study briefly reviews density effects and investigates the sequestration potential of CO_2 in a shallow saline aquifer in Qatar.

1.2 CO_2 in Enhanced Oil Recovery

The CO_2 enhanced oil recovery (EOR) has been applied in petroleum production for many years. The first large-scale, commercial CO_2 EOR project began operations in 1972 at the SACROC field in West Texas, and continues to this date (Sweatman et al. 2009). A large number of CO_2 EOR projects have started since then. Based on the 2010 EOR survey by the Oil and Gas Journal there are a total of 129 projects globally (120 of them in the US and Canada). In the US alone, CO_2 injection has accounted for the recovery of about 1.5 billion barrels of oil. CO_2 injection in oil reservoirs (for sequestration purposes) has also become more attractive from a global warming standpoint. The increase in CO_2 concentration in atmosphere due to burning fossil fuels and deforestation may be one of the main causes for the acceleration of global warming. Since fossil fuels will be a critical component of world energy supply for the coming decades, methods for disposal of CO_2 that do not involve long residence of CO_2 in the atmosphere (such as injection in oil and gas reservoirs) are considered as part of a possible solution.

CO_2 injection may improve oil recovery through three main mechanisms: 1) swelling, 2) reducing viscosity, and 3) decreasing residual oil saturation. Diffusion of CO_2 in the oil phase may also contribute to recovery in highly heterogeneous and fractured reservoirs (Hoteit and Firoozabadi 2009).

In CO_2 injection schemes, the minimum miscibility pressure (MMP) from 1D horizontal slim-tube measurements is often thought to be a key parameter. The MMP is defined as minimum pressure that is required to achieve multiple contact miscibility between the injected fluid and oil at the reservoir temperature. However, the flow path may be very different in a slim tube and in a reservoir.

In a slim-tube experiment, a long (say 10 m or longer) small diameter (say 0.5 cm) tube packed with sand or glass beads is saturated with oil that is then displaced by injection gas at a fixed pressure and temperature. The oil recovery after injection of some fixed amount of gas (usually 1.1 or 1.2 pore volume) is measured at different pressures. Typically, recovery increases with an increase in pressure and then levels off. In a recovery vs. pressure plot, the MMP is usually taken to be the point where the recovery starts to level off. The measured MMP from slim tube is used for the purpose of field evaluation or tuning equations of state.

The question is how relevant slim tube MMP is to performance of CO_2 injection in 2D and 3D reservoirs. The slim tube, because of its small diameter, represents a 1D horizontal flow. The flow in reservoir conditions even in homogenous domains is 2D or 3D. As CO_2 dissolves in the oil, the density often increases. On the other hand, when a gas phase evolves from mixing of CO_2 and the oil, the gas phase is often lighter than CO_2 and the oil. The evolved gas phase moves upward due to buoyancy. These density effects under the influence of gravity in reservoir conditions will change the flow path from 1D to 2D or 3D. In a 1D slim tube, there is no gravity effect.

There has been extensive research on the effect of CO_2 dissolution on oil viscosity and many correlations have been developed. Density effects from mixing have not been taken into account in the past; they often are ignored in modeling of CO_2 injection (Bangia et al. 1993; Cardenas et al. 1984; Johnston 1988; Palmer et al. 1984; Perry 1982) . A clear example of neglect of density effect is the pilot performance in the Weeks Island from CO_2 injection, which showed an early breakthrough of injected CO_2 (Johnston 1988). A number of other papers which are based on the assumption that when the injected CO_2 is lighter than the oil, the CO_2 injection is a stable gravity drainage process (Bangia et al. 1993; Cardenas et al. 1984). As will be shown in this study, this may not be true when the permeability is high. CO_2 dissolution in water also results in a density increase (Garcia 2001; Han and McPherson 2009; Tabasinejad et al. 2010). The density increase in water may have a significant effect on the mixing and the flow path and affects the sequestration potential (Farajzadeh 2008; Firoozabadi and Cheng 2010).

In this study, literature on change in density from CO_2 dissolution in a petroleum fluid is first briefly reviewed. The procedure to model the density increase from CO_2 dissolution (while preserving the viscosity reduction effect) using the Peng-Robinson equation of state (Peng and Robinson 1976) is then discussed. The density effect is then examined for CO_2 injection in a 2D vertical cross section and in a 3D reservoir and the results are compared for cases with and without the density increase. This effect is investigated in: homogenous 2D domains with two different permeabilities and a heterogeneous 3D domain with random permeability distribution.

1.3 CO_2 Sequestration in Saline Aquifers

Studies on CO_2 sequestration in saline aquifers have been performed since the early 90's. The first study of the reservoir simulation of CO_2 sequestration in a saline aquifer reported by van der Meer (1992). In the geological considerations for the storage site, he stated that an aquifer must be at a depth of at least 800 m for the injected CO_2 to remain in the supercritical state. This constraint has been followed in all the published work since. Gravity segregation and viscous fingering were found to be dominant CO_2 water displacement mechanisms.

Holt et al. (1995) used a black oil simulator to model CO_2 sequestration. Their aquifer model consisted of 4800 grid blocks and permeabilities ranged from 100-2000 mD with an average of 340 mD. The ratios between vertical and horizontal permeabilities varied from 0.02 to 0.045. The reservoir pressure and temperature was set to 2900 psi and 144 °F. The base case model has a CO_2 injection rate of 1.6 PV/year and the injection well was perforated through all layers. Based on the simulation results, they concluded that CO_2 storage in a heterogeneous aquifer depends strongly on injection rate and permeabilities. An injection rate below 0.4% PV/year gave gravity stabilized displacement and high storage capacity (>30%). At rates of 1.6% PV/year and higher, the storage capacity became 16% PV and was rate independent.

Pruess et al. (2003) studied the amount of CO_2 that can be trapped into the various phases (gas, aqueous, and solid) for a range of conditions encountered in typical disposal aquifers. They estimated the combined storage capacity of CO_2 at 30 kg per unit of reservoir volume.

Kumar et al. (2005) performed simulation studies using the GEM compositional simulator to study CO_2 storage in saline aquifers. Simulations of a few decades of CO_2 injection followed by several thousand years of natural gradient flow were done. They concluded that the effect of residual gas on CO_2 storage was significant compared to storage in brine or minerals. Injecting CO_2 from the bottom half of the aquifer enhanced residual trapping and reduced the amount of mobile gas before it migrated to the aquifer seal. They also found that injecting water after the CO_2 injection period increases the storage capacities of solubility and mineral trapping.

Ennis-King and Paterson (2005) studied the role of convective mixing in the long-term storage of CO_2 in deep saline aquifers. The density of formation water increases upon dissolution with CO_2 which creates density instability. They used linear stability analysis to estimate when this instability would occur in anisotropic systems. This was compared with numerical simulations performed using the TOUGH2 simulator. The simulator used a detailed equation of state (EOS) for CO_2-brine systems on a 2D grid 500 m wide (50 grid blocks) and 400 m thick (100 blocks refined to 0.5 m at the top). The pressure at the top was 2610 psi and the temperature was 172 °F. They found that the time required for the convective instability to begin ranges from less than a year to hundreds of years depending on the permeability. This time is less than the total time required to dissolve CO_2 in a typical storage project, which can be up to tens of thousands of years.

Bryant et al. (2008) investigated whether the intrinsic instability of buoyancy driven flow leads to fingering of CO_2. The mechanisms governing this type of displacement were studied in a series of fine grid simulations with a finite volume of CO_2 placed at the bottom of a 2D aquifer and only buoyancy driving the displacement. The GEM-GHG simulator was used in this study and simulation used 40,000 grid blocks. There were several fine-scale geostatistical realizations of permeability and the effect of capillary pressure and dip angle were also investigated. They found that CO_2 rises along preferential flow paths that are a consequence of rock properties (permeability, drainage capillary pressure curve and anisotropy). Capillary pressure broadens the lateral extent of the flow paths.

Burton et al.(2008) developed an analytical model using Darcy's Law and a modified form of the Buckley-Leverett theory. The long term injection of CO_2 dries out the near-wellbore region. Drying removes the water from the near wellbore region but also precipitates salts altering the permeability. From their model, they concluded that quantifying the relative permeability curve is very important in determining achievable injection rate and therefore determining the well count for CO_2 sequestration projects. The well count in return strongly affects the economics of sequestration projects.

More recently, storage in shallow saline aquifers has also been investigated. Tiamiyu et al. (2010) used CMG-GEM in a study to find the optimal combination of operational parameters: injection rates, well completion types, and brine withdrawal strategy to harness CO_2 storage potential and leakage risk mitigation in shallow saline aquifers. The motivation behind this study was that deep saline aquifers may not always be present near the CO_2 source. The aquifer top was set at 550 m (1804 ft.) and the initial reservoir pressure of 810 psi was used. This is well below the critical pressure of CO_2. They found that the potential of CO_2 storage in shallow saline aquifers can be greatly enhanced using brine withdrawal. Using horizontal wells that completed in the bottom of a moderately heterogeneous aquifer helps mitigate CO_2 leakage through the cap rock. Well perforation and orientation while having a negligible effect on CO_2 injectivity, extended the injection period until the aquifer reached the maximum allowable injection pressure.

Many of the studies discussed above assume a constant pressure outer boundary. Economides and Ehlig-Economides (2009) through a simple analytical model showed that assuming a constant pressure boundary neglects the critical point that reservoir pressure will build up under a constant injection rate. They concluded that CO_2 can occupy no more than 1% of the pore volume. Barrufet et al. (2010) performed a comparison study of the CO_2 storage capacity between a depleted gas condensate reservoir and equivalent saline aquifer. They found that due to the low overall compressibility of aquifers, the mass of CO_2 sequestered per pore volume is approximately 13 times lower than that of a depleted gas condensate model. However, due to their large extent, aquifers still can provide storage for significant volumes of CO_2.

First-order finite difference methods present numerical dispersion errors unless very fine gridding is used. This can be computationally expensive. Moortgat and Firoozabadi (2010) modeled two phase compositional flow in anisotropic media using a combination of high-order finite element methods. They used the mixed hybrid finite element method to solve for pressure and fluxes, and the discontinuous Galerkin method to update the mass transport. This method reduced numerical dispersion, captured shock fronts more accurately and lowered the dependence on mesh quality and orientation. By using this higher-order method, coarser meshes can be used at a lower CPU cost, compared to traditional finite difference methods. In a later work (Moortgat et al. 2011), they also suggested the use of cubic-plus-association (CPA) equation of state, instead of Henry's law to more accurately model the effect of cross association of water and CO_2 molecules on phase behavior.

1.3.1 Field Injection Studies

The Sleipner project in offshore Norway is the world's first commercial-scale CO_2 storage project injecting CO_2 in the sands of the Utsira formation at 1million tons per year (Gale et al. 2001). The Utsira formation is a moderately sorted, uncemented sand that has a high porosity The Saline Aquifer Carbon Dioxide Storage (SACS) project consisted of the Statoil and partners along with several independent research organizations to plan and monitor the storage of CO_2. They performed a simulation study using a modified black oil simulator. The reservoir pressure ranged from 8 to 10 MPa (1160 - 1450 psi) and temperature of 37 °C (98.6 °F). The formation porosity ranged from 27 to 30 % and permeability from 1 to 8 Darcy. Results of the injection planning studies revealed that CO_2 should be injected near the bottom of the formation to minimize areal distribution and maximize the dissolution in formation water. Up to 18% of the CO_2 injected was dissolved in the formation water. They predicted that the maximum extension of CO_2 after 20 years would be 3 km and supercritical conditions resulted in wider distribution of free CO_2.

1.3.2 Sources of CO_2 in Qatar

In 2009, Qatar produced 3,154 billion cubic feet (Bcf) of natural gas which is approximately 8.6 bcf/day. The natural gas produced from the North field, Qatar's largest gas field, consists of 3.5 wt% CO_2 (Whitson and Kuntadi 2005). If the average gas density is 0.05 lb/ft3, then this translates to 2.54 million metric tons (tonnes) of CO_2 produced every year. The average daily design injection rate for CO_2 sequestration in this case would need to be 132 million SCF/day. This rate was calculated by noting that 1 million tons is 50,045,455 lbmoles of CO_2, and 1 lbmole of CO_2 occupies 379.4 SCF at standard conditions (House et al. 2003).

Real estate development in Qatar during recent years has also led to an increase in cement production. Producing 1 tonne of cement generates 0.83 tonnes of CO_2. But fossil fuel combustion still remains the largest source of CO_2 emissions. According to the Carbon Dioxide Information Analysis Center (CDIAC), Qatar produced 17.1 million tonnes of CO_2 in 2007 (Fig. 1.1), out of which 10 million tonnes were produced from combustion of gas fuels. Cement production emitted 340,000 tonnes of CO_2. Qatar has the highest per capita emissions of CO_2 in the world (14.02 tonnes). Comparatively, the US ranks as the 11^{th} highest CO_2 emitter per capita (5.2 tonnes). There is a need for CO_2 mitigation in Qatar.

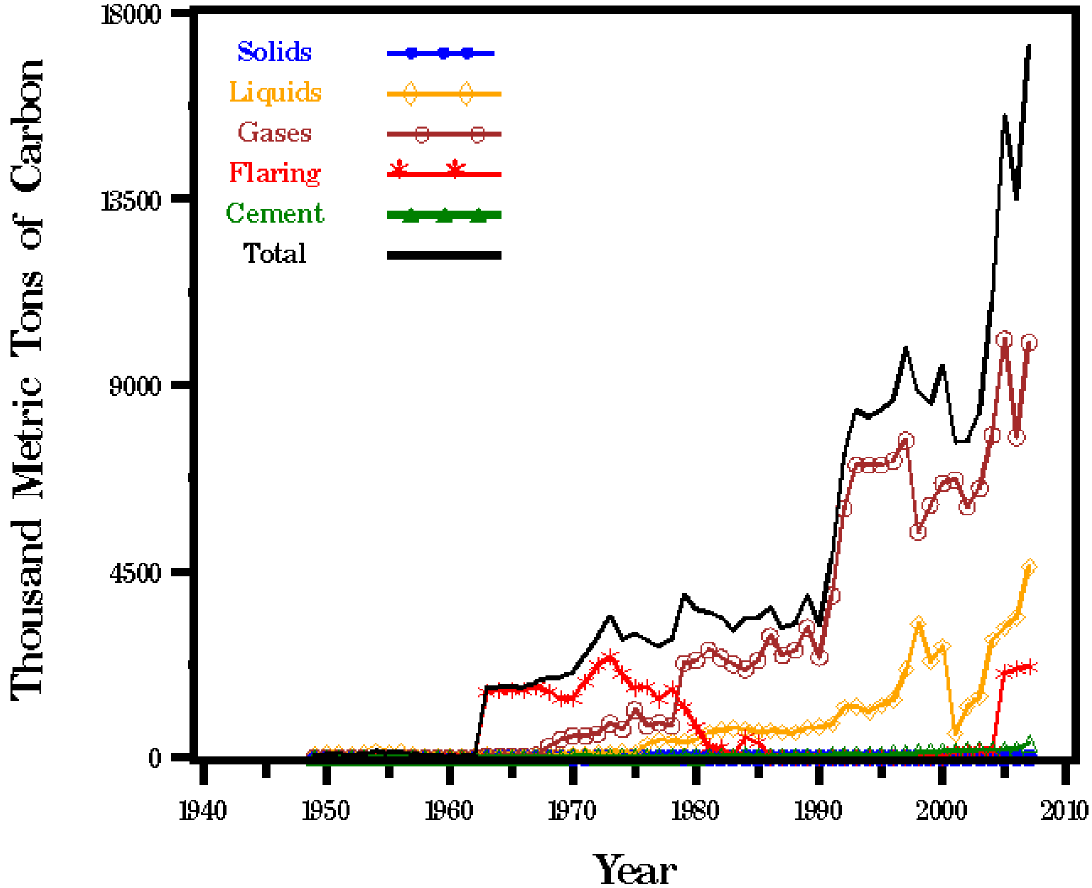

Fig. 1.1 —Fossil-Fuel CO_2 Emissions for Qatar from 1949 to 2007. (CDIAC 2007)

1.4 Review of Sections

Section 2 describes the process of modeling the abnormal density behavior seen in CO_2/crude oil mixtures. A brief literature review about effect of CO_2 solubility on oil density is presented. A fluid model for the GEM compositional simulation is then developed.

Section 3 describes the 2D and 3D models developed for the GEM simulator. The fluid model capturing the density increase is compared with the default model. The effect of injection depth is also investigated in homogenous and heterogeneous models.

Section 4 discusses the transport processes and trapping mechanisms involved in CO_2 sequestration.

Section 5 discusses the development of a CO_2 sequestration reservoir model for a saline aquifer in Qatar. The geology of the Aruma aquifer along with the data used to build the base case model is described briefly. The effects of diffusion are also investigated.

Section 6 outlines conclusions and recommendations for further work.

2. MODELING THE ABNORMAL DENSITY BEHAVIOR IN CO_2/CRUDE OIL MIXTURES

2.1 Effect of CO_2 Solubility on Oil Density

There are several published data that report an increase in liquid hydrocarbon density upon CO_2 dissolution. Lansangan and Smith (1993a) have found that mixtures of CO_2 and a West Texas crude oil show monotonic viscosity decrease and the density increase with increased CO_2 concentration. They suggest that the increase in density might be caused by strong intermolecular Coulombic interactions between CO_2 and hydrocarbon molecules.

DeRuiter et al. (1994) studied the solubility and displacement of viscous crudes with CO_2 and have found that the oils exhibit an increase in density due to CO_2 solubility. The two samples in their study with API gravities of 18.5 and 14 exhibited an increase in density upon CO_2 dissolution. In a study of a West Texas crude oil, Grigg (1995) observed a 2% increase in oil density (after the addition of CO_2 and before the phase split) while the viscosity decreased. After the phase split, the traditional viscosity-density relationship was observed; viscosity increased (decreased) when density increased (decreased).

Ashcroft and Ben-Isa (1997) report on the effect of dissolved air, nitrogen, oxygen, methane, and carbon dioxide on the densities of liquid hydrocarbons. The hydrocarbons include heptanes, octane, nonane, decane, dodecane, tetradecane, hexadecane, cyclohexane, methylcyclohexane, and methylbenzene (toluene). Their data shows that saturation of hydrocarbon liquids with gases other than CO_2 results in a decrease in density while saturation with CO_2 causes an increase in density.

2.2 Fluid Selection

As discussed in the previous section, there may be an increase in oil density and a decrease in viscosity with CO_2 dissolution. Lansangan and Smith (1993b) report density and viscosity measurement trends for oil samples from West Texas. The fluid sample (RO-B) from their paper was used in this study as it shows relatively high increase in density (about 5%) with CO_2 dissolution. They report a density of 0.74 g/cc and viscosity of 0.77 cp at 1700 psia and 116 °F for this fluid.

2.3 Fluid Characterization

The CMG WINPROP software is used to match the density and viscosity of the oil sample by performing regression on critical properties, binary interaction coefficients, and shift parameters for the heavy fractions and viscosity correlation parameters. In this work, the Peng-Robinson EOS is used to calculate phase behavior, and density (with volume shift parameters) and the Pedersen et al. (1987) correlation to calculate viscosity. To improve the accuracy of predictions, the original C_{7+} heavy fraction (reported by Lansangan and Smith (1993b)) was split into three pseudo-components.

Table 2.1 lists the fluid composition with the heavy fraction split and Table 2.2 shows the measured density and viscosity with CO_2 dissolution in single phase. The calculated density and viscosity of the CO_2/oil mixtures for increasing CO_2 solubility using the tuned EOS parameters are reported in Table 2.3. To predict the increasing density trend, the volume shift parameter of CO_2 was modified. By changing the CO_2 volume shift parameter, the density increase in the fluid from CO_2 dissolution can be modeled without affecting the calculated viscosity. This is due to the fact that in the Pedersen correlation the viscosity of the mixture depends on the viscosity (and density) of a reference component (usually methane) and other factors that are independent of mixture density. Therefore, modifying the shift parameter of CO_2 does not affect the viscosity of the mixture.

Table 2.1 – Fluid composition (Fluid 'RO-B' from Lansangan and Smith (1993b))

Components	Initial composition (mole fraction)
CO_2	0.0220
C_1	0.2228
C_2	0.1285
C_3	0.1235
C_4	0.0819
C_5	0.0386
C_6	0.0379
$C_{7\text{-}12}$	0.1301
$C_{13\text{-}21}$	0.1085
C_{22+}	0.1062

Table 2.2 – Measured density and viscosity vs. CO_2 composition in CO_2/oil mixture (Fluid 'RO-B' from Lansangan and Smith (1993b))		
CO_2 composition	measured viscosity (cp)	measured density (g/cc)
0.022	0.770	0.744
0.034	0.683	0.745
0.1506	0.530	0.749
0.3498	0.419	0.761
0.5482	0.380	0.782

Table 2.3 – Fluid critical properties and other relevant data						
Components	T_c (K)	P_c (atm)	MW (g/mole)	ω	*BIC* CO_2 -comp$_i$	BIC C_1 -comp$_i$
CO_2	304.2	73.76	44.01	0.2250	0.000	0.100
C_1	190.6	46.00	16.04	0.0080	0.100	0.000
C_2	305.4	48.84	30.07	0.0980	0.100	0.003
C_3	369.8	42.46	44.10	0.1520	0.100	0.009
C_4	425.2	38.00	58.12	0.1930	0.100	0.015
C_5	469.6	33.74	72.15	0.2510	0.100	0.021
C_6	507.5	32.89	86.00	0.2750	0.100	0.025
C_{7-12}	569.6	21.11	126.19	0.3462	0.100	0.038
C_{13-21}	790.3	15.00	218.64	0.4636	0.080	0.070
C_{22+}	1075.4	9.65	442.38	0.8050	0.100	0.129

2.3.1 Basis for Modification of CO_2 Volume Shift Parameter

The CO_2 density is calculated using the Peng-Robinson EOS with the default volume shift parameter that WINPROP uses. This data is compared to the isothermal CO_2 density data at 116 °F from the National Institute of Standards and Technology (NIST).

NIST uses an equation of state developed for CO_2 by Span and Wagner (1996) with estimated density uncertainty ranging from 0.03% to 0.05%. The correlation of Jhaveri and Youngren (1988), used in many commercial simulators (including WINPROP) to calculate the volume shift parameters, may not be accurate for CO_2. The default volume shift parameter by the Jhaveri and Youngren correlation underestimates the density as the pressure increases (Fig. 2.1). At 1700 psi and 116 ˚F, the correct CO_2 volume shift parameter is found to be 0.2569 which is significantly different from the value given by the Jhaveri and Youngren correlation (-0.09434). To model the increasing oil density with CO_2 dissolution, the initial oil density (without CO_2) is first matched by adjusting the volume shift parameters of the heavy fractions. Then the CO_2 volume shift parameter is adjusted based on the pure CO_2 density.

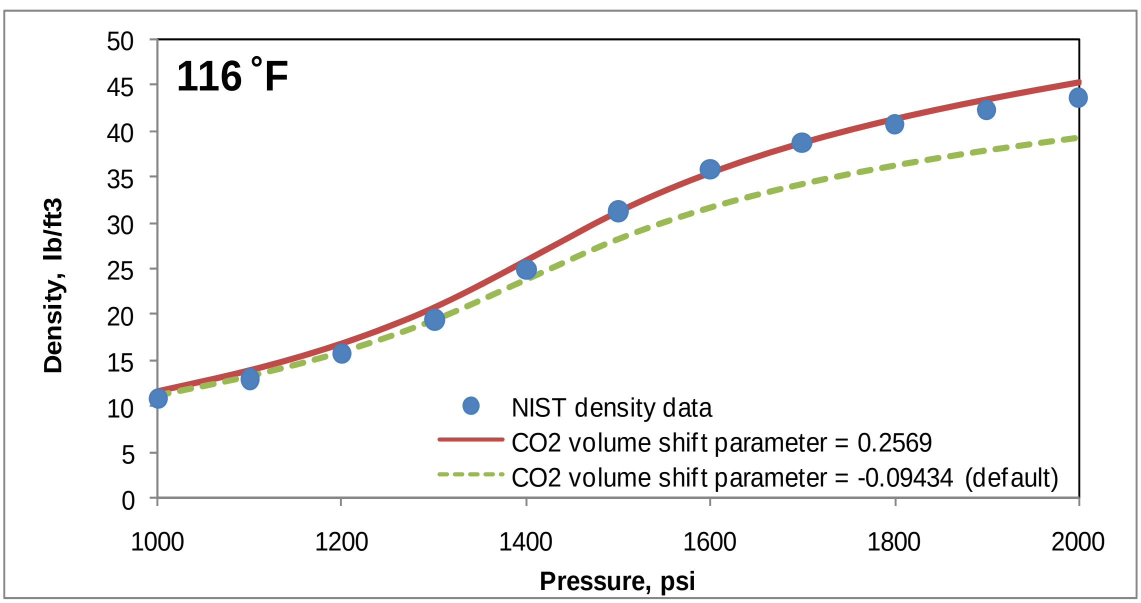

Fig. 2.1 —Density of pure CO_2 at 116 ˚F from 1000-2000 psi (from the NIST Chemistry WebBook). The CO_2 density calculated with the Peng-Robinson EoS using the default volume shift parameter and an optimum value are compared against the NIST data.

Table 2.4 lists the volume shift parameters of different components for the default case (decreasing density with CO_2 dissolution) and for the proper prediction of density (increasing density with CO_2 dissolution). Using the default CO_2 volume shift parameter gives an 11.7% difference in the value of pure CO_2 density at 1700 psia and 116 ˚F as can be seen in Fig. 2.1. Table 2.5 lists the Pedersen et al. correlation for viscosity model parameters. The results of density and viscosity predictions using parameters listed in Tables 2.3-2.5 are compared with measured values in Fig. 2.2. The densities and viscosities shown in Fig. 2.2 are the single phase liquid and two-phase liquid densities and viscosities. The phase-split occurs when the overall CO_2 mole composition is approximately 0.55. The calculated data match the increasing density trend in the single phase quite well but deviate when in the two-phase liquid region (max error of 7.8%). This can also be partially due to error in the two-phase composition measurements and limited available data to characterize EOS parameters.

Table 2.4 – Volume shift parameters

Components	Default (decrease in density with CO_2 dissolution)	Adjusted (increase in density with CO_2 dissolution)
CO_2	-0.09434	0.2569
C_1	-0.15386	-0.15386
C_2	-0.1021	-0.1021
C_3	-0.0733	-0.0733
C_4	-0.05706	-0.05706
C_5	-0.03446	-0.03446
C_6	-0.00499	-0.00499
$C_{7\text{-}12}$	0.065225	0.1000
$C_{13\text{-}21}$	0.14672	0.1900
C_{22+}	0.06936	0.4700

Table 2.5 – Parameter values for Pedersen et al. (1987) viscosity correlation

MW mixing rule coefficient	MW mixing rule exponent	Coupling factor correlation coefficient	Coupling factor correlation density exponent	Coupling factor correlation MW exponent
0.0001304	2.303	0.007378	1.847	0.5173

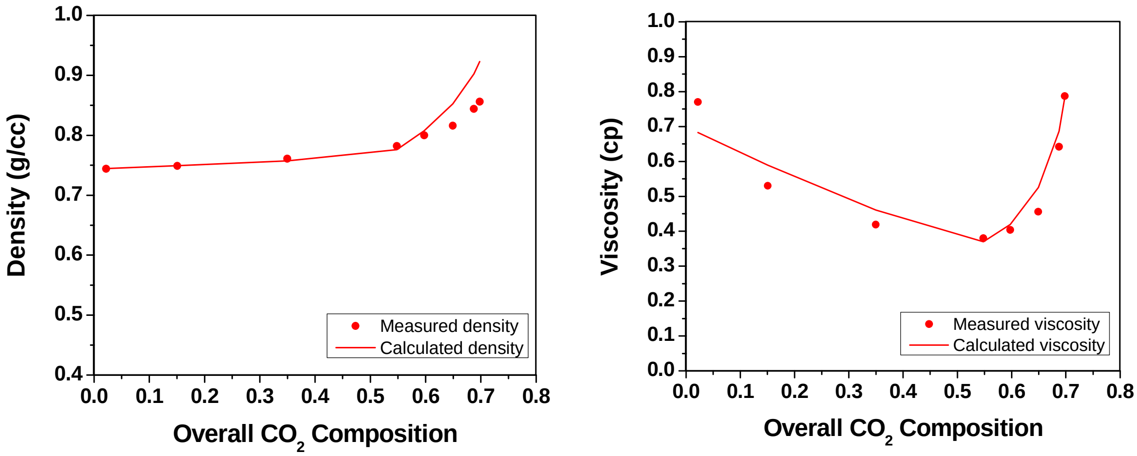

Fig. 2.2 —Variation of density and viscosity with overall CO_2 composition (mole fraction) in CO_2/oil mixtures for: Oil 'RO-B' (Table 2.1), *P* = 1700 psi, *T* = 116 °F. Measured values are from Lansangan and Smith (1993b). Computed density values are based on adjusted volume shift parameters.

2.4 Validation of the Fluid Model through MMP Simulation

The characterized fluid is used to saturate a slim tube simulation model to validate the MMP. Data from Yellig and Metcalfe (1980) are used to simulate the slim-tube experiment. These authors employ a stainless steel tube with length of 40 ft (12.2 m) and diameter of ¼-in. (6.3 mm) packed with 160-200 mesh sand. They report a permeability of approximately 2.5 Darcy and pore volume of 85 cm^3. A constant injection rate of 0.00305 ft^3/day is used (Yellig and Metcalfe 1980) to carry out the simulation runs for pressures ranging from 1100-2500 psi. Uniform initial composition and initial pressure are assumed. The oil recoveries at 1.2 PVI are plotted for each pressure (Fig. 2.3). A MMP of around 1650 psi is obtained. This is very close to the reported value of 1700 psi for this oil sample. Lansangan and Smith (1993b) do not report other measurements related to fluid properties such as saturation pressure but based on the density, viscosity, and MMP comparisons between experimental and simulated data, the characterized fluid is representative of the original reported fluid.

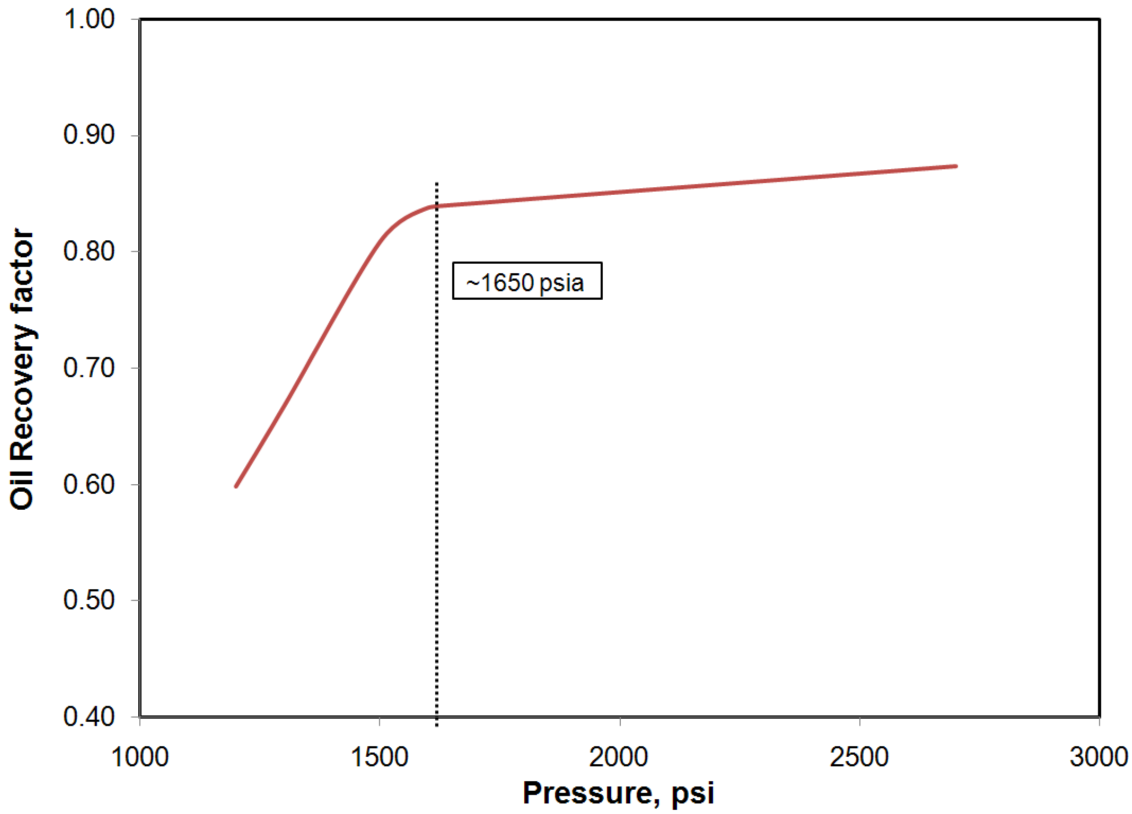

Fig. 2.3 —MMP validation of the characterized reservoir fluid RO-B in a slim tube simulation model. Simulated oil recoveries for different pressures are plotted at 1.2 PVI.

3. 2D AND 3D SIMULATION RUNS

3.1 Model Descriptions

To study the effect of density increase from mixing in flow path and recovery, CO_2 is injected in a 2D vertical cross-section and in a 3D domain. A commercial compositional simulator (CMG GEM) with a fully-implicit scheme is used for simulations.

3.1.1 2D Model Description

A domain with a length of 1200 ft (365 m) and depth of 200 ft (61 m) and width of 16.4 ft (5 m) is used in the 2D model. There are 240 grids in the *x*-direction (length) and 40 grids in *z*-direction (depth). Grid sensitivity tests show that the gridding is adequate for the 2D examples. The use of finer gridding also corrected the numerical diffusion seen in the CO_2 flow path. A constant porosity of 22.35% is used in this model.

3.1.2 3D Model Description

In the 3D domain, a ¼ five-spot pattern with an injector-producer spacing of 1200 ft (365 m) and a depth of 200 ft (61 m) is modeled. The total pattern area is 60 acres and the length and width of the ¼ five-spot pattern is 848 ft (258 m). This model has the same porosity as the 2D domain except for the random heterogeneity example. In 3D examples, there are 21 grids in *x*-direction, 21 grids in *y*-direction (width), and 20 grids in *z*-direction. Grid sensitivity tests showed that this level of gridding was accurate.

3.1.3 Well Constraints

In both 2D and 3D examples, the injector is located at the top (bottom) on one side of the formation and the producer is located at the bottom (top) on the opposite side. In these examples, the injection rate is constant (approximately 0.05 PV/year) and the pressure at the producing well is set equal to 1700 psi, the reported reservoir pressure of the fluid.

3.1.4 Rock-Fluid Data

The gas and oil relative permeability data used in all the examples are listed in Table 2.6. The capillary pressure is assumed to be zero.

Table 2.6 – Gas and oil relative permeabilities

Oil Saturation	k_{ro}	k_{rg}
0.3	0	1
0.344	0.003	0.879
0.388	0.011	0.766
0.431	0.025	0.660
0.475	0.044	0.563
0.519	0.068	0.473
0.563	0.098	0.391
0.606	0.134	0.316
0.650	0.175	0.250
0.694	0.221	0.191
0.738	0.273	0.141
0.781	0.331	0.098
0.825	0.394	0.063
0.869	0.462	0.035
0.913	0.536	0.016
0.956	0.615	0.004
1	0.7	0

3.1.5 Numerical Model Parameters

Initial runs with fine grids gave a high material balance error. Therefore the following steps were taken to reduce the material balance error in GEM:

- The maximum change in pressure, saturation and global composition were changed to account for the high flow rates at the wellbore. The keywords associated with this are *NORM (*PRESS, *SATUR,* and **GMOLAR).*
- The convergence tolerance for the linear solver was reduced. (*PRECC*).
- The minimum time-step size (*DTMIN*) was reduced. The default maximum time-step (*DTMAX* = 365 days) was used.
- The calculation settings for GMRES were changed. GMRES is an acceleration procedure to solve the linear systems in compositional simulations. The keywords associated this are *NORTH* and *ITERMAX.*

The detailed values of the parameters stated above can be found in the example data file in Appendix A. This numerical scheme gave material balance errors of less than 1% for all of the simulation runs.

3.2 Simulation Results

To show the effect of density on CO_2 flow path and oil recovery, a number of 2D and 3D simulations were performed. In each case, there were two different density change case as CO_2 dissolved in oil. The reference case has the default volume shift parameters (used in the commercial simulator) where there is a decrease in oil density with CO_2 dissolution. In the other case, the modified CO_2 shift parameter (as in Table 2.4) is used, where the oil density increases with CO_2 dissolution. In both 2D and 3D examples it is observed that the effect of increasing density with CO_2 dissolution can have a significant effect on the flow path, time of breakthrough and recovery. The results are presented in the sections below.

3.2.1 Homogenous Domains

In the first example a constant permeability of 100 mD was used in the domain. Fig. 3.1 compares CO_2 composition profiles in the domain at 0.05, 0.1, 0.3, and 0.7 PV injection for both the default case (where oil density decreases with CO_2 dissolution) and for the case with increasing oil density with CO_2 dissolution. The injector is located at the top-left corner and the producer is located at the right-bottom corner of the domain. The results show the effect of increasing density on CO_2 composition in flow path and front shape. There is a slight difference in the flow path between the increasing density and decreasing density cases when CO_2 is injected from the top.

There is, however, a drastic change in the flow path when CO_2 is injected from the bottom and produced at the top. Fig. 3.2 depicts simulation results for this case with k = 100 mD. In some CO_2 injection schemes the density of CO_2 is close to the oil density and CO_2 may be injected in the bottom. At the injection point, the CO_2 density ranges from 0.59 to 0.63 g/cc; the oil density is approximately 0.74 g/cc before mixing with CO_2. Unlike the decreasing density case in Fig. 3.1 where CO_2 tends to move upward and then right towards the producer at the top, with increasing density, there is a tendency for CO_2 to move along the bottom/middle of the domain. Results at 0.7 PVI show a high CO_2 sweep efficiency with increasing density. The high sweep efficiency results in a significantly longer breakthrough time and ultimate recovery (Fig. 3.3). For bottom injection, with increasing density, the predicted recovery is 59% whereas for the decreasing density, the predicted recovery is 51%. In the top injection, with increasing density, the predicted recovery is 52% whereas for the decreasing density, the predicted recovery is 53%. In this example, bottom injection (including the density effects) resulted in more recovery than top injection which is a common industry practice. The GEM simulation data file used for the 100 mD case is provided in Appendix A.

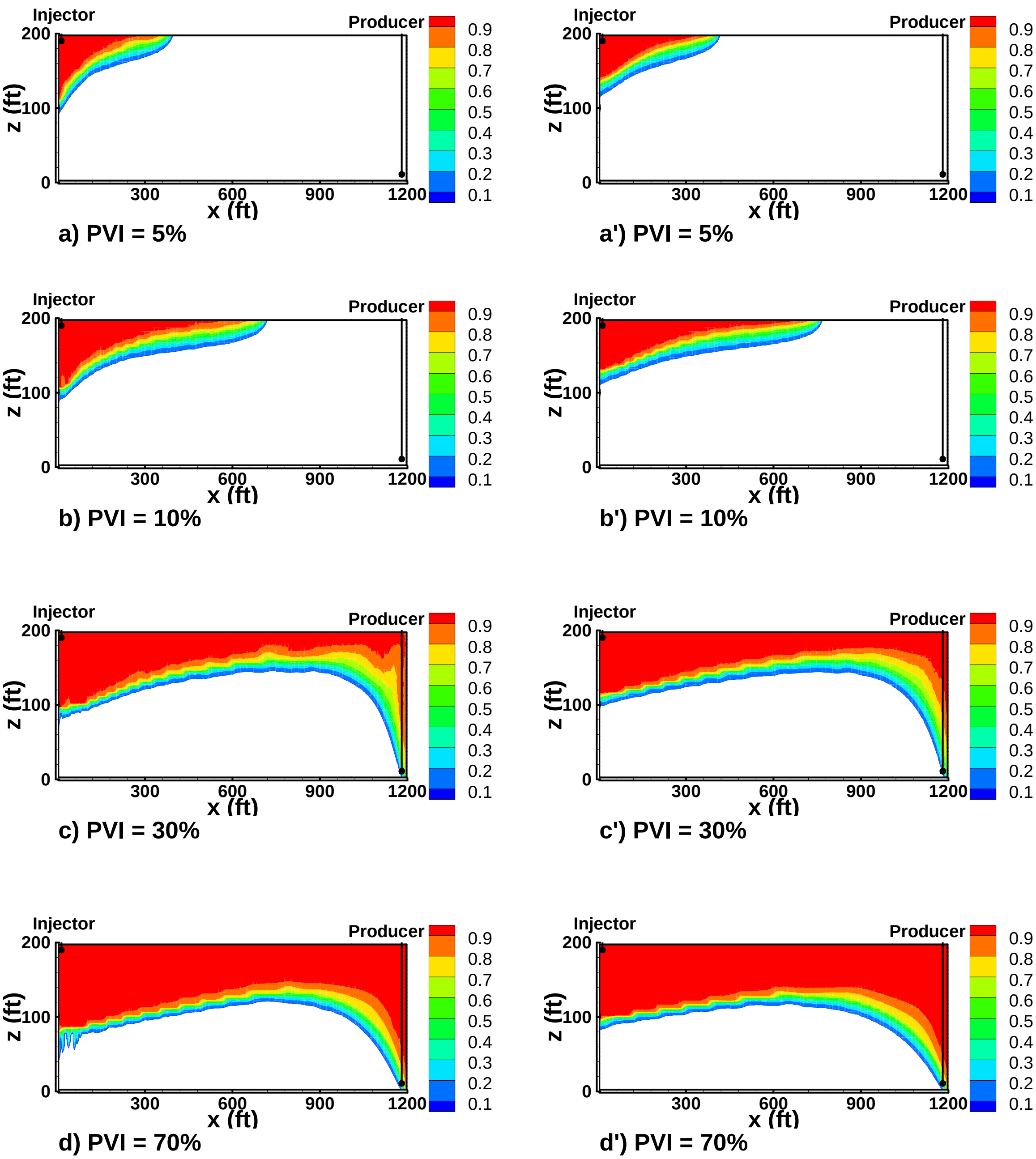

Fig. 3.1 —Overall CO_2 composition (mole fraction) at different PVI for (a, b, c, d) increasing density with CO_2 dissolution and (a', b', c', d') decreasing density with CO_2 dissolution: top injection, homogenous 2D media, k = 100 mD.

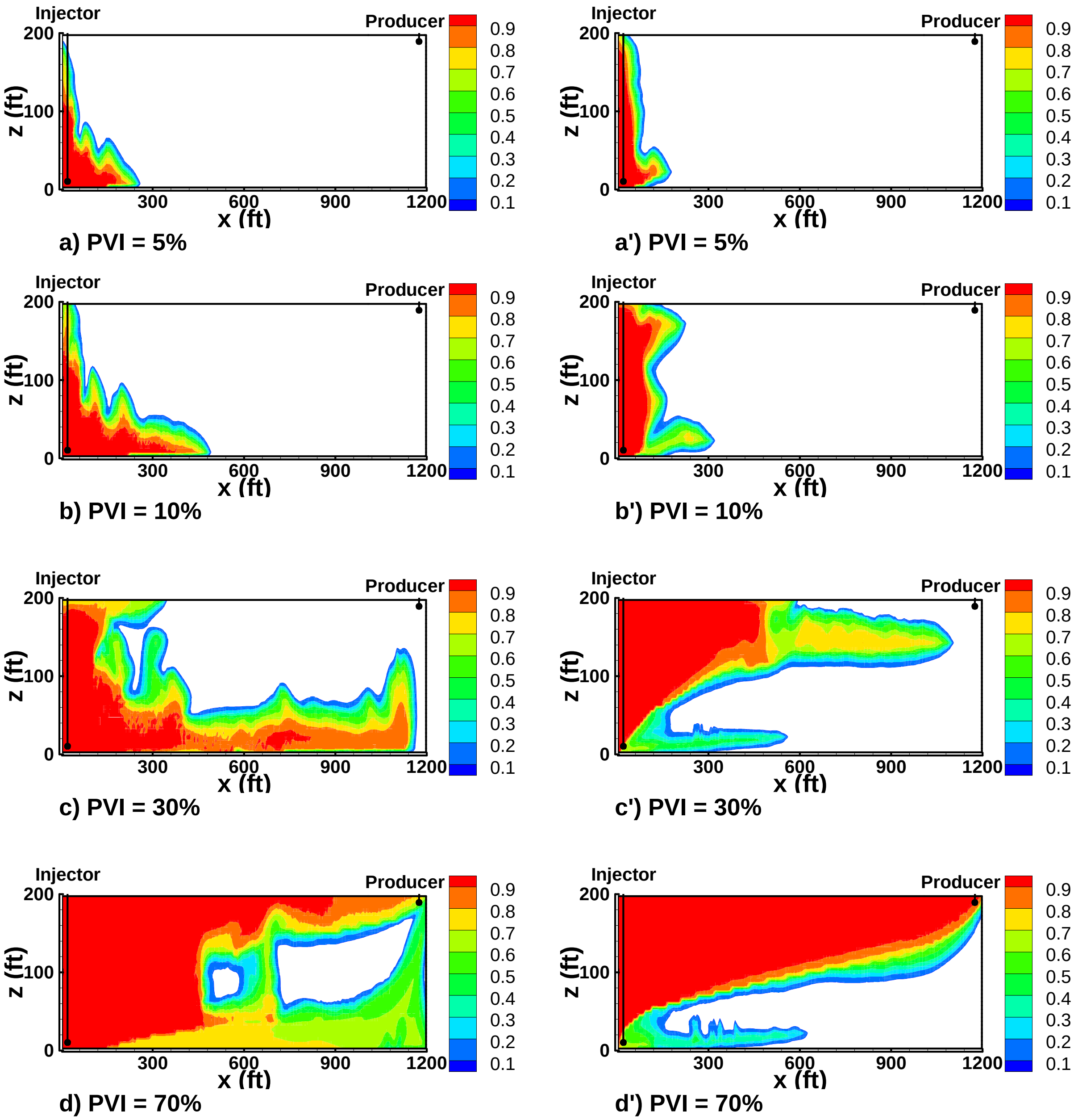

Fig. 3.2 —Overall CO_2 composition (mole fraction) at different PVI for (a, b, c) increasing density with CO_2 dissolution and (a', b', c') decreasing density with CO_2 dissolution: bottom injection, homogenous 2D media, *k* = 100 mD.

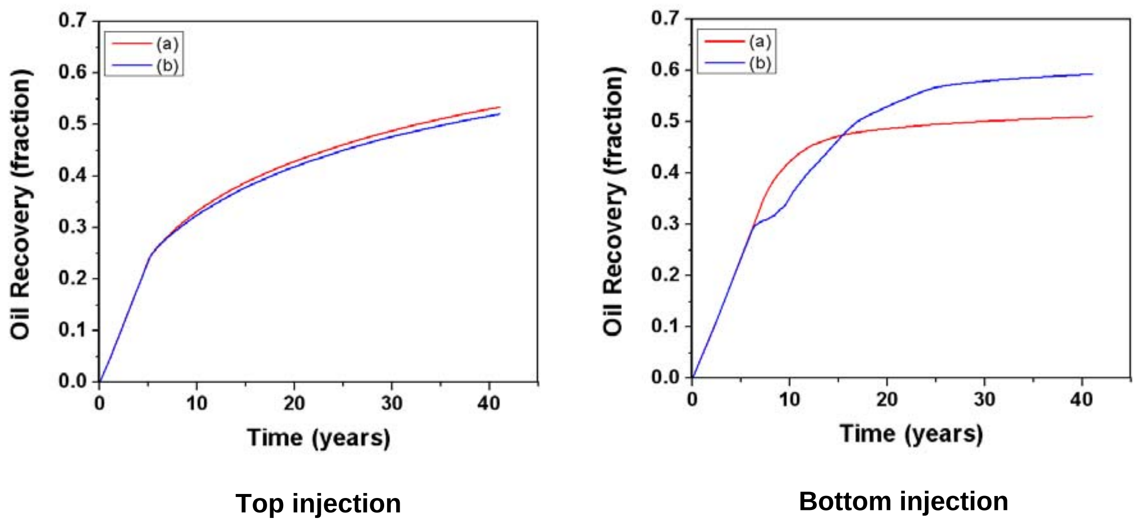

Fig. 3.3 —Oil recovery vs. time for (a) decreasing density with CO_2 dissolution and (b) increasing density with CO_2 dissolution: homogenous 2D media, k = 100 mD.

For a permeability of 1000 mD, there is a pronounced occurrence of gravity fingers especially for the top injection case with increasing density (Fig. 3.4). If the producer well is located below the injector well, there will be a breakthrough as was the case for CO_2 injection in the Weeks Island study (Johnston 1988). There is also an increase in density for the case of decreasing density with CO_2 dissolution due to vaporization of methane from the liquid phase in the gas phase giving rise to gravity fingers as can be seen in Fig. 3.4 c'. Due to the position of the producer, the breakthrough time and recovery for the two cases is nearly the same. The 3D results in the homogeneous domain with k = 100 mD and k = 1000 mD are qualitatively similar in 2D and 3D and are not discussed for the sake of brevity.

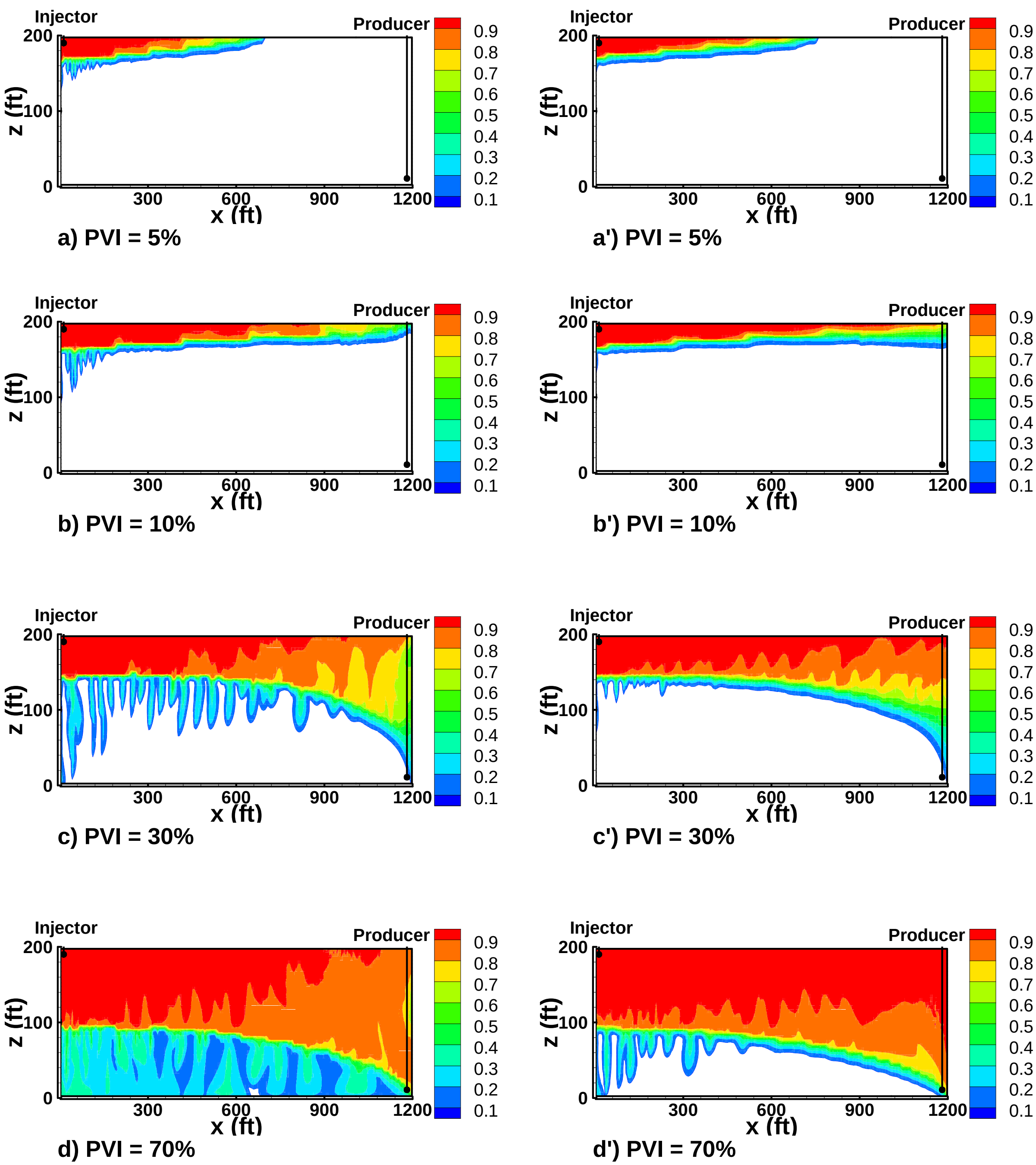

Fig. 3.4 – Overall CO_2 composition (mole fraction) at different PVI for (a, b, c) increasing density with CO_2 dissolution and (a', b', c') decreasing density with CO_2 dissolution: top injection, homogenous 2D media, k = 1000 mD.

3.2.2 Heterogeneous Domains

To study the density effect in heterogeneous domains, two examples are considered. Both examples have random permeability distribution and differ only in the degree of heterogeneity. In the first example, Gaussian geostatistical simulation is used to assign permeabilities to the grid blocks ranging from 10 mD to 500 mD (Fig. 3.5a). The porosity (Fig. 3.5b) in each grid block is related to permeability by:

$\phi_i = 0.11889 + 0.02277 \log(k_i)$ (k_i in mD).

This method produces a highly heterogeneous domain. Fig. 3.6 shows the density effect on CO_2 flow path for the top and bottom injection scenarios; both exhibit better vertical sweep efficiency when the increasing density is modeled. Fig. 3.7 shows the recovery profiles for the top and bottom injection scenarios. For both cases, the recovery with density increase is higher than that with density decrease. The recovery from bottom injection is about 48% with density increase while it is 31% with density decrease. The breakthrough time for bottom injection is extended by 2 years when the density effect is included. There is less gas production in the top injection cases than the bottom injection cases.

In the next example, ordinary kriging is used to assign permeabilities to the grid blocks ranging from 10 mD to 500 mD (Fig. 3.8a). The porosity is related to the permeability using the same expression as the previous example (Fig. 3.8b). Even though the permeability distributions in the two examples are quite different, the density effects on flow path are very similar (Fig. 3.9). Fig. 3.10 shows the recovery profiles for the top and bottom injection scenarios. For both cases, the recovery with density increase is higher than that with density decrease. The recovery from bottom injection is about 47% with density increase while it is 30% with density decrease. Breakthrough occurs after 2 years with density decrease, while it occurs after 4 years with density increase.

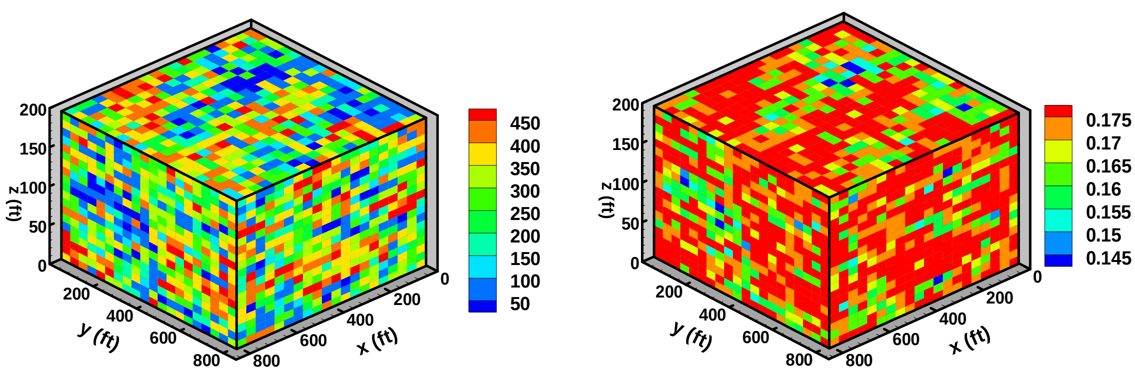

(a) (b)

Fig. 3.5 —Distribution of (a) permeability (mD) and (b) porosity(fraction) in the heterogeneous 3D media using Gaussian geostatistical simulation.

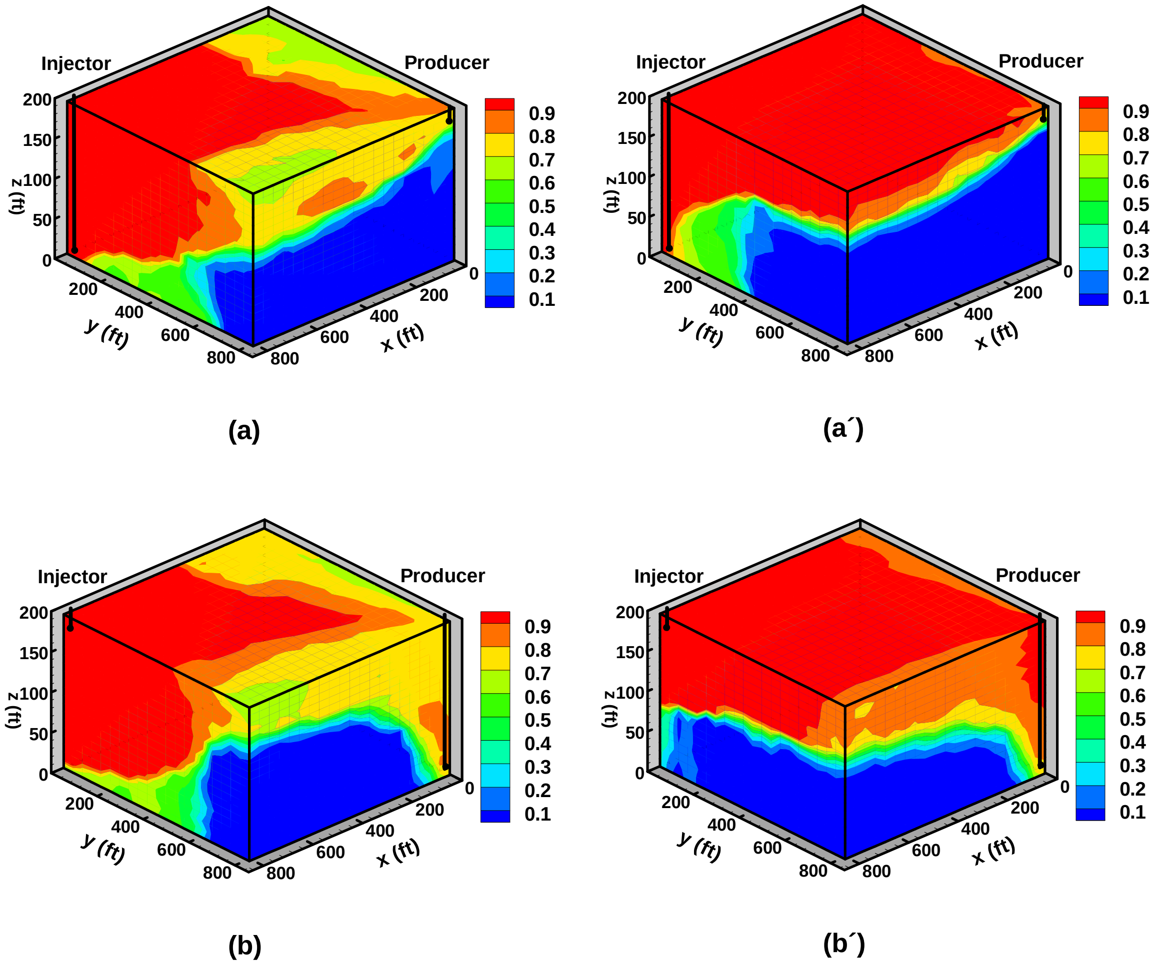

Fig. 3.6 —Overall CO_2 composition (mole fraction) at 70% PVI for (a, b) increasing density with CO_2 dissolution and (a´, b´) decreasing density with CO_2 dissolution: heterogeneous 3D media using Gaussian geostatistical simulation.

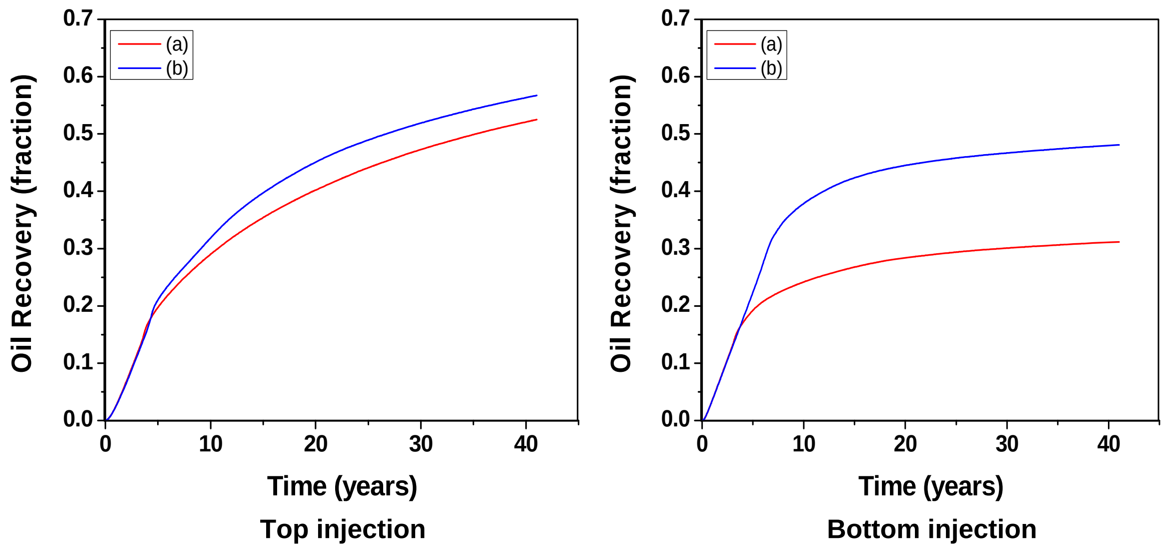

Fig. 3.7 —Oil recovery vs. time for (a) decreasing density with CO_2 dissolution and (b) increasing density with CO_2 dissolution: heterogeneous 3D media using Gaussian geostatistical simulation.

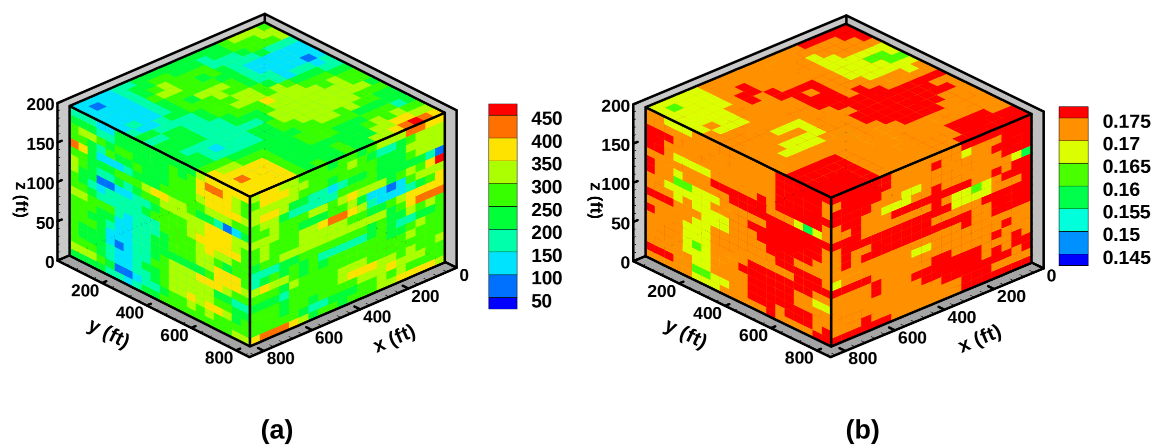

Fig. 3.8 —Distribution of (a) permeability (mD) and (b) porosity(fraction) in the heterogeneous 3D media using ordinary kriging.

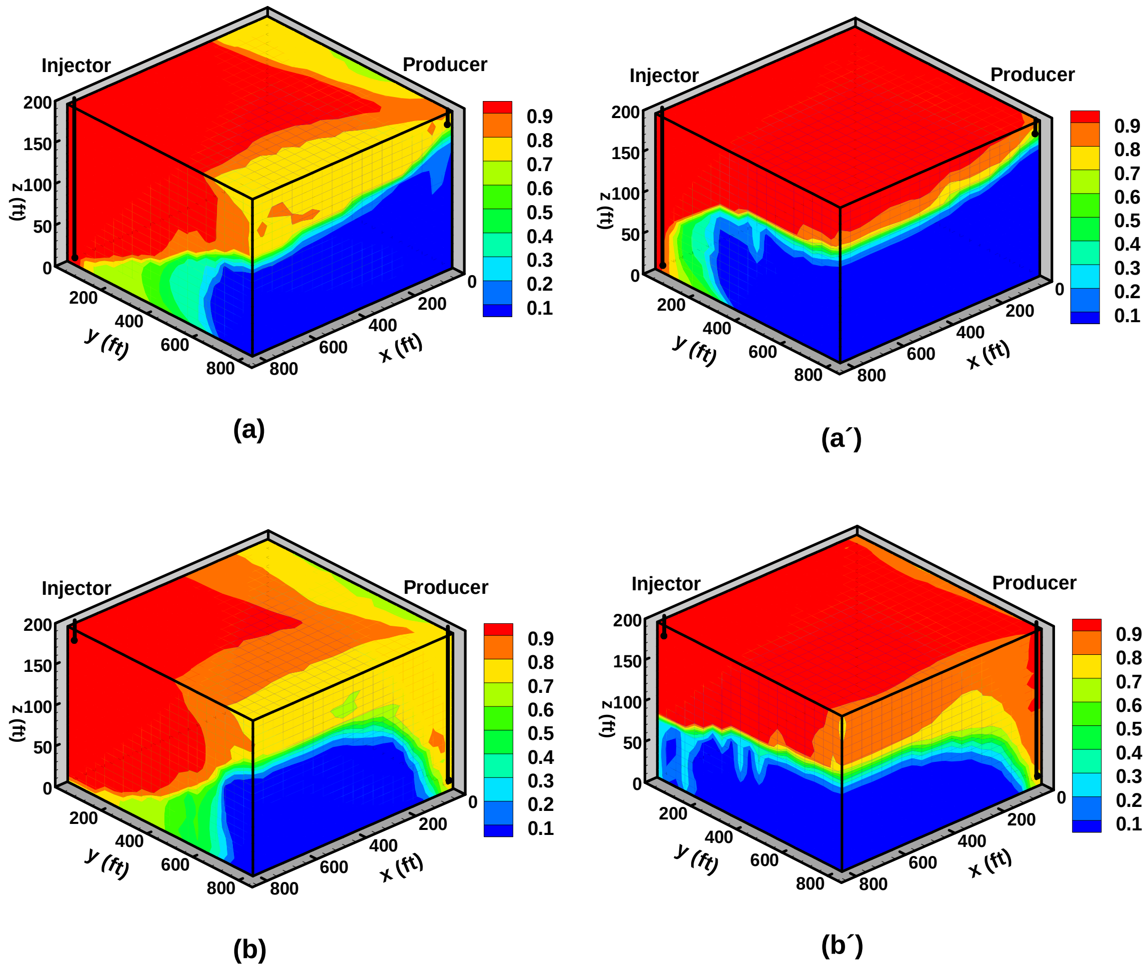

Fig. 3.9 —Overall CO_2 composition (mole fraction) at 70% PVI for (a, b) increasing density with CO_2 dissolution and (a´, b´) decreasing density with CO_2 dissolution: heterogeneous 3D media using ordinary kriging.

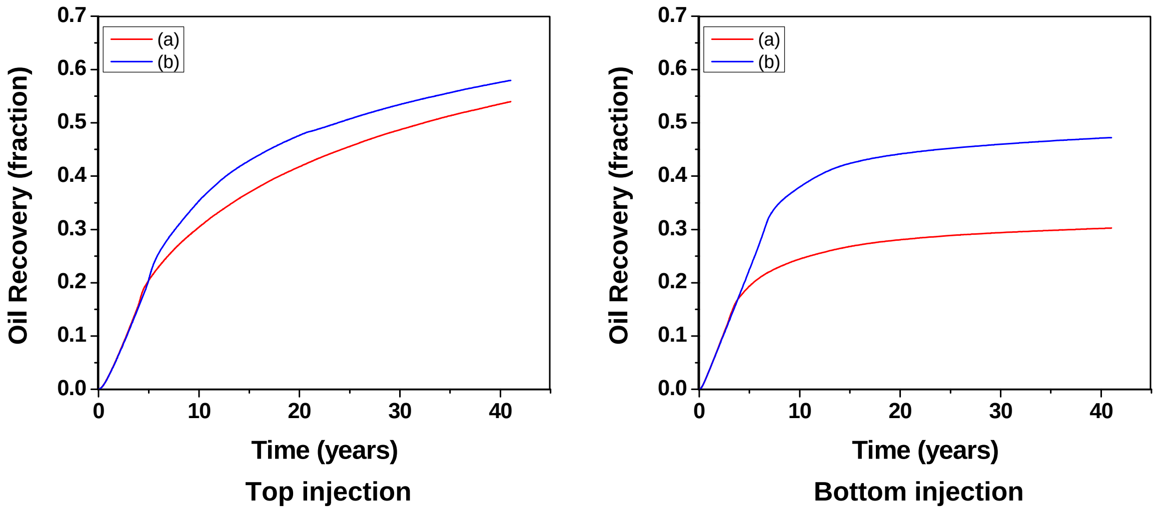

Fig. 3.10 —Oil recovery vs. time for (a) decreasing density with CO_2 dissolution and (b) increasing density with CO_2 dissolution: heterogeneous 3D media using ordinary kriging.

3.3 Section Summary

A simple approach to model the increase in oil density with CO_2 dissolution using the Peng-Robinson EOS and the Pedersen viscosity correlation is presented. By changing the volume shift parameter of CO_2, one can model the increase in oil density with CO_2 dissolution while preserving the viscosity match. The Peng-Robinson EOS can predict the density of pure CO_2 by adjusting the CO_2 volume-shift parameter. The use of the existing correlations for predicting the volume-shift parameters do not perform well for CO_2 injection at high pressures. While the slim tube MMP is independent of density effects, the oil density change from CO_2 dissolution can have a drastic effect on recovery performance as seen in the simulation results. Due to the 1D nature of flow in slim tube experiments, the density effect is not taken into account. In 2D and 3D, when injected

CO_2 is lighter than the oil phase, there may be no gravity stable displacement due to increase in oil density from solubility. When the density of the injected gas is less than the oil density, CO_2 injection may result in unstable gravity drainage. Past literature has neglected density effects in the study and evaluation of CO_2 injection. Density measurements for CO_2/oil mixtures at different CO_2 compositions and prediction of these results in the fluid model can increase the reliability of the simulation results and decrease the degree of uncertainty. Heterogeneity may also have a significant effect as would be expected. The depth of injection and production wells with respect to the top of the reservoir may also have a major impact on recovery.

CO_2 SEQUESTRATION IN SALINE AQUIFERS

In this section, the processes involved in CO_2 sequestration are discussed. Section 4.1 discusses the transport processes involved in CO_2 sequestration, followed by Section 4.2 discussing the various trapping mechanisms.

4.1 Transport Processes

The following transport processes are relevant to CO_2 storage in saline aquifers (Ukaegbu et al. 2009):

1. Advection is the movement of CO_2 caused by pressure gradients. When CO_2 is injected into saline aquifers, it flows away from the high-pressure injection points in a radial direction towards areas of low pressure according to Darcy's Law.
2. Buoyancy is caused by the density differences between the gas and the liquid phases. CO_2 being less dense will rise upwards as the brine sinks.
3. Diffusion is caused by the concentration gradients. Molecules of CO_2 will migrate from regions of higher concentration to regions of lower concentration to achieve equilibrium in chemical potential.

Advection is dominant during the injection period. Buoyancy is also an important transport mechanism since CO_2 is typically 40-60% less dense than the formation brine. Including diffusion in the modeling of CO_2 sequestration can have a significant effect on the storage of CO_2. This is addressed in this study.

4.2 Trapping Mechanisms

When injected in saline aquifers, CO_2 can be trapped through a combination of one or more chemical and physical processes. Orr et al. (2005) tried to postulate the time and length scales that characterize the sequestration of CO_2 and introduced two time periods: injection period and post-injection period. During the injection period, advection and gravity segregation are the dominant transport mechanisms. Heterogeneity determines the movement of low viscous CO_2 and appropriate representation of heterogeneity is important. Structural trapping of CO_2 and CO_2 trapping as a residual gas (hysteresis) are the main sequestration mechanisms during this phase. In the post-injection period (100 to 10000 years), buoyancy and capillary forces dominate over the viscous forces. Dissolution of CO_2 in brine and mineralization of CO_2 become more important as time progresses. These trapping mechanisms are discussed in detail below.

4.2.1 Structural Trapping

Structural trapping consists of trapping CO_2 in a flow system with low flow velocity over geologic periods of time (Nghiem et al. 2004). Being less dense than brine, CO_2 will rise upwards as a plume until it encounters the low permeability cap rock. CO_2 will then migrate laterally up dip along the seal if it is not horizontal. This is the first and most basic screening criteria for CO_2 sequestration in saline aquifers.

4.2.2 Residual Trapping

Residual trapping is another effective trapping mechanism and is also most effective when the immobile gas is away from the cap rock. CO_2 trapped in pore spaces, from which water was displaced, will remain locked in place because of the capillary effect and cannot be displaced by imbibitions of any fluid (Tiamiyu et al. 2010). Kumar et al. (2005), through an inject low and let rise approach, have shown that residual trapping plays a dominant role in CO_2 storage. Bryant et al. (2008) further investigated whether the intrinsic instability of buoyancy driven flow leads to fingering of CO_2. The mechanisms governing this type of displacement were studied in a series of fine grid simulations with a finite amount of CO_2 at the bottom of a 2D aquifer and only buoyancy driving the displacement. There were several fine-scale geostatistical realizations of permeability and the effect of capillary pressure and dip angle were also investigated. They found that CO_2 follows preferential flow paths that are a consequence of rock properties (permeability, drainage capillary pressure curve and anisotropy). Capillary pressure broadens the lateral extent of the flow paths.

4.2.3 Solubility Trapping

Solubility trapping involves the dissolution of CO_2 in the formation brine. The mixture of CO_2 and brine is denser than the fresh brine and this sets up a convective process in which the denser brine sinks to the bottom. The percentage of CO_2 dissolved in brines during the upward migration of CO_2 is typically less than 10%. Over a long period of time, the injected CO_2 will form a thin layer of CO_2 free phase which will slowly dissolve in the underlying brine. There are several correlations available to calculate the density of CO_2 dissolved brine. Duan and Sun (2003) have the most comprehensive model for calculating CO_2 solubility in pure water and NaCl solutions from 273 to 533 K and 0 to 2000 bar. Their model is based on the equation of state of Duan et al. (1992) and the work on thermodynamics of electrolytes by Pitzer (1973). Comparison of their equation of state predictions with experimental data show that their results are close to experimental uncertainty which is about 7% in CO_2 solubility. The model is also extended to model CO_2 solubility in complex brines such as seawater with good accuracy.

Using the equation of state developed by Duan and Sun (2003), Burton and Bryant (2009) calculated the solubility of CO_2 in brine as a function of depth with the temperature and pressure gradients assumed to be 0.01 °F/ft and 0.44 psi/ft respectively. They found that beyond 2000 ft the solubility in brine remains constant (Fig. 4.1). Thus the formation depth presents neither advantage nor disadvantage for this process. They found the solubility of CO_2 at aquifer conditions to be around 2.1 mol%. This can be achieved with several combinations of pressure and temperature.

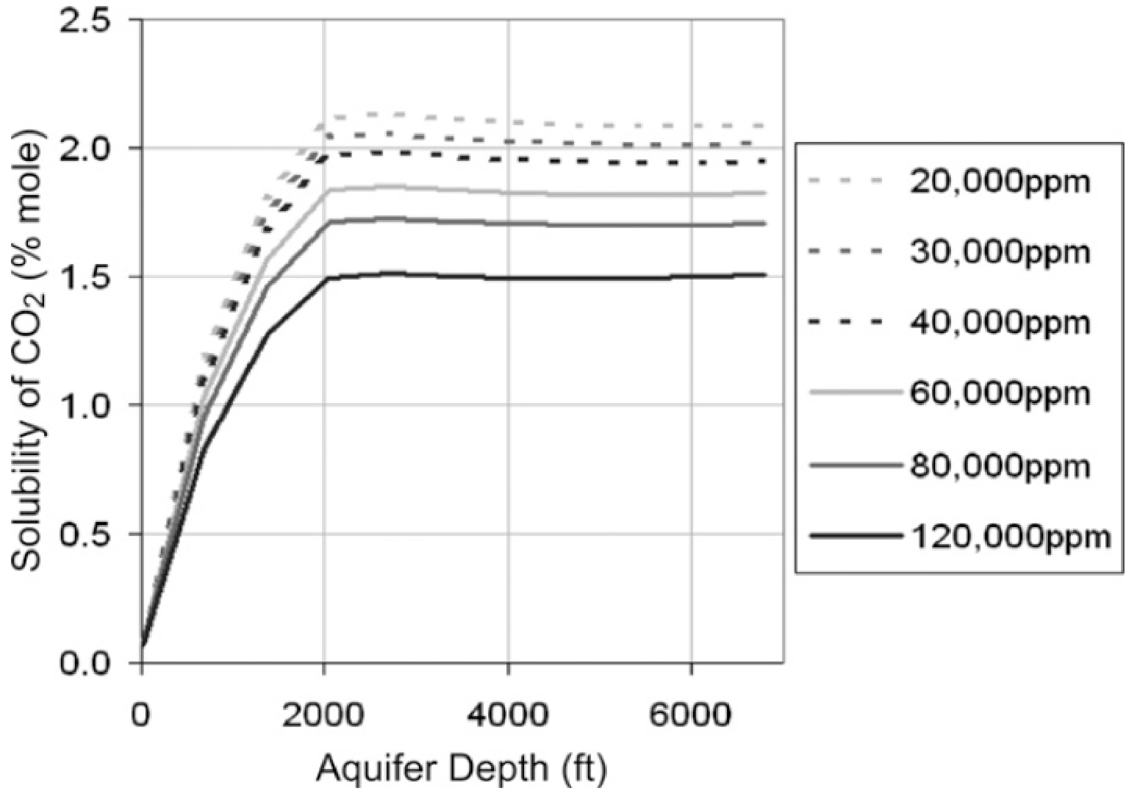

Fig. 4.1 —The solubility of CO_2 in brine as a function of temperature pressure and salinity determined by the Duan and Sun EOS (Burton and Bryant 2008). Solubility increases with depth to ~2000 ft, and then remains constant. A geothermal gradient of 0.01 °F/ft and a hydrostatic gradient of 0.44 psi/ft are used. Brine salinity effects the plateau solubility.

Fig. 4.1 cannot be reproduced directly by the Peng Robinson EOS. The solubility is tuned by the binary interaction coefficients (BICs), which are functions of temperature and salinity (Kumar 2004). If one set of BICs are used, the solubility will continue to increase even after 2000 ft, failing to capture the plateau. Recalculating the BICs at each depth captures the plateau, but this is a very inefficient process. Therefore the Peng Robinson EOS cannot model solubility in thick aquifers and aquifers with large temperature or salinity variations.

4.2.4 Aqueous Phase Diffusion

Molecular diffusion describes the passive movement of molecules, due to random motion (Brownian motion), or due to a compositional gradient in the mixture, and is quantified by molecular diffusion coefficients (Leahy-Dios and Firoozabadi 2007). To include the effect of molecular diffusion, the diffusion coefficients of CO_2 in water are required. There is a lot of experimental data available for measuring molecular diffusion. Tamimi et al.(1994) reported the diffusion coefficients of CO_2 in water from 298 to 368K. For this study, (~313K) the diffusivity reported was 2.93×10^{-5} cm^2/s. Frank et al. (1996) measured the diffusion coefficients and viscosities for CO_2/H_2O systems. At 318K, they reported a diffusion coefficient of 3.07×10^{-5} cm^2/s. Renner (1988) developed a novel in-situ method to calculate the diffusion coefficients of CO_2 and other solvent gases in consolidated media at high pressures. The diffusion coefficient of CO_2 in 0.25 M NaCl brine at 100 F and pressures ranging from 647 to 846 psi was reported to be ranging from $3.64 – 7.35 \times 10^{-5}$ cm^2/s. Renner concluded that the diffusion coefficient of CO_2 in water or brine was an empirical function of liquid and CO_2 viscosities.

There have been diverging opinions in the literature on the effect of diffusion on the CO_2 sequestration process. Ukaegbu et al. (2009) found through a simulation study that the diffusion of CO_2 in the aqueous phase increases the amount of dissolved CO_2. This increase was as much as 18% after 20 years into the simulation. They explained that the increase in CO_2 concentration in the gridblock cause CO_2 to migrate to areas of lower concentration to reduce the concentration difference, which allows greater dissolution.

On the other hand, Ennis-King and Paterson (2005) have shown through linear stability analysis that the dominant mechanism for dissolution of CO_2 in water is convective mixing rather than diffusion. Moortgat and Firoozabadi (2010) state that current correlations used assume an effective diffusivity in which the diffusive flux of the component *i* only depends on its own compositional gradient. This could lead to an oversimplification, especially for 3 component systems. They suggest the use of Fickian diffusion.

4.3 Section Summary

There has been a lot of work on CO_2 sequestration in recent years. Researchers have investigated the dominant physical and chemical processes involved. Solubility and mineral trapping are the most desirable trapping mechanisms because the CO_2 is sequestered in a form that is safe for the environment. The Peng Robinson EOS is not a suitable method to model CO_2 solubility in brine. The literature discussed in this section along with published experimental data will be used in the development of a simulation model in the next section.

CO_2 SEQUESTRATION CASE STUDY: ARUMA AQUIFER

5.1 Aquifer Description and Hydrogeology

The Aruma aquifer is located in southwest Qatar. It occupies an area of about 1985 km^2 on land which is approximately 16% of Qatar's area. The Qatar Department of Agricultural and Water Research have drilled four deep wells in this aquifer to characterize it better. Regional monitoring of the groundwater levels and comprehensive logging were performed to better understand the aquifer. Water quality analysis was also performed at the four deep wells. Details of the drilling report completed by Al-Baida Technical Services (ATS) are presented in the next section (ATS 2004).

The Aruma aquifer comprises approximately 130 m (426 ft) of granular limestone belonging to the Aruma Formation. The top of the aquifer ranges from 380 to 550 m within southwest Qatar. The aquifer is overlain by thick relatively impermeable deposits of the lower Umm Er Radhuma (UER) aquifer and is underlain by a sequence of shales of up to 100 m thickness belonging to the lower Aruma Formation. These strata bound the aquifer and serve to isolate it from groundwater movement in other formations. The aquifer is highly confined within its bounding strata and this is confirmed by a very low "storativity" value. The storativity of an aquifer is a dimensionless number that equals to the volume of water released from a unit volume of aquifer per unit decline in pressure. There was also no evidence of leakage or drainage while testing. The overall thickness of the Aruma formation declines moving northwards from approximately 265 m in the south to less than 240 m in the north. Within the formation, the upper limestone becomes thicker moving northwards while the shales at base become thinner.

5.2 Data Processing

The approximate limits of the project area are shown in Fig. 5.1. There are 11 pre-existing deep wells in the project area numbered DW-1 through to DW-11. The new deep wells drilled were numbered DW-12, DW-13, DW-14 and DW-15. DW-12 and DW-13 were located adjacent to existing wells DW-03 and DW-11 in order to perform aquifer tests while observing water levels in the nearby deep wells. The new wells are located around the flanks of the Dukhan anticline which has a dip that exceeds 0.5°. DW-14 and DW-15 are located in the neighboring syncline while DW-12 and DW-13 are located on the anticlinal crest. Detailed logging was performed at each new deep well location. This data along with the limited log data of the existing deep wells was used to map the Aruma aquifer top and bottom. The log data of the wells available and those that are used in this study are provided in the Table 5.1. Table 5.2 provides a summary of the aquifer properties measured from log data and flow tests.

Using the log data and the results of the flow tests, maps were created for porosity, permeability, formation depth and thickness. Geographix software was used for the log analysis and creating the maps. These maps were then exported to CMG to create the static reservoir model. SI units were used in the static reservoir model as most of the data was reported in SI units. The results are reported in field units for ease of understanding.

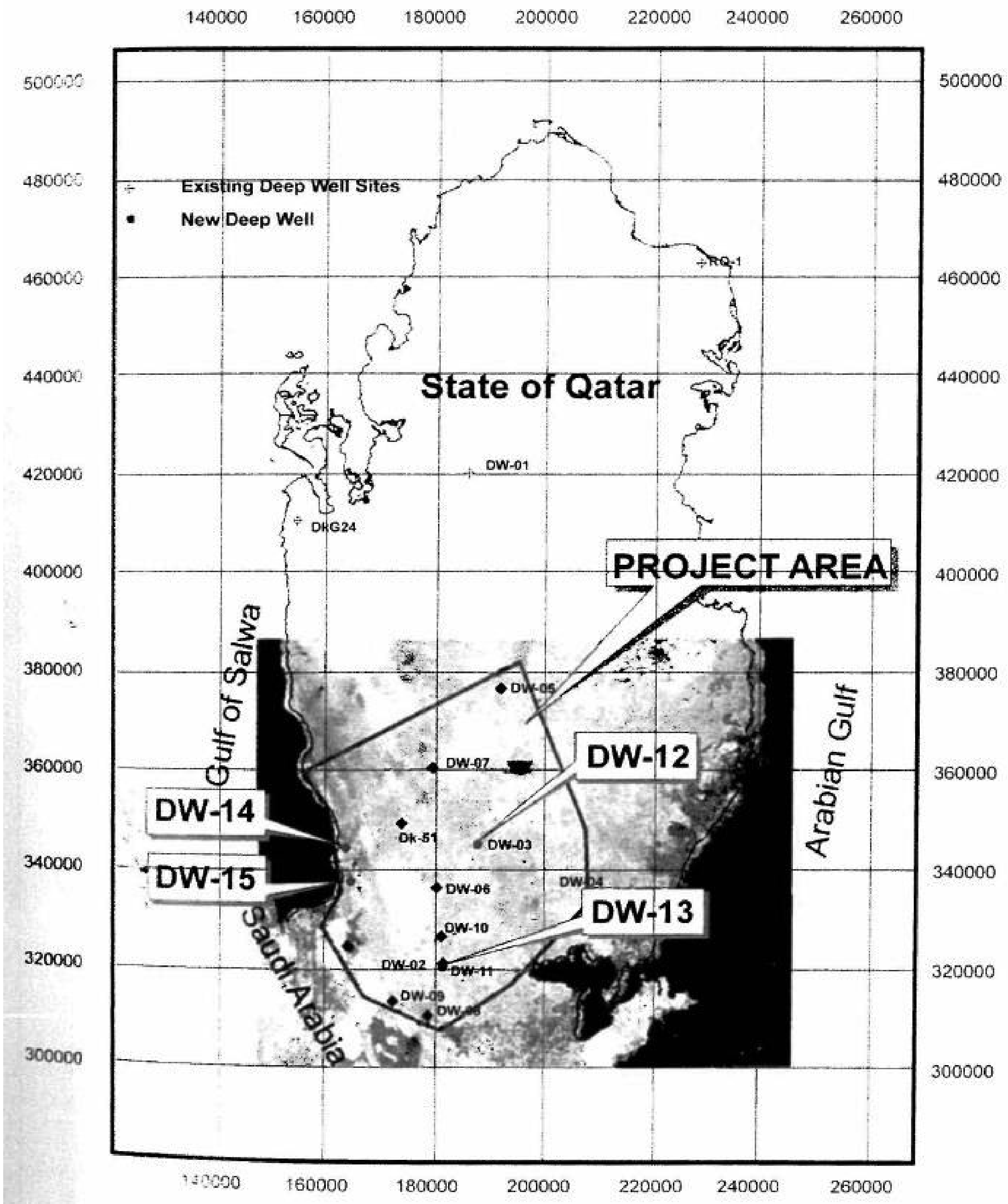

Fig. 5.1 —The project area and location of the deep wells (ATS 2004)

Table 5.1 – Log data available for the Aruma aquifer

Well	Gamma Ray	Sonic Log	Neutron Log	Density Log	Temperature	Resistivity
DW-6	X					X
DW-7	X					X
DW-8	X					X
DW-10	X					X
DW-12 *	X	X	X	X	X	X
DW-13 *	X	X	X	X	X	X
DW-14 *	X	X	X	X	X	X
DW-15 *	X	X	X	X	X	X

*** = newly drilled wells***

Table 5.2 – Aruma Aquifer properties

Well	Top (ft)	Bottom (ft)	Thickness (ft)	Porosity (fraction)	Permeability (mD)	Temperature (°F)
DW-12	1585	2028	443	0.162	4187	112.8
DW-13	1503	1936	433	0.149	3395	115.5
DW-14	1880	2388	509	0.111	2263	116.9
DW-15	1854	2336	482	0.123	3508	118.2
Total Dissolved Solids, ppm			5000			
k_v/k_h			0.1			

It is important to note that the Aruma aquifer is highly permeable (Table 5.2). Firoozabadi and Cheng (2010) emphasize the selection of high permeability aquifers to store CO_2 because they aid in the rapid dissolution of CO_2 in brine.

5.3 Base Case Model Description

A three dimensional corner point fine grid was used to model the project area. The model consists of 106 grids in the *x*-direction, 145 grids in the *y*-direction (width), and 7 grids in the *z*-direction. The Aruma aquifer is modeled with five layers in the *z*-direction. The two layers above it represent the seal and the overlying UER formation. Each gridblock is 500 meters in the *x*- and *y*-directions. Isopachs generated from the log analysis were used to assign thickness for each layer in the *z*-direction. The permeability of the seal is assumed to be 0.01 mD due to a lack of permeability measurements of the seal rock. A k_v/k_h value of 0.1 was used. Null blocks were assigned to cells outside the project area. The eight existing deep wells shown in Table 5.1 were converted to CO_2 injectors. They were all set to inject equal amounts of CO_2 in the bottom layer for 30 years. The simulation stops after 200 years to observe the gradient flow. Fig. 5.2 shows the reservoir model with the well locations. The selection of the injection rates and well constraints are discussed in the next section.

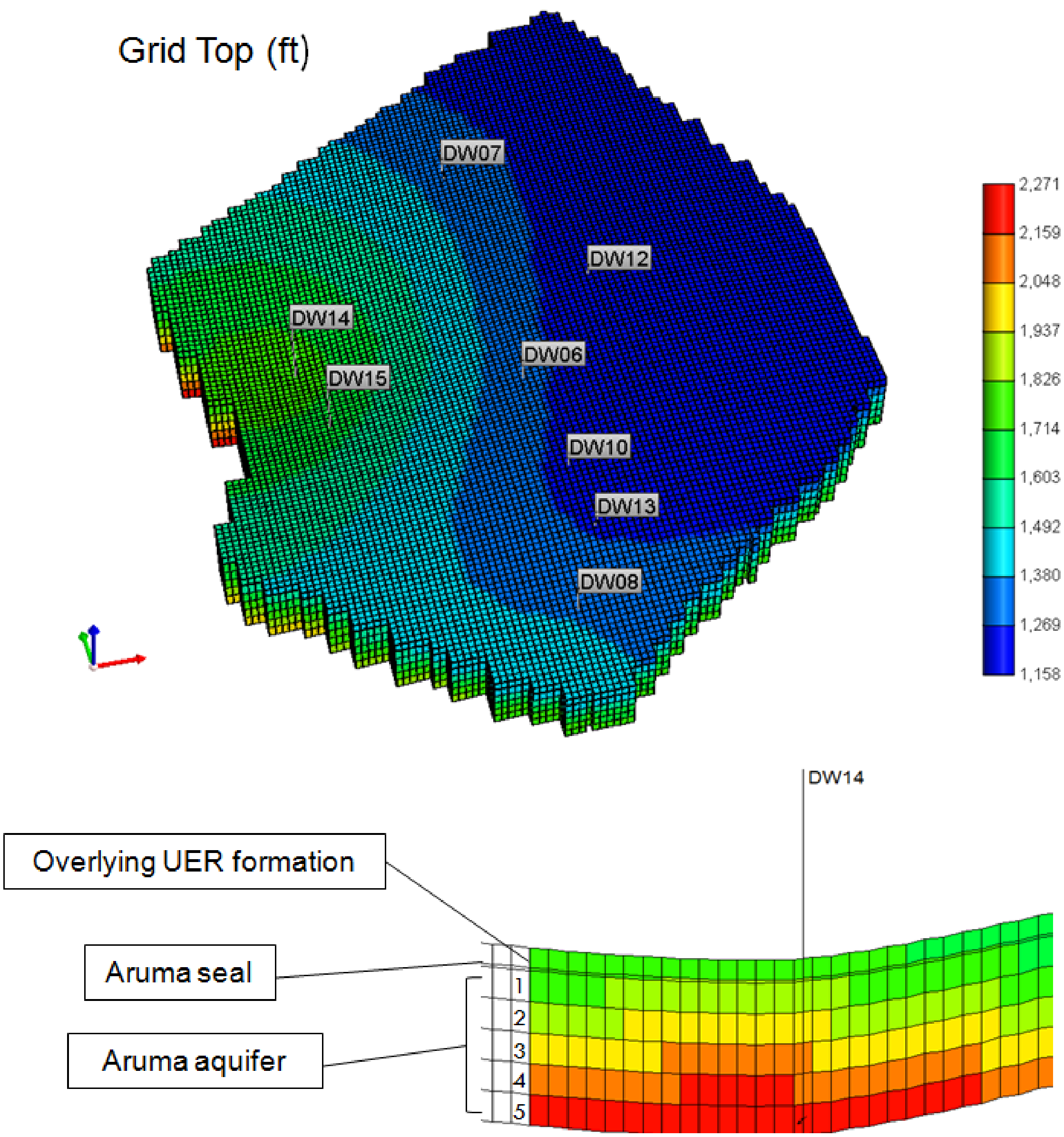

Fig. 5.2 —The reservoir model showing well locations and the description of the layers.

5.3.1 Injection Design and Well Constraints

A realistic injection scenario is developed taking into account existing sequestration projects. The Sleipner project was chosen as a facilities design analog. In terms of pore volume, the Utsira formation is 10 times larger than the Aruma formation modeled. CO_2 is being injected into the Utsira Formation at a rate of 1 million tonnes/year. This translates to average daily injection rate of 52 million SCF/day. Since the Aruma formation is 10 times smaller, a daily injection rate of 5.2 million SCF/day is used. This rate is divided equally among the eight wells giving each an injection rate of 650000 SCF/day (18406 sm^3/day). CO_2 is injected through perforations made in the bottom layer of the Aruma aquifer.

The change in pressure at the well will have an impact on the pressure at the caprock, which affects the seal integrity. The bottomhole pressure constraint was set such that injection pressure would not exceed the fracture gradient. Using the formula proposed by Eaton (1969) to predict fracture gradient, a fracture gradient of 0.68 psi/ft (15.7 kPa/m) was obtained. This means that at a depth of 500 m (1640 ft), the fracture pressure of the rock is 1115 psia. All the wells are present at depths exceeding 500 m. The ideal injection wells are located in the syncline (DW-14 and DW-15). Injection from these points allows the gas to migrate up dip and get trapped under the anticline.

5.3.2 Fluid Phase Behavior

The Peng-Robinson EOS was used to model phase behavior. The model consists of CO_2, H_2O and C_1 as pure components. Table 5.3 shows the different property values used by the Peng-Robinson EOS. It should be noted that the Peng-Robinson EOS is only used to calculate the gas phase behavior. C_1 is used as a trace component to add compressibility to the near incompressible system. This helps in the convergence of the equations in the reservoir simulator. The aqueous phase density is calculated from the Rowe and Chou correlation, while aqueous viscosity is calculated using the Kestin correlation. These correlations are built into GEM and are functions of pressure, temperature and salinity. The Peng-Robinson EOS predicts the CO_2 gas density accurately within the pressure range of this study when a volume shift parameter of zero is used. The Pedersen correlation is used to calculate the viscosity of the components. The values of the five coefficients used in this study were those obtained by Kumar (2004) after matching experimental data (Table 5.4).

Table 5.3 – Component properties used in the aquifer model

Components	T_c (K)	P_c (atm)	MW (g/mole)	ω	*BIC* CO_2 -comp$_i$	Volume Shift
CO_2	304.2	73.76	44.01	0.2250	0.000	0.000
C_1	190.6	46.00	16.04	0.0080	0.103	0.000
H_2O	647.3	217.60	18.01	0.3440	0.200	0.000

Table 5.4 – Parameter values for Pedersen et al. (1984) viscosity correlation for a CO_2 – brine system obtained by Kumar (2004)				
MW mixing rule coefficient	MW mixing rule exponent	Coupling factor correlation coefficient	Coupling factor correlation density exponent	Coupling factor correlation MW exponent
0.291	1.4	0.0005747	4.265	1.0579

5.3.3 CO_2 Solubility in Brine

In this study, Henry's Law is used to model CO_2 solubility in brine. The solubility of CO_2 in brine is a reversible reaction given by:

CO_2 (g) ⇋ CO_2 (aq)

Thermodynamic equilibrium between the gas and aqueous phase requires that the fugacities of CO_2 in the gas and aqueous phase be equal:

$$f_{CO_2(g)} = f_{CO_2(w)}$$

The gas fugacity, $f_{CO2\ (g)}$ is calculated using the Peng-Robinson EOS. But the equation of state fails to model the behavior of the aqueous phase properly. Therefore the fugacity of CO_2 in the aqueous phase is calculated using Henry's Law, i.e.

$$f_{CO_2(w)} = y_{CO_2(w)} H_{CO_2(w)}$$

The Henry's constant, $H_{CO_2(w)}$, is calculated at the reservoir temperature is also dependent on salinity (Nghiem et al. 2004). It is calculated at the reservoir pressure, P, as follows:

$$\ln(H) = \ln(h) + \frac{v^{\infty}(P - P_{ref})}{RT}$$

where P_{ref} is the reference pressure

v^{∞} is the partial volume at infinite dilution

h is the Henry's constant at P_{ref}

Accurate correlations for the Henry's constants of CO_2, N_2, H_2S and CH_4 have already been implemented in GEM. These correlations take into account the pressure, temperature and salinity. The Harvey model (1996) for calculating the Henry's constant of CO_2 is activated with the keyword *HENRY-CORR-CO2*.

5.3.4 Rock-Fluid Data

Relative permeability data was obtained by using the following equations and parameters (Table 5.5)(Anchliya 2009; Kumar 2004):

For $S_g \leq S_{gcr}$: $k_{rg} = 0$

For $S_g > 1 - S_{wrg}$: $k_{rwg} = 0$

For $S_g \geq S_{gcr}$:

$$k_{rg} = k_{rg}^{\circ}\left(\frac{S_g - S_{gcr}}{1 - S_{wrg} - S_{wirg}}\right)^{N_g}$$

For $S_g \leq 1 - S_{wrg}$:

$$k_{rwg} = k_{rw}^{\circ}\left(\frac{S_g - S_{gcon}}{1 - S_{wrg} - S_{gcon}}\right)^{N_w}$$

where k_{rg}° is gas end point relative permeability

k_{rw}° is water end point relative permeability

S_g is gas saturation

S_{gcr} is critical gas saturation

S_{wirg} is irreducible water saturation

S_{wrg} is residual water saturation during gas flood

S_{gcon} is connate gas saturation

N_g is gas relative permeability exponent

N_w is water relative permeability exponent

Table 5.5 – Relative permeability parameters for the base case (Kumar 2004)

Gas end point relative permeability	1.0
Water end point relative permeability	0.334
Connate gas saturation	0.25
Critical gas saturation	0.25
Residual water saturation	0.25
Irreducible water saturation	0.25
Water relative permeability exponent	2
Gas relative permeability exponent	2.5

Relative permeability data published by Bennion and Bachu (2008) was not used as it was obtained using highly saline brine and supercritical CO_2. The capillary pressure for the base case was assumed to be zero from the lack of experimental data. Other works have used the Brooks-Corey approach (Brooks and Corey 1966) to predict capillary pressure. The Brooks-Corey relation is given by:

$$P_c = P_d S_w^{*-1/\lambda}$$

where P_d is threshold or displacement pressure

λ is pore geometric factor

S_w^* is effective water saturation

The effective water saturation, S_w^* is calculated by

$$S_w^* = \frac{S_w - S_{wr}}{1 - S_{wr}}$$

where S_{wr} is irreducible water saturation

The pore geometric factor and displacement pressure are determined experimentally. Values of $\lambda = 2$ and $P_d = 10$ Pa are used in the literature for CO_2 sequestration (Bielinski et al. 2008; Ukaegbu et al. 2009).

5.3.5 Initial Conditions

The initial overall mole fraction of CO_2 in the aquifer is zero, where the global mole fraction of water is one. The initial reservoir pressure at 500 m (1640 ft) is 721 psi, which is calculated using a hydrostatic gradient of 0.44 psi/ft. Pure CO_2 is not in a supercritical state when it is injected into this aquifer.

5.4 Simulation Results for the Base Case

Fig. 5.3 shows the cumulative gas injected with time. At shut-in (30 years),pproximately 57 BSCF of gas has been injected, translating to 3 million tonnes. After injecting a constant rate for a period of 30 years the average aquifer pressure has increased only by 7 psia. The well bottom-hole pressure profiles in Fig. 5.4 show that average increase in bottom-hole pressure during the injection period was only about 17 psia. The overall difference in pressure between the wells is due to the fact they are all injecting from different depths into the lowest layer of the Aruma aquifer. DW-14 and DW-15, located in a syncline as mentioned previously, have the highest bottom-hole pressure. Due to the size of the aquifer, the increase in pressure is negligible with respect to the fracture pressure of the rock. The GEM data file for the base case is provided in Appendix B.

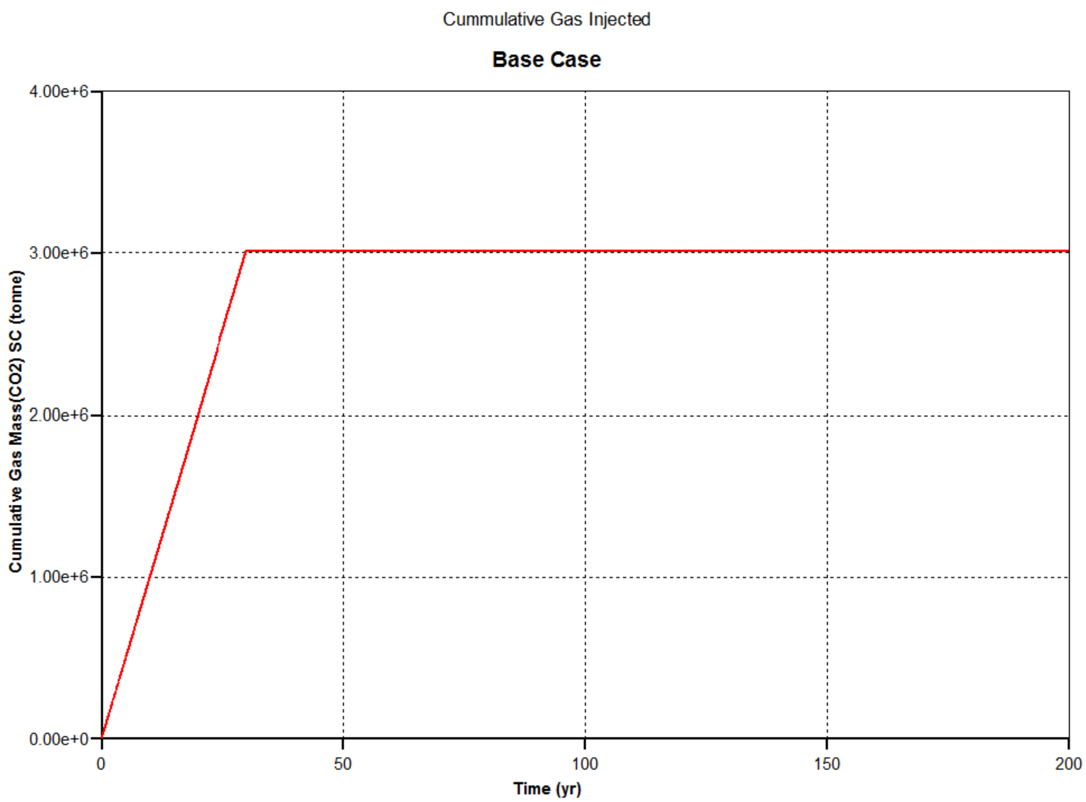

Fig. 5.3 —Cumulative gas injected with time for the base case. Approximated 3 million tonnes are injected at the end of a 30 year injection period.

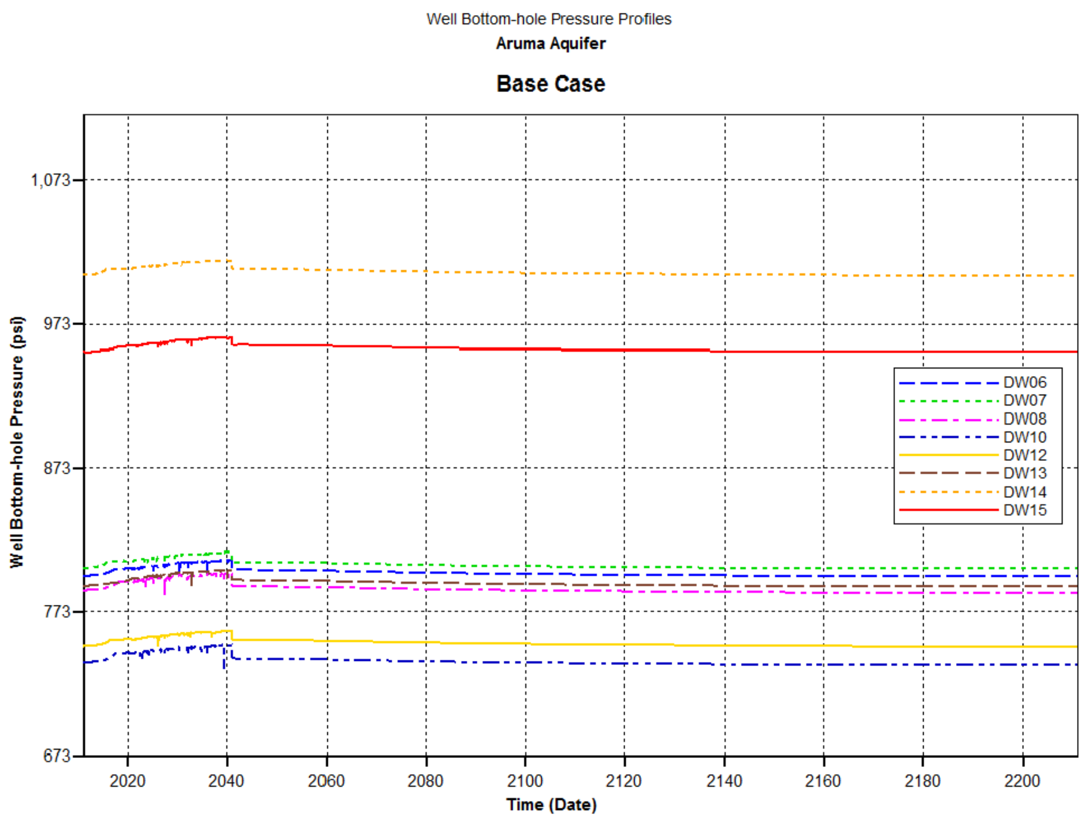

Fig. 5.4 —Well Bottom-hole Pressure profiles for the base case.

Fig.5.5 shows the global mole composition of CO_2 in the overlying UER formation. It is interesting to note that CO_2 does not breakthrough into the UER and the seal manages to contain the CO_2. The selection of the injection rate also plays an important role on the effect of seal integrity. If a very high CO_2 injection rate is used, the pressure under the seal will rapidly increase surpassing the fracture pressure and causing leakage of CO_2. It should be noted that CO_2 cannot be prevented from reaching the seal in this case. The average permeability of the Aruma aquifer is 3340 mD. Assuming a kv/kh value of 0.1, there is still a vertical permeability of 334 mD. It has also been speculated that the seal rock may have a higher capillary pressure than the reservoir rock. Bryant et al. (2008) have shown that if the rising CO_2 encounters a layer whose capillary pressure exceeds the capillary pressure of CO_2 phase, then the CO_2 is completely diverted to flow updip in the layer beneath the barrier. This process is not modeled in this study due to lack of capillary pressure data.

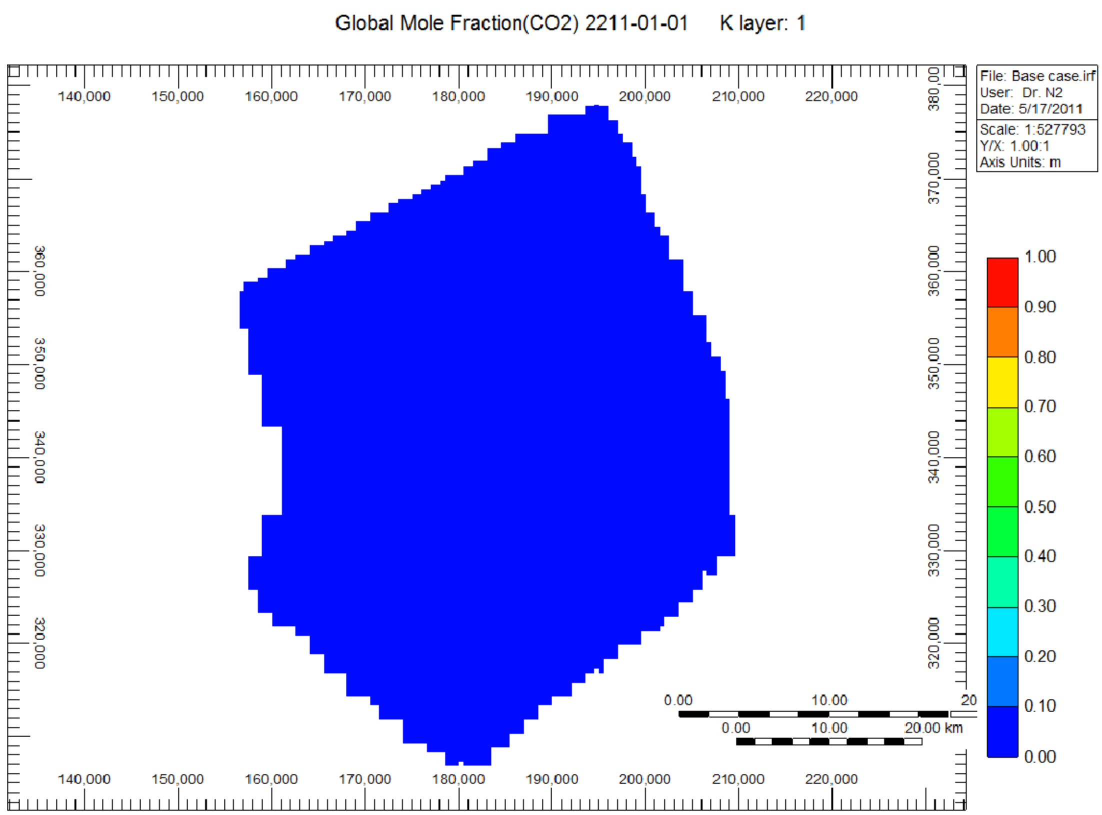

Fig. 5.5 —The CO_2 global mole fraction in the overlying formation at the end of the simulation. There is no leakage for CO_2 into the UER after 200 years with the proposed injection scheme.

The CO_2 global mole fraction in the lowest layer of the aquifer (layer 7) is shown in Fig. 5.6. We observe that due to high permeability, there is a greater radial spread of CO_2 at bottom of the aquifer. A vertical cross section around the well DW-12 shows the shape and propagation of the CO_2 plume.

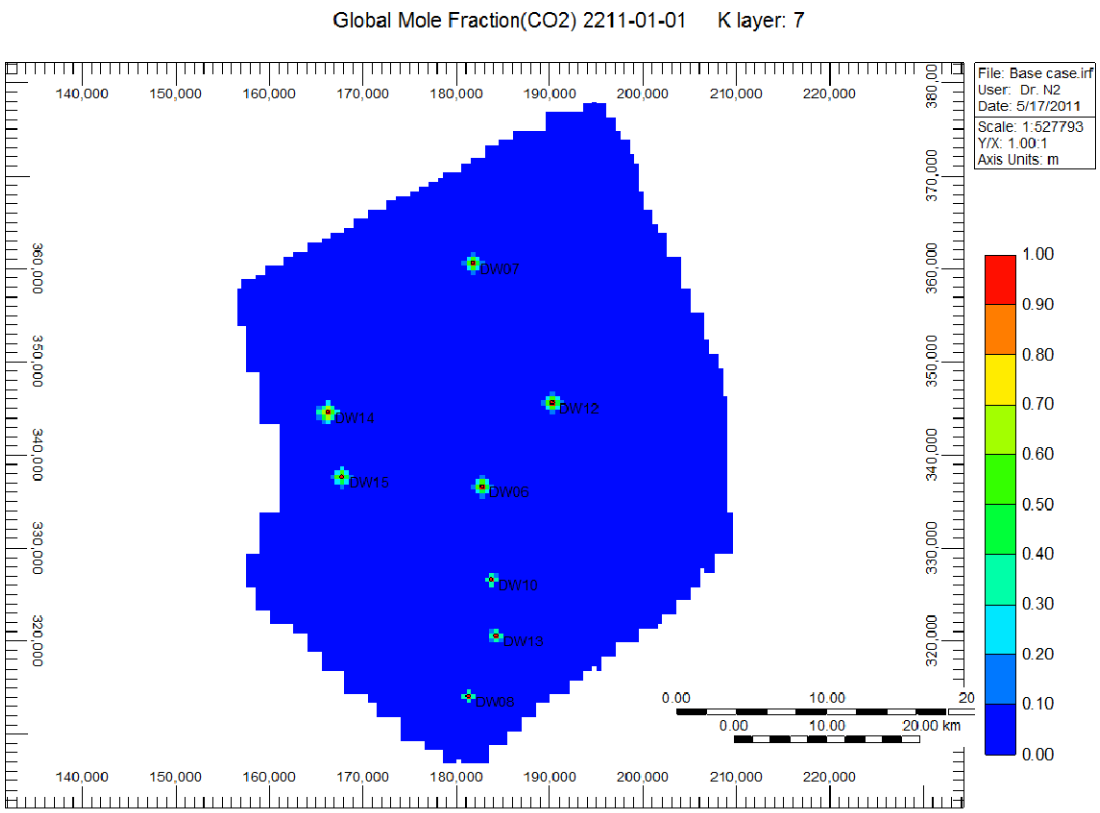

Fig. 5.6 —The CO_2 global mole fraction in the lowest layer of Aruma aquifer. CO_2 is being injected in this layer.

It is observed from Figs. 5.6 and 5.7 that a large portion of the Aruma aquifer has still not been affected by 30 years of CO_2 injection. A closed boundary system was modeled in order to represent a confined aquifer.

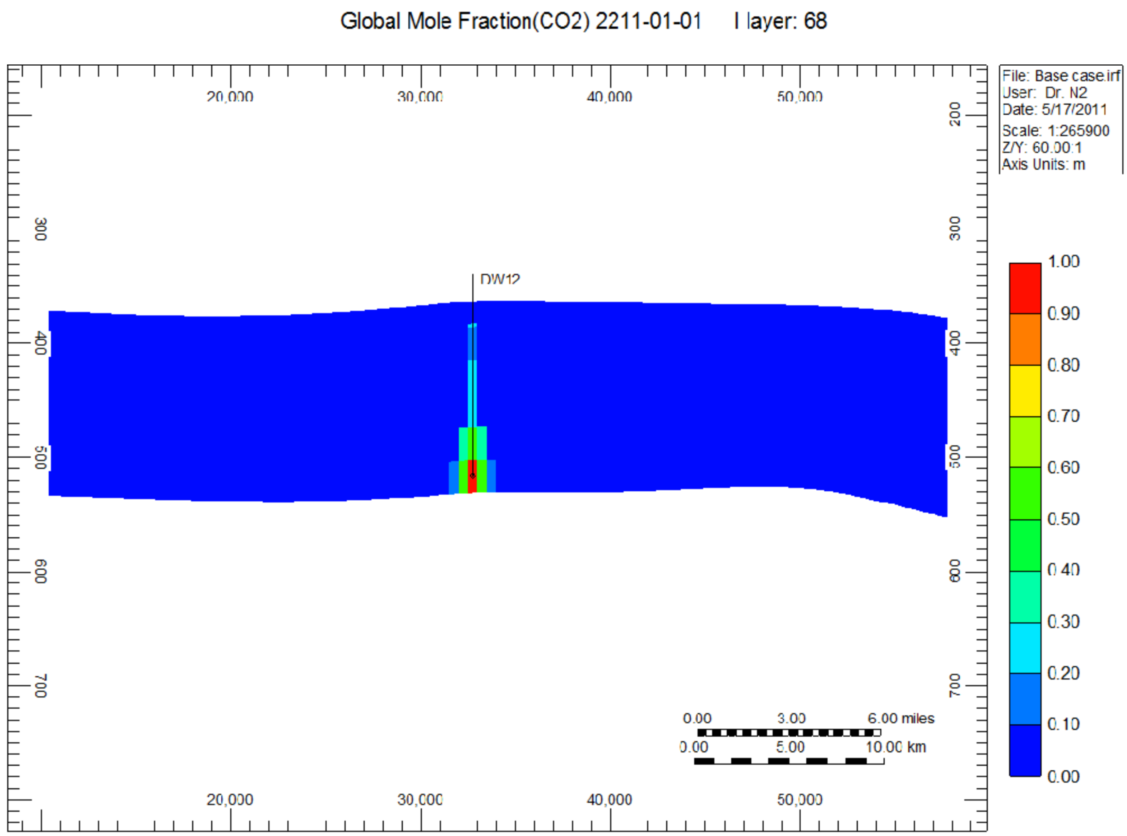

Fig. 5.7 —Propagation of the CO_2 plume from DW-12.

5.5 Including Diffusion in the Base Case

The keyword in GEM to model diffusion in the aqueous phase is *DIFFC-AQU*. The diffusion coefficient of the components in cm^2/s must be provided to use this option. GEM has the Sigmund (1976) correlation and the Wilke-Chang (1955) correlation built in to calculate the diffusion coefficient in oil and gas phases. Previous works to model diffusion have used a CO_2 diffusion coefficient of 2×10^{-5} cm^2/s (Anchliya 2009; Ukaegbu et al. 2009). The diffusion coefficient is primarily a function of temperature. The average temperature of the Aruma aquifer is 115 °F (319 K). Based on experimental data (Frank et al. 1996; Tamimi et al. 1994) a CO_2 diffusion coefficient of 3×10^{-5} cm^2/s is used in this study.

5.5.1 Simulation Results

The same injection scheme as the base case was used in the simulation run. There was almost no difference in the bottom-hole pressure profiles. Fig. 5.8 compares the number of moles of CO_2 in the aqueous phase with and without diffusion. It was found that diffusion enhances the solubility of CO_2 in brine.

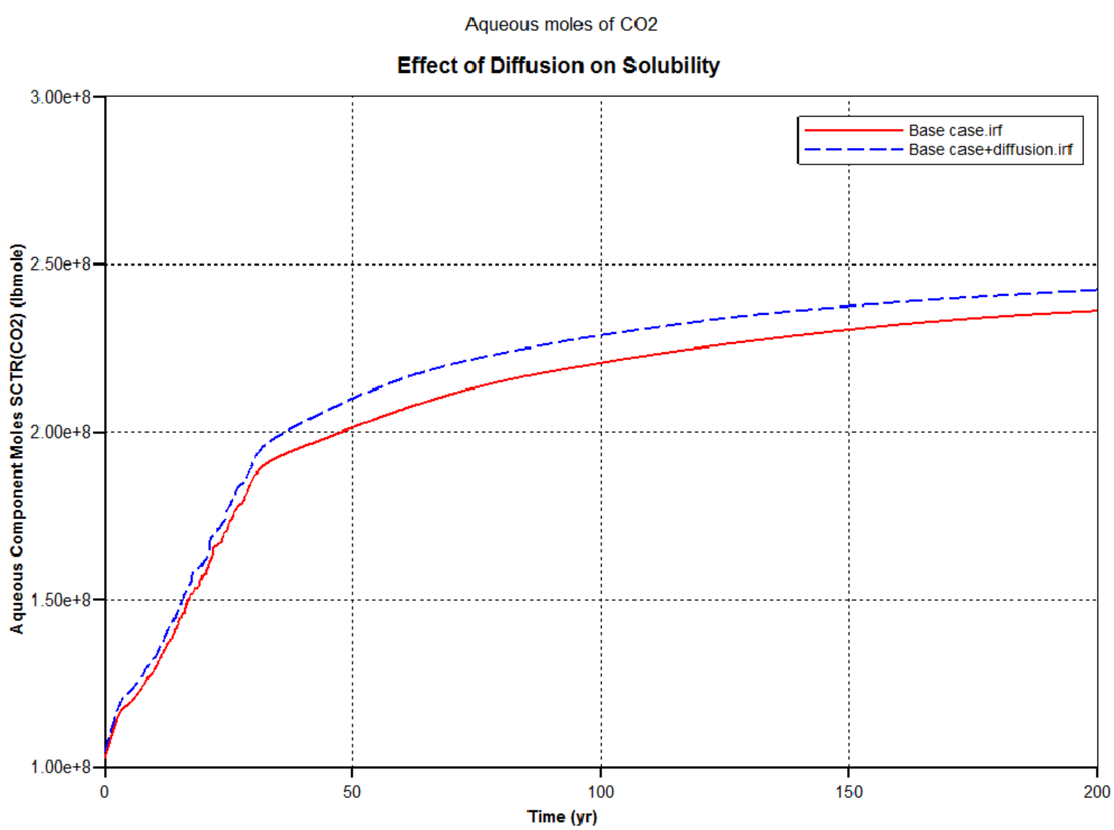

Fig. 5.8 —The effect of diffusion on the solubility of CO_2 in brine.

5.6 Grid Sensitivity Analysis

The current dimensions of each grid block in the base case are 500 m in the *x*- and *y*-directions. To study the effect of the gridding size on the propagation of the CO_2 plume, a sub-model containing a single well (DW-12) was used. The sub-model dimensions are 4500 m in the *x*- and *y*-directions with the well placed in the center. The dimensions of the grid blocks are the same as the base case (Fig. 5.9). The sub-model contains 567 cells.

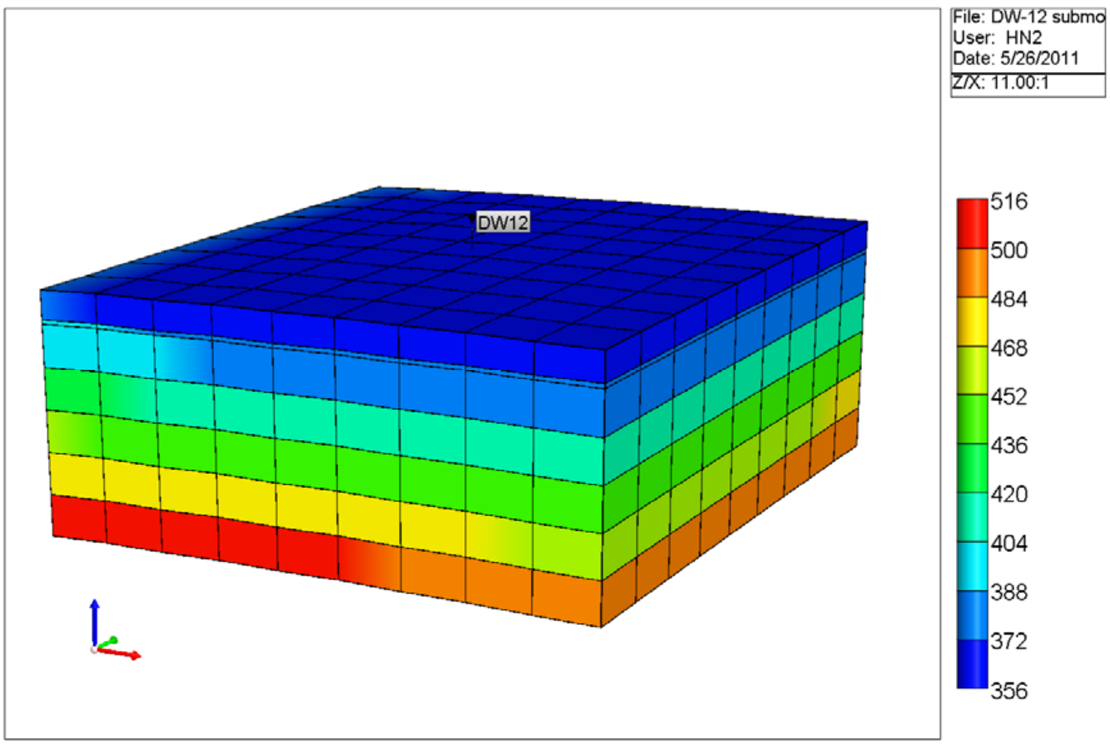

Fig. 5.9 —Extraction of a sub-model containing the well DW-12 for grid sensitivity tests. The current gridding dimensions are used in the base case. The sub-model contains 567 grids.

In the fine grid sub-model, the dimensions of the grid blocks representing the Aruma aquifer are reduced by one-third in each direction. The grid blocks of the seal and the overlying UER formation are reduced by one-third in the *x*- and *y*-directions. This model now contains 12960 cells (Fig. 5.10). The effect of grid size on diffusion is also investigated.

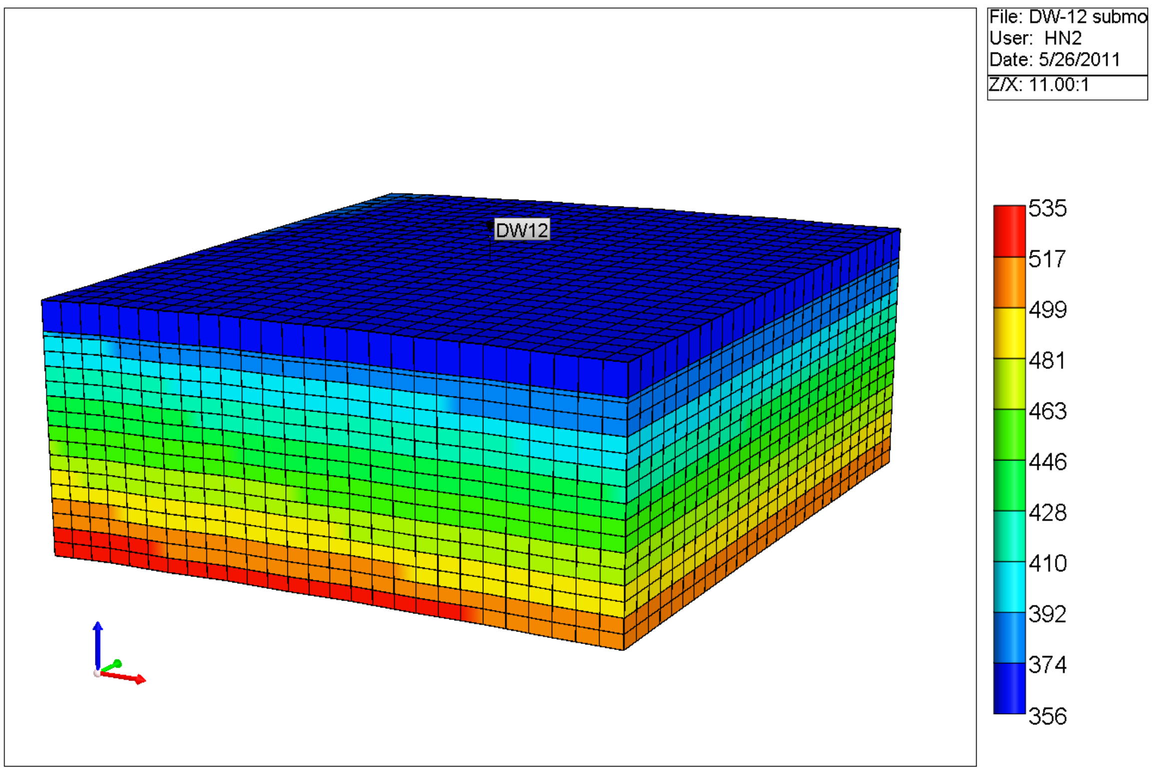

Fig. 5.10 —The fine grid sub-model containing the well DW-12 for grid sensitivity tests. The sub-model contains 12960 grid blocks.

5.6.1 Grid Sensitivity Results

The use of finer grids shows a significant difference in the propagation of CO_2 plume. Fig. 5.11 compares the global mole fraction of CO_2 between the two cases after 200 years.

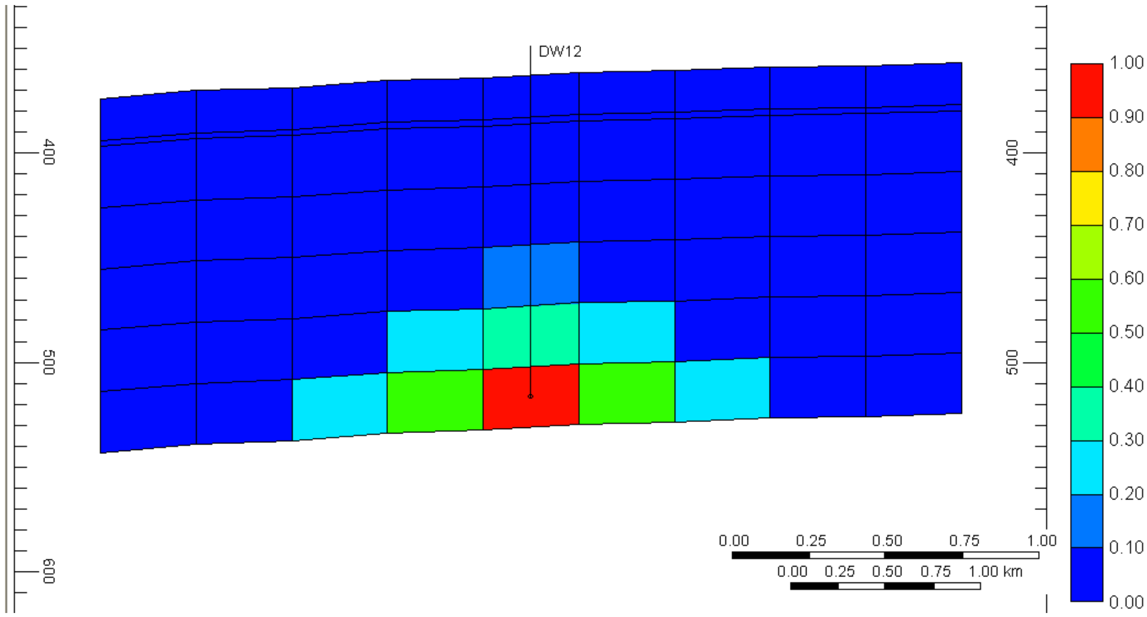

(a)

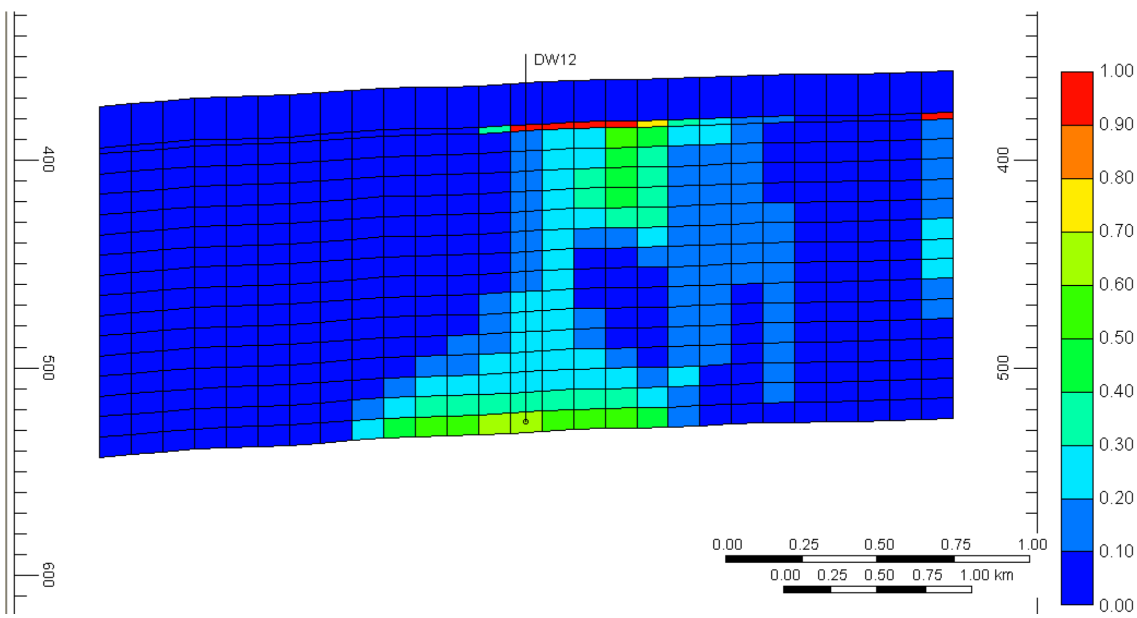

(b)

Fig. 5.11 —Comparison of CO_2 plume propagation after 200 years: (a) coarse gridding and (b) fine gridding.

With coarse gridding, upward movement of CO_2 is limited. CO_2 spreads radially from the injection point. The use of fine grids shows the CO_2 plume reaching the seal and beginning to move up dip below the seal. As the CO_2 dissolves in the brine below the seal, the increase in the brine density triggers convective mixing of CO_2. The use of coarse grids also overestimates the amount of CO_2 dissolved in brine as can be seen in Fig. 5.12.

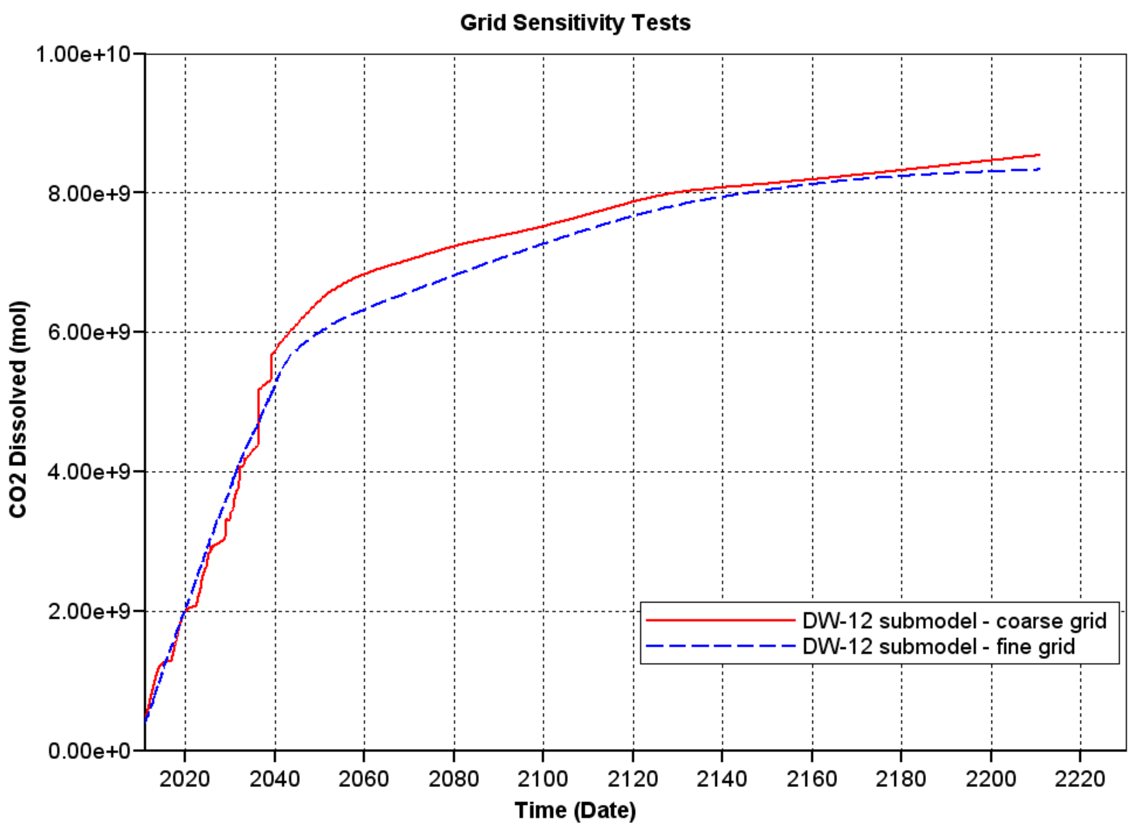

Fig. 5.12 —Effect of grid size on CO_2 solubility in brine – base case.

When diffusion is included in the models, the use of fine grids enhances the effect of diffusion. Fig. 5.13 shows an increase in the rate of dissolved CO_2 when fine grids are used.

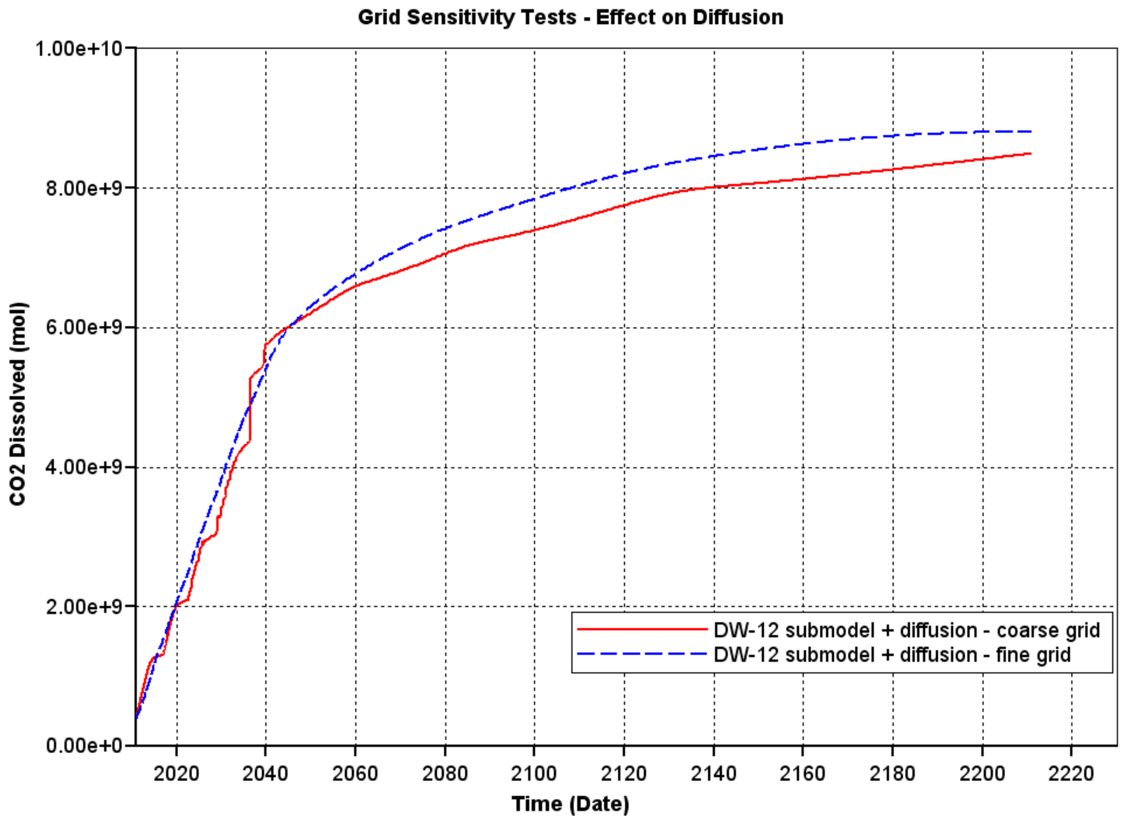

Fig. 5.13 —Effect of grid size on CO_2 solubility in brine – with diffusion.

In the case where finer grids were used, the CO_2 dissolved in brine increased by 3.6%. Selection of the right grid size is very important for accurate modeling of CO_2 sequestration. However, the use of fine grids is computationally expensive. The simulation run time increased by factor of 92 when finer grids are used in the sub-model. Local grid refinement is a useful technique for increasing the numerical accuracy of the simulations without refining the entire grid, which would take more simulation time. This feature is available in GEM, and is described in the next section.

5.7 Including Local Grid Refinement in the Aquifer Modeling

Based on the results of Section 5.6, local grid refinement (LGR) was used in the Aruma model (Fig. 5.14). Grid refinement was done around the wellbore, in the region where CO_2 was expected to migrate, based upon the results presented in Section 5.4. Approximately 5000 acres around the wellbore were refined. The grid size along all three dimensions was reduced by a factor of three for the bottom five layers representing the Aruma aquifer. The grid size in the top two layers was reduced by a factor of three only along the *x*- and *y*-directions.

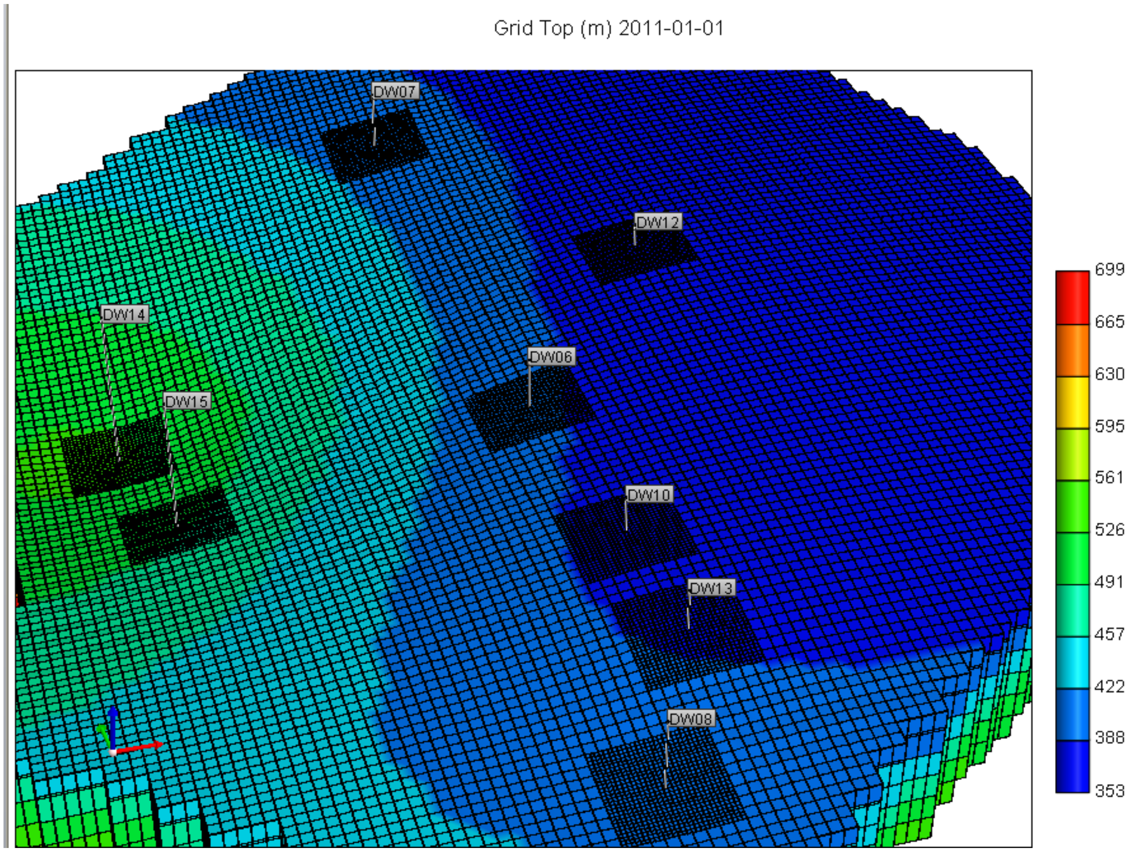

Fig. 5.14 —Including local grid refinement to the Aruma aquifer model.

Fig. 5.15 shows the global mole composition of CO_2 in the overlying UER formation (layer 1). The use of LGR shows that CO_2 breakthrough occurs in the UER at the end of the simulation run. This was not observed when coarser grids were used.

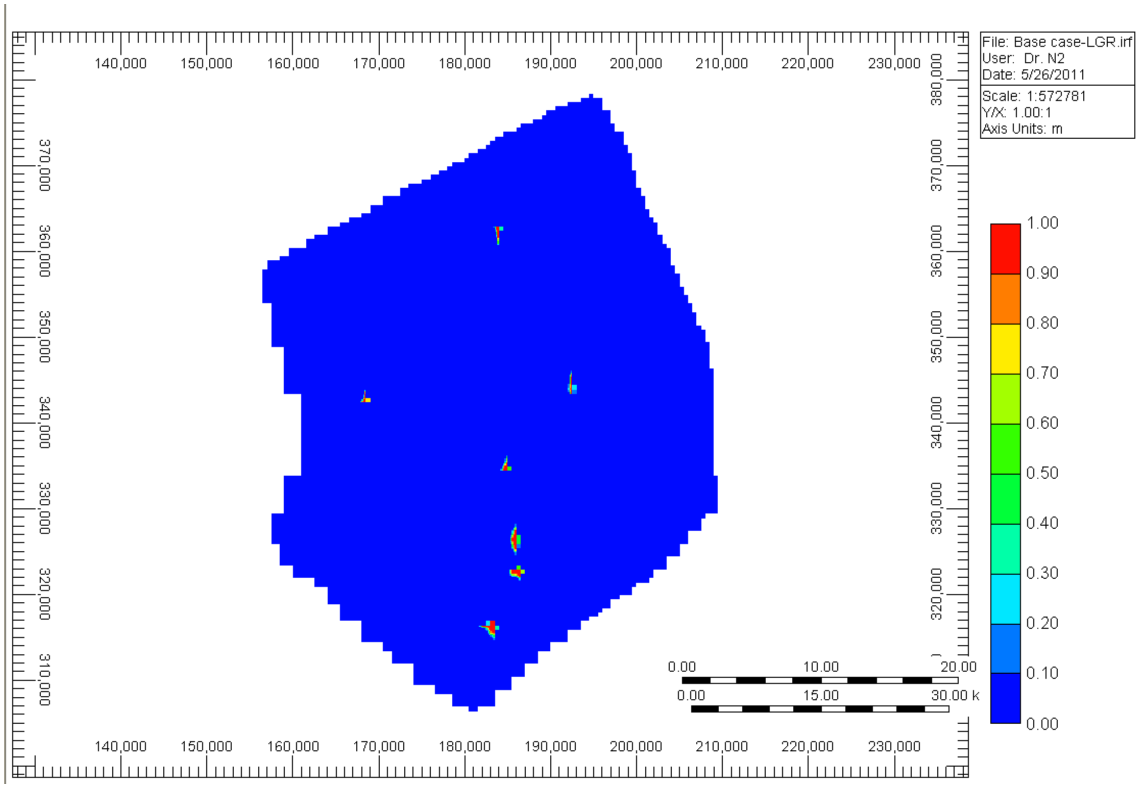

Fig. 5.15 —The CO_2 global mole fraction in the overlying formation at the end of the simulation. There is CO_2leakage into the UER after 200 years when local grid refinement is used.

Fig. 5.16 shows the movement of CO_2 around the well DW-12 after 200 years. Greater vertical movement of CO_2 is observed in this case. The profile of the plume is very different of that which is seen when course grids are used throughout the aquifer.

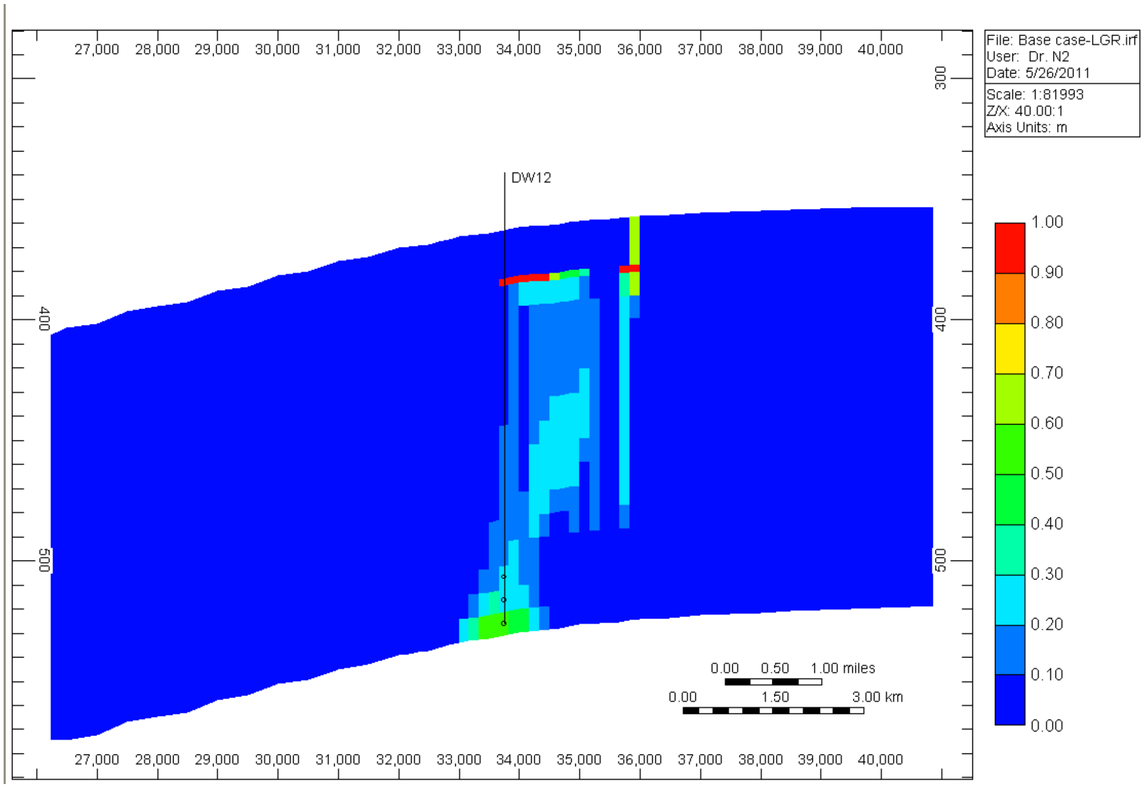

Fig. 5.16 —Cross-section of DW-12 showing the CO_2 global mole fraction after 200 years. Vertical movement of CO_2 is observed.

As seen in the previous section, when diffusion is not included, the model without LGR overestimates the amount of CO_2 dissolved (Fig. 5.17). When diffusion is included, the model without LGR underestimates the amount of CO_2 dissolved (Fig. 5.18).

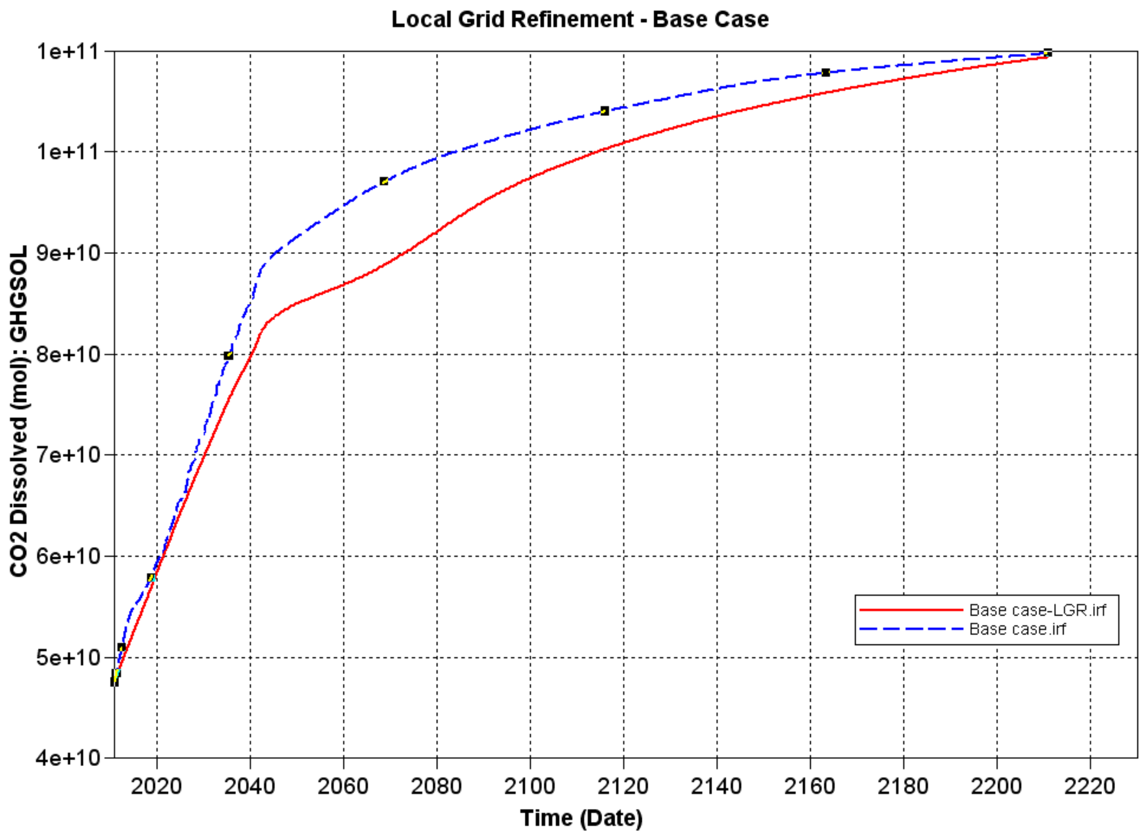

Fig. 5.17—Comparison of the CO_2 dissolved with local grid refinement – without diffusion.

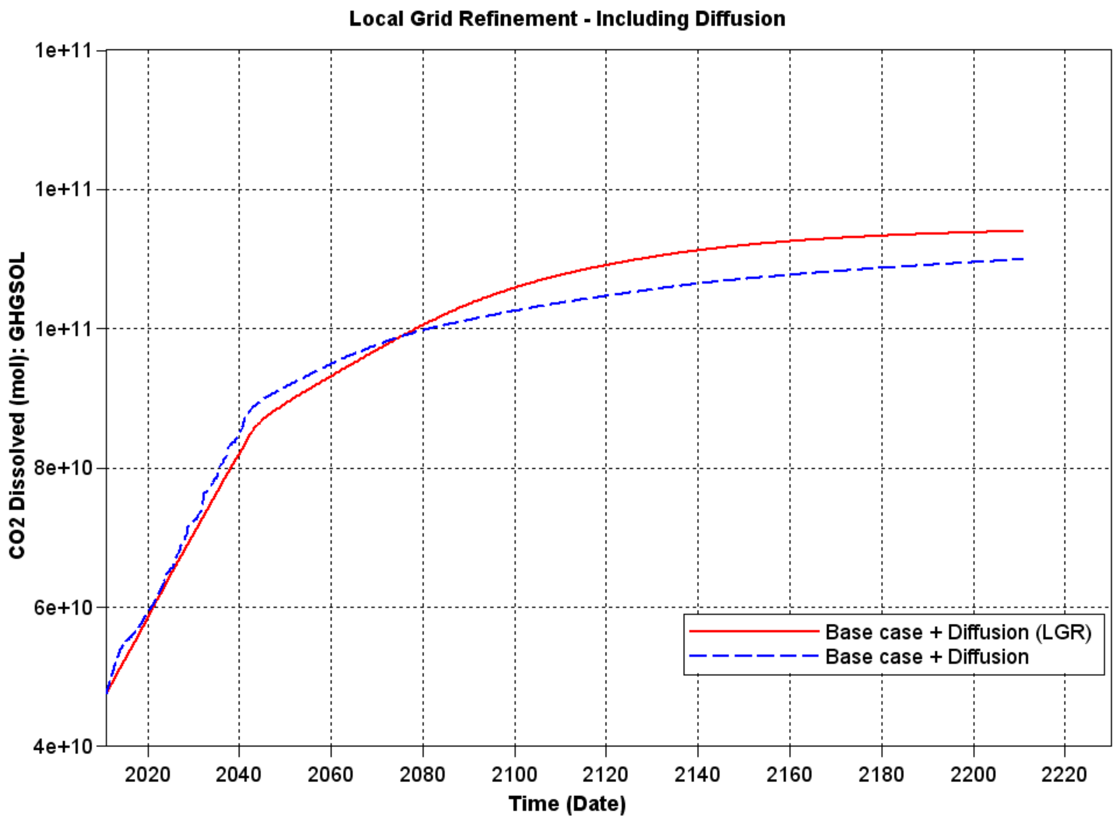

Fig. 5.18 —Comparison of the CO_2 dissolved with local grid refinement – with diffusion.

5.8 Section Summary

A simulation model is prepared for the Aruma aquifer using the available log data and flow test data. The existing deep wells were converted to CO_2 injectors. CO_2 was injected at a constant rate for a period of 30 years. The inclusion of diffusion enhances the rate of CO_2 dissolution in brine. The grid size affects the movement of the CO_2 plume and the propagation of vertical fingers (caused by the density instability).

4. CONCLUSIONS AND RECOMMENDATIONS

6.1 Conclusions

To address the issue of including abnormal density effects arising from CO_2 solubility in crude oils, a simple approach to model the increase in oil density with CO_2 dissolution using the Peng-Robinson EOS and the Pedersen viscosity correlation is presented. By changing the volume shift parameter of CO_2, the increase in oil density with CO_2 dissolution can be modeled while preserving the viscosity match. The Peng-Robinson EOS can predict the density of pure CO_2 by adjusting the CO_2 volume shift parameter. The use of the existing correlations for predicting the volume shift parameters do not perform well for CO_2 injection at high pressures. Due to 1D nature of flow in slim tube experiments, the density effect is not taken into account. In 2D and 3D, when injected CO_2 is lighter than the oil phase, there may be no gravity stable displacement due to increase in oil density from solubility. CO_2 injection when the density of the injected gas is less than the oil density may result in unstable gravity drainage.

Past literature has neglected density effects the study and evaluation of CO_2 injection in the crest. Density measurements for CO_2/oil mixtures at different CO_2 compositions and prediction of these results in the fluid model can significantly increase the reliability of the simulation results and decrease the degree of uncertainty. Heterogeneity may also have a significant effect as expected. The depth of injection and production wells with respect to the top of the reservoir may also have a large impact on recovery.

Saline aquifers hold a lot of potential for sequestering CO_2. The important transport processes and trapping mechanisms are identified and discussed. A simulation model is prepared for the Aruma aquifer using the available log data and flow test data. The existing deep wells were converted to CO_2 injectors. CO_2 was injected at a constant rate for a period of 30 years. There was no leakage of CO_2 through the seal using the proposed injection scheme. The inclusion of diffusion increased the amount of CO_2 dissolved in brine.

6.2 Recommendations

The acquisition of more experimental data that captures the density effect would greatly help in modeling this phenomenon. The creation of a database with experimental data would be the next step. Though Lansangan and Smith (1993) proposed a theory that increase in density might be caused by strong intermolecular Coulombic interactions between CO_2 and hydrocarbon molecules, this would need to be verified at a molecular level. There is a lot we still need to understand about these complex fluid systems.

The Aruma aquifer in Qatar, though being a shallow saline aquifer, has been shown to have potential in CO_2 sequestration. A seismic study should be conducted to obtain a more detailed structure of the aquifer. This would also help in the prediction of the CO_2 migration flow paths. There is also a possibility that discovery of extensive faults could greatly increase the leakage risk of this project. More data needs to be collected to make a thorough and informed decision. The diffusion coefficients and rock capillary pressure data should be determined experimentally. Including geochemistry in the aquifer model and its effect on CO_2 injectivity would be the next step.

REFERENCES

Anchliya, A. 2009. Aquifer Management for CO_2 Sequestration. MS thesis, Texas A&M University, College Station, Texas.

Ashcroft, S.J. and Ben-Isa, M. 1997. Effect of Dissolved Gases on the Densities of Hydrocarbons. *J. Chem. & Eng. Data* **42** (6): 1244-1248.

Al-Baida Technical Services. 2004. *Drilling of Four Deep Wells (Aruma Formation) Project South West Qatar*. Doha: Department of Agriculture and Water Research.

Bangia, V.K., Yau, F.F., and Hendricks, G.R. 1993. Reservoir Performance of a Gravity-Stable, Vertical CO_2 Miscible Flood: Wolfcamp Reef Reservoir, Wellman Unit. *SPE Res Eng* **8** (4): 261-269. doi: 10.2118/22898-PA.

Barrufet, M.A., Bacquet, A., and Falcone, G. 2010. Analysis of the Storage Capacity for CO_2 Sequestration of a Depleted Gas Condensate Reservoir and a Saline Aquifer. *J Can Pet Technol* **49** (8) : 23-31. doi: 10.2118/139771-PA.

Beecy, D.J. and Kuuskraa, V.A. 2001. Status of U.S. Geologic Carbon Sequestration Research and Technology. *Envir Geosci* **8** (3): 152-159.

Bennion, B. and Bachu, S. 2008. Drainage and Imbibition Relative Permeability Relationships for Supercritical CO_2/Brine and H_2S/Brine Systems in Intergranular Sandstone, Carbonate, Shale, and Anhydrite Rocks. *SPE Res Eval & Eng* **11** (3): 487-496. doi: 10.2118/99326-PA.

Bielinski, A., Kopp, A., Schütt, H. et al. 2008. Monitoring of CO_2 Plumes During Storage in Geological Formations Using Temperature Signals: Numerical Investigation. *Int J Green Gas Con* **2** (3): 319-328.

Brooks, R.H. and Corey, A.T. 1966. Properties of Porous Media Affecting Fluid Flow. *Journal of the Irrigation and Drainage Division, Proc., ASCE* **92** (2): 61-88

Bryant, S.L., Lakshminarasimhan, S., and Pope, G.A. 2008. Buoyancy-Dominated Multiphase Flow and its Effect on Geological Sequestration of CO_2. *SPE J.* **13** (4): 447-454. doi: 10.2118/99938-PA.

Burton, M. and Bryant, S.L. 2009. Eliminating Buoyant Migration of Sequestered CO_2 through Surface Dissolution: Implementation Costs and Technical Challenges. *SPE Res Eval & Eng* **12** (3): 399-407. doi: 10.2118/110650-PA.

Burton, M., Kumar, N., and Bryant, S.L. 2008. Time-Dependent Injectivity During CO_2 Storage in Aquifers. Paper SPE 113937 presented at the SPE/DOE Symposium on Improved Oil Recovery, Tulsa, Oklahoma, USA, 19–23 April 2008. doi: 10.2118/113937-MS.

Cardenas, R.L., Alston, R.B., Nute, A.J. et al. 1984. Laboratory Design of a Gravity-Stable Miscible CO_2 Process. *J Pet Technol* **36** (1): 111-118. doi: 10.2118/10270-PA.

DeRuiter, R.A., Nash, L.J., and Singletary, M.S. 1994. Solubility and Displacement Behavior of a Viscous Crude with CO_2 and Hydrocarbon Gases. *SPE Res Eng* **9** (2): 101-106. doi: 10.2118/20523-PA.

Duan, Z., Møller, N., and Weare, J.H. 1992. An Equation of State for the CH_4- CO_2-H_2O System: I. Pure Systems from 0 to 1000°C and 0 to 8000 Bar. *Geochimica et Cosmochimica Acta* **56** (7): 2605-2617.

Duan, Z. and Sun, R. 2003. An Improved Model Calculating CO_2 Solubility in Pure Water and Aqueous Nacl Solutions from 273 to 533 K and from 0 to 2000 Bar. *Chem. Geol.* **193** (3-4): 257-271.

Eaton, B.A. 1969. Fracture Gradient Prediction and Its Application in Oilfield Operations. *J Pet Technol* **21** (10): 1353-1360. doi: 10.2118/2163-PA.

Economides, M.J. and Ehlig-Economides, C. 2009. Sequestering Carbon Dioxide in a Closed Underground Volume. Paper SPE 124430 presented at the SPE Annual Technical Conference and Exhibition, New Orleans, Louisiana, USA, 4–7 October. doi: 10.2118/124430-MS.

Ennis-King, J.P. and Paterson, L. 2005. Role of Convective Mixing in the Long-Term Storage of Carbon Dioxide in Deep Saline Formations. *SPE J.* **10** (3): 349-356. doi: 10.2118/84344-PA.

Farajzadeh, R. 2008. Enhanced Transport Phenomena in CO_2 Sequestration and CO_2 EOR. PhD dissertation, Delft U. of Tech., The Netherlands.

Firoozabadi, A. and Cheng, P. 2010. Prospects for Subsurface CO_2 Sequestration. *AIChE J.* **56** (6): 1398-1405.

Frank, M.J.W., Kuipers, J.A.M., and van Swaaij, W.P.M. 1996. Diffusion Coefficients and Viscosities of $CO_2 + H_2O$, $CO_2 + CH_3OH$, $NH_3 + H_2O$, and $NH_3 + CH_3OH$ Liquid Mixtures. *J. Chem. & Eng. Data* **41** (2): 297-302.

Gale, J., Christensen, N.P., Cutler, A. et al. 2001. Demonstrating the Potential for Geological Storage of CO_2: The Sleipner and Gestco Projects. *Environmental Geoscience.* **8** (3): 160-165.

Garcia, J. 2001. *Density of Aqueous Solutions of CO_2*. Berkley, California: Lawrence Berkley National Laboratory.

Grigg, R.B. 1995. Dynamic Phase Composition, Density, and Viscosity Measurements During CO_2 Displacement of Reservoir Oil. Paper SPE 28974 presented at the SPE International Symposium on Oilfield Chemistry, San Antonio, Texas, USA, 14–17 February. doi: 10.2118/28974-MS.

Han, W.S. and McPherson, B.J. 2009. Optimizing Geologic CO_2 Sequestration by Injection in Deep Saline Formations Below Oil Reservoirs. *Energy Conversion and Management* **50** (10): 2570-2582.

Harvey, A.H. 1996. Semiempirical Correlation for Henry's Constants over Large Temperature Ranges. *AIChE J.* **42** (5): 1491-1494.

Holt, T., Jensen, J.I., and Lindeberg, E. 1995. Underground Storage of CO_2 in Aquifers and Oil Reservoirs. *Energy Conversion and Management* **36** (6-9): 535-538.

Hoteit, H. and Firoozabadi, A. 2009. Numerical Modeling of Diffusion in Fractured Media for Gas-Injection and -Recycling Schemes. *SPE J.* **14** (2). 323-337. doi: 10.2118/103292-PA.

House, N.J., Faulder, D.D., Olson, G.L. et al. 2003. Simulation Study of CO_2 Sequestration in a North Sea Formation. Paper SPE 81202 presented at the SPE/EPA/DOE Exploration and Production Environmental Conference, San Antonio, Texas, USA, 10–12 March. doi: 10.2118/81202-MS.

IPCC. 2008. Contribution of Working Group III to the Fourth Assessment Report of the Intergovernmental Panel on Climate Change, Metz, B., Davidson, O.R., Bosch, P.R., Dave R., Meyer, L.A., editors. Cambrige University Press: New York.

Jhaveri, B.S. and Youngren, G.K. 1988. Three-Parameter Modification of the Peng-Robinson Equation of State to Improve Volumetric Predictions. *SPE Res Eng* **3** (3): 1033-1040. doi: 10.2118/13118-PA.

Johnston, J.R. 1988. Weeks Island Gravity Stable CO_2 Pilot. Paper SPE 17351 presented at the SPE Enhanced Oil Recovery Symposium, Tulsa, Oklahoma, USA, 17–20 April. doi: 10.2118/17351-MS.

Kumar, A. 2004. A Simulation Study of Carbon Sequestration in Deep Saline Aquifers. MS thesis, University of Texas, Austin, Texas.

Kumar, A., Noh, M.H., Ozah, R.C. et al. 2005. Reservoir Simulation of CO_2 Storage in Aquifers. *SPE J.* **10** (3). 336-348. doi: 10.2118/89343-PA.

Lansangan, R.M. and Smith, J.L. 1993a. Viscosity, Density, and Composition Measurements of CO_2/West Texas Oil Systems. *SPE Res Eng* **8** (3). 175-182. doi: 10.2118/21017-PA.

Lansangan, R.M. and Smith, J.L. 1993b. *Supplement to SPE 21017, Viscosity, Density, and Composition Measurements of Certain CO_2 /West Texas Oil Systems*. doi: 10.2118/26300-MS.

Leahy-Dios, A. and Firoozabadi, A. 2007. Unified Model for Nonideal Multicomponent Molecular Diffusion Coefficients. *AIChE J.* **53** (11): 2932-2939.

Moortgat, J. and Firoozabadi, A. 2010. Higher-Order Compositional Modeling with Fickian Diffusion in Unstructured and Anisotropic Media. *Advances in Water Resources* **33** (9): 951-968.

Moortgat, J., Li, Z., and Firoozabadi, A. 2011. Three-Phase Compositional Modeling of CO_2 Injection by Higher-Order Finite Element Methods with CPA Equation of State. Paper SPE 141907 presented at the SPE Reservoir Simulation Symposium, The Woodlands, Texas, USA, 21–23 February. doi: 10.2118/141907-MS.

Nghiem, L., Sammon, P., Grabenstetter, J. et al. 2004. Modeling CO_2 Storage in Aquifers with a Fully-Coupled Geochemical EOS Compositional Simulator. Paper SPE 89474 presented at the SPE/DOE Symposium on Improved Oil Recovery, Tulsa, Oklahoma, USA, 17–21 April. doi: 10.2118/89474-MS.

Orr, F.M.J., Kovscek, A., Jessen, K. et al. 2005. CO_2 Sequestration in Oil/Gas Reservoirs, Saline Aquifers and Coal Beds. *Energy Research at Stanford 2005-2006*.

Palmer, F.S., Nute, A.J., and Peterson, R.L. 1984. Implementation of a Gravity-Stable Miscible CO_2 Flood in the 8000 Foot Sand, Bay St. Elaine Field. *J Pet Technol* **36** (1): 101-110. doi: 10.2118/10160-PA.

Pedersen, K.S., Fredenslund, A., Christensen, P. and Thomassen P. 1984. Viscosity of crude oils. *Chem. Eng. Sci.* **39** (6): 1011–1016.

Pedersen, K.S. and Fredenslund, A. 1987. An improved corresponding states model for the prediction of oil and gas viscosities and thermal conductivities. *Chem. Eng. Sci.* **42** (1): 182–186.

Peng, D.Y. and Robinson, D.B. 1976. A New Two-Constant Equation of State. *American Chemical Society*: 46-51.

Perry, G.E. 1982. Weeks Island "S" Sand Reservoir B Gravity Stable Miscible CO_2 Displacement, Iberia Parish, Louisiana. Paper SPE 10695 presented at the SPE Enhanced Oil Recovery Symposium, Tulsa, Oklahoma, USA, 4–7 April. doi: 10.2118/10695-MS.

Pitzer, K.S. 1973. Thermodynamics of Electrolytes. I. Theoretical Basis and General Equations. *Journal of Physical Chemistry* **77** (2): 268-277.

Pruess, K., Xu, T., Apps, J. et al. 2003. Numerical Modeling of Aquifer Disposal of CO_2. *SPE J.* **8** (1): 49-60. doi: 10.2118/83695-PA.

Renner, T.A. 1988. Measurement and Correlation of Diffusion Coefficients for CO_2 and Rich-Gas Applications. *SPE Res Eng* **3** (2): 517-523. doi: 10.2118/15391-PA.

Sigmund, P.M. 1976. Prediction of Molecular Diffusion at Reservoir Conditions. Part 1-Measurement and Prediction of Binary Dense Gas Diffusion Coefficients. *J Can Pet Technol* **15** (2): 48-57.

Span, R. and Wagner, W. 1996. A New Equation of State for Carbon Dioxide Covering the Fluid Region from the Triple-Point Temperature to 1100 K at Pressures up to 800 Mpa. *J. Phy. & Chem. Ref. Data* **25** (6): 1509-1596.

Sweatman, R.E., Parker, M.E., and Crookshank, S.L. 2009. Industry Experience with CO_2-Enhanced Oil Recovery Technology. Paper SPE 126446 presented at the SPE International Conference on CO_2 Capture, Storage, and Utilization, San Diego, California, USA, 2–4 November. doi:10.2118/126446-MS.

Tabasinejad, F., Barzin, Y., Moore, R.G. et al. 2010. Water/ CO_2 System at High Pressure and Temperature Conditions: Measurement and Modeling of Density in Equilibrium Liquid and Vapor Phases. Paper SPE 131636 presented at the SPE EUROPEC/EAGE Annual Conference and Exhibition, Barcelona, Spain, 14–17 June. doi: 10.2118/131636-MS.

Tamimi, A., Rinker, E.B., and Sandall, O.C. 1994. Diffusion Coefficients for Hydrogen Sulfide, Carbon Dioxide, and Nitrous Oxide in Water over the Temperature Range 293-368 K. *J Chem. & Eng. Data* **39** (2): 330-332.

Tiamiyu, O.M., Nygaard, R., and Bai, B. 2010. Effect of Aquifer Heterogeneity, Brine Withdrawal, and Well-Completion Strategy on CO_2 Injectivity in Shallow Saline Aquifer. Paper SPE 139583 presented at the SPE International Conference on CO_2 Capture, Storage, and Utilization, New Orleans, Louisiana, USA, 12–12 November. doi: 10.2118/139583-MS.

Ukaegbu, C., Gundogan, O., Mackay, E. et al. 2009. Simulation of CO_2 Storage in a Heterogeneous Aquifer. *Proc. Institution of Mechanical Engineers, Part A: Journal of Power and Energy* **223** (3): 249-267.

van der Meer, L.G.H. 1992. Investigations Regarding the Storage of Carbon Dioxide in Aquifers in the Netherlands. *Energy Conversion and Management* **33** (5-8): 611-618.

Whitson, C.H. and Kuntadi, A. 2005. Khuff Gas Condensate Development. Paper SPE 10692 presented at the International Petroleum Technology Conference, Doha, Qatar, 21–23 November. doi: 10.2118/10692-MS.

Wilke, C.R. and Chang, P. 1955. Correlation of Diffusion Coefficients in Dilute Solutions. *AIChE J.* **1** (2): 264-270.

Yellig, W.F. and Metcalfe, R.S. 1980. Determination and Prediction of CO_2 Minimum Miscibility Pressures. *J Pet Technol.* **32** (1): 160-168. doi: 10.2118/7477-PA.

APPENDIX A

EXAMPLE CO_2/OIL DATA FILE

Following in the GEM input file used for simulating the CO_2 injection from the bottom of a 2D domain that has a homogenous permeability of 100 mD.

```
RESULTS SIMULATOR GEM 200800

DIM MDV 57600
DIM MDLU 2684304
DIM MDALP 5448984
DIM MDDD 691200



INUNIT FIELD
WSRF WELL 1
WSRF GRID TIME
OUTSRF GRID DENG DENO K 'C1' K 'CO2' KRG KRO PRES SG SO SW
TSO
            X 'C1' X 'CO2' Y 'C1' Y 'CO2' Z 'C1' Z 'CO2'
OUTSRF RES NONE
OUTSRF WELL ZWEL 'CO2' 'Well-2'
WPRN GRID 0
OUTPRN GRID NONE
OUTPRN RES NONE
**$  Distance units: ft
RESULTS XOFFSET           0.0000
RESULTS YOFFSET           0.0000
RESULTS ROTATION           0.0000  **$  (DEGREES)
RESULTS AXES-DIRECTIONS 1.0 -1.0 1.0


**-------------------- RESERVOIR DATA ---------------------

GRID VARI 240 1 40
```

```
KDIR DOWN
DI IVAR  240*5
DJ JVAR  16.4042
DK ALL  9600*5
DTOP  240*1000
**$ Property: NULL Blocks  Max: 1  Min: 1
**$  0 = null block, 1 = active block
NULL CON           1
**$ Property: Porosity  Max: 0.2235  Min: 0.2235
POR CON       0.2235
**$ Property: Permeability I (md)   Max: 100  Min: 100
PERMI CON         100
PERMJ EQUALSI
PERMK EQUALSI
**$ Property: Pinchout Array  Max: 1  Min: 1
**$  0 = pinched block, 1 = active block
PINCHOUTARRAY CON           1
CPOR 3e-5


**---------------- FLUID COMPONENT DATA ------------------

MODEL PR
NC 10 10
COMPNAME 'CO2' 'C1' 'C2' 'C3' 'NC4' 'NC5' 'FC6' 'C7+'
'C13+' 'C22+'
HCFLAG
0 0 0 0 0 0 0 0 0 0
VISCOR MODPEDERSEN
VISCOEFF 1.3040000E-04 2.3030000E+00 7.3780000E-03
1.8470000E+00 5.1730000E-01
MW
4.4010000E+01 1.6043000E+01 3.0070000E+01 4.4097000E+01
5.8124000E+01 7.2151000E+01 8.6000000E+01 1.2619000E+02
2.1864000E+02 4.4238000E+02
AC
0.225 0.008 0.098 0.152 0.193 0.251 0.27504 0.34615 0.46364
0.80496
PCRIT
7.2800002E+01 4.5400051E+01 4.8200051E+01 4.1900026E+01
3.7500026E+01 3.3299977E+01 3.2460006E+01 2.0830990E+01
1.4803850E+01 9.5238099E+00
VCRIT
```

```
9.4000000E-02 9.9000000E-02 1.4800000E-01 2.0300000E-01
2.5500000E-01 3.0400000E-01 3.4400000E-01 4.6250000E-01
8.1500000E-01 1.8580000E+00
TCRIT
3.0420000E+02 1.9060000E+02 3.0540000E+02 3.6980000E+02
4.2520000E+02 4.6960000E+02 5.0750000E+02 5.6964311E+02
7.9025476E+02 1.0754300E+03
PCHOR
78 77 108 150.3 189.9 231.5 250.1 361.2 589.6 986.9
SG
0.818 0.3 0.356 0.507 0.584 0.631 0.69 0.71224 0.78276
0.84911
TB
-109.21 -258.61 -127.57 -43.69 31.19 96.89 146.93 239.189
480.328 921.603
OMEGA
0.457236 0.457236 0.457236 0.457236 0.457236 0.457236
0.457236 0.457236 0.457236 0.457236
OMEGB
0.0777961 0.0777961 0.0777961 0.0777961 0.0777961 0.0777961
0.0777961 0.0777961 0.0777961 0.0777961
VSHIFT
-0.0943467 -0.153861 -0.102103 -0.0733009 -0.0570559 -
0.0344627 -0.004992 0.1 0.19 0.47
BIN
1.0000000E-01
1.0000000E-01 2.6890022E-03
1.0000000E-01 8.5370405E-03 1.6620489E-03
1.0000000E-01 1.4748531E-02 4.9143360E-03 8.6625350E-04
1.0000000E-01 2.0640839E-02 8.5779330E-03 2.7121325E-03
5.1467786E-04
1.0000000E-01 2.5345101E-02 1.1747825E-02 4.6198099E-03
1.4920539E-03 2.5462307E-04
1.0000000E-01 3.8419394E-02 2.1279999E-02 1.1202389E-02
5.8809841E-03 2.9279823E-03 1.4586581E-03
1.0000000E-01 7.0018325E-02 4.6738564E-02 3.1412902E-02
2.2113722E-02 1.6006595E-02 1.2281260E-02 5.3273178E-03
8.0000000E-02 1.2883664E-01 9.8473647E-02 7.6801306E-02
6.2529225E-02 5.2384492E-02 4.5721369E-02 3.1440562E-02
1.1219313E-02

TRES 116

**-------------------- ROCK FLUID ------------------------
```

```
ROCKFLUID
RPT 1
SWT
**$        Sw          krw        krow
            0            0         0.7
      0.04375   0.00390625    0.615234
       0.0875     0.015625    0.535937
      0.13125    0.0351562    0.462109
        0.175       0.0625     0.39375
      0.21875    0.0976563    0.330859
       0.2625     0.140625    0.273438
      0.30625     0.191406    0.221484
         0.35         0.25       0.175
      0.39375     0.316406    0.133984
       0.4375     0.390625   0.0984375
      0.48125     0.472656   0.0683594
        0.525       0.5625     0.04375
      0.56875     0.660156   0.0246094
       0.6125     0.765625   0.0109375
      0.65625     0.878906  0.00273437
          0.7            1           0
SLT
**$        Sl          krg        krog
          0.3            1           0
      0.34375     0.878906  0.00273437
       0.3875     0.765625   0.0109375
      0.43125     0.660156   0.0246094
        0.475       0.5625     0.04375
      0.51875     0.472656   0.0683594
       0.5625     0.390625   0.0984375
      0.60625     0.316406    0.133984
         0.65         0.25       0.175
      0.69375     0.191406    0.221484
       0.7375     0.140625    0.273438
      0.78125    0.0976563    0.330859
        0.825       0.0625     0.39375
      0.86875    0.0351562    0.462109
       0.9125     0.015625    0.535937
      0.95625   0.00390625    0.615234
            1            0         0.7

**----------------- INITIAL CONDITION ---------------------

INITIAL
```

```
USER_INPUT
**$ Property: Pressure (psi)   Max: 1700  Min: 1700
PRES CON         1700
**$ Property: Water Saturation  Max: 0  Min: 0
SW CON            0
**$ Property: Global Composition(NC5)  Max: 0.0386  Min:
0.0386
ZGLOBALC 'NC5' CON       0.0386
**$ Property: Global Composition(C1)  Max: 0.2228  Min:
0.2228
ZGLOBALC 'C1' CON       0.2228
**$ Property: Global Composition(CO2)  Max: 0.022  Min:
0.022
ZGLOBALC 'CO2' CON        0.022
**$ Property: Global Composition(C2)  Max: 0.1285  Min:
0.1285
ZGLOBALC 'C2' CON       0.1285
**$ Property: Global Composition(C3)  Max: 0.1235  Min:
0.1235
ZGLOBALC 'C3' CON       0.1235
**$ Property: Global Composition(NC4)  Max: 0.0819  Min:
0.0819
ZGLOBALC 'NC4' CON       0.0819
**$ Property: Global Composition(FC6)  Max: 0.0379  Min:
0.0379
ZGLOBALC 'FC6' CON       0.0379
**$ Property: Global Composition(C13+)  Max: 0.10851  Min:
0.10851
ZGLOBALC 'C13+' CON      0.10851
**$ Property: Global Composition(C7+)  Max: 0.13008  Min:
0.13008
ZGLOBALC 'C7+' CON      0.13008
**$ Property: Global Composition(C22+)  Max: 0.10621  Min:
0.10621
ZGLOBALC 'C22+' CON      0.10621

**-----------------------  NUMERICAL ---------------------

NUMERICAL
*NORM *PRESS  500.0
*NORM *SATUR    0.1    ** expected changes in one time-step
*NORM *GMOLAR   0.1

*DTMIN 1.0E-3          ** timestep size
*PRECC 1.0D-04         ** set convergence tolerance
```

```
*ITERMAX 50
*NORTH 20

**---------------------- WELL DATA ---------------------

RUN
DATE 2009 1 20
**$
WELL  'Well-1'
INJECTOR 'Well-1'
INCOMP  SOLVENT  1.  0.  0.  0.  0.  0.  0.  0.  0.  0.
OPERATE  MAX  BHG  126.66  CONT
**$          rad  geofac  wfrac  skin
GEOMETRY  K  0.25  0.37  1.  0.
PERF  GEOA  'Well-1'
**$ UBA     ff  Status  Connection
    1 1 40  1.  OPEN    FLOW-FROM  'SURFACE'
**$
WELL  'Well-2'
PRODUCER 'Well-2'
OPERATE  MIN  BHP  1700.  CONT
**$          rad  geofac  wfrac  skin
GEOMETRY  K  0.25  0.37  1.  0.
PERF  GEOA  'Well-2'
**$ UBA      ff  Status  Connection
    240 1 1  1.  OPEN    FLOW-TO  'SURFACE'
**$ Property: Implicit flag  Max: 3  Min: 3
AIMSET CON           3
DATE 2009 4 20.00000
DATE 2009 7 20.00000
DATE 2009 10 20.00000
DATE 2010 1 20.00000
DATE 2010 4 20.00000
DATE 2010 7 20.00000
DATE 2010 10 20.00000
DATE 2011 1 20.00000
DATE 2011 4 20.00000
DATE 2011 7 20.00000
DATE 2011 10 20.00000
DATE 2012 1 20.00000
DATE 2012 4 20.00000
DATE 2012 7 20.00000
DATE 2012 10 20.00000
DATE 2013 1 20.00000
DATE 2013 4 20.00000
```

```
DATE 2013 7 20.00000
DATE 2013 10 20.00000
DATE 2014 1 20.00000
DATE 2014 4 20.00000
DATE 2014 7 20.00000
DATE 2014 10 20.00000
DATE 2015 1 20.00000
DATE 2015 4 20.00000
DATE 2015 7 20.00000
DATE 2015 10 20.00000
DATE 2016 1 20.00000
DATE 2016 4 20.00000
DATE 2016 7 20.00000
DATE 2016 10 20.00000
DATE 2017 1 20.00000
DATE 2017 4 20.00000
DATE 2017 7 20.00000
DATE 2017 10 20.00000
DATE 2018 1 20.00000
DATE 2018 4 20.00000
DATE 2018 7 20.00000
DATE 2018 10 20.00000
DATE 2019 1 20.00000
DATE 2019 4 20.00000
DATE 2019 7 20.00000
DATE 2019 10 20.00000
DATE 2020 1 20.00000
DATE 2020 4 20.00000
DATE 2020 7 20.00000
DATE 2020 10 20.00000
DATE 2021 1 20.00000
DATE 2021 4 20.00000
DATE 2021 7 20.00000
DATE 2021 10 20.00000
DATE 2022 1 20.00000
DATE 2022 4 20.00000
DATE 2022 7 20.00000
DATE 2022 10 20.00000
DATE 2023 1 20.00000
DATE 2023 4 20.00000
DATE 2023 7 20.00000
DATE 2023 10 20.00000
DATE 2024 1 20.00000
DATE 2024 4 20.00000
DATE 2024 7 20.00000
```

```
DATE 2024 10 20.00000
DATE 2025 1 20.00000
DATE 2025 4 20.00000
DATE 2025 7 20.00000
DATE 2025 10 20.00000
DATE 2026 1 20.00000
DATE 2026 4 20.00000
DATE 2026 7 20.00000
DATE 2026 10 20.00000
DATE 2027 1 20.00000
DATE 2027 4 20.00000
DATE 2027 7 20.00000
DATE 2027 10 20.00000
DATE 2028 1 20.00000
DATE 2028 4 20.00000
DATE 2028 7 20.00000
DATE 2028 10 20.00000
DATE 2029 1 20.00000
DATE 2029 4 20.00000
DATE 2029 7 20.00000
DATE 2029 10 20.00000
DATE 2030 1 20.00000
DATE 2030 4 20.00000
DATE 2030 7 20.00000
DATE 2030 10 20.00000
DATE 2031 1 20.00000
DATE 2031 4 20.00000
DATE 2031 7 20.00000
DATE 2031 10 20.00000
DATE 2032 1 20.00000
DATE 2032 4 20.00000
DATE 2032 7 20.00000
DATE 2032 10 20.00000
DATE 2033 1 20.00000
DATE 2033 4 20.00000
DATE 2033 7 20.00000
DATE 2033 10 20.00000
DATE 2034 1 20.00000
DATE 2034 4 20.00000
DATE 2034 7 20.00000
DATE 2034 10 20.00000
DATE 2035 1 20.00000
DATE 2035 4 20.00000
DATE 2035 7 20.00000
DATE 2035 10 20.00000
```

```
DATE 2036 1 20.00000
DATE 2036 4 20.00000
DATE 2036 7 20.00000
DATE 2036 10 20.00000
DATE 2037 1 20.00000
DATE 2037 4 20.00000
DATE 2037 7 20.00000
DATE 2037 10 20.00000
DATE 2038 1 20.00000
DATE 2038 4 20.00000
DATE 2038 7 20.00000
DATE 2038 10 20.00000
DATE 2039 1 20.00000
DATE 2039 4 20.00000
DATE 2039 7 20.00000
DATE 2039 10 20.00000
DATE 2040 1 20.00000
DATE 2040 4 20.00000
DATE 2040 7 20.00000
DATE 2040 10 20.00000
DATE 2041 1 20.00000
DATE 2041 4 20.00000
DATE 2041 7 20.00000
DATE 2041 10 20.00000
DATE 2042 1 20.00000
DATE 2042 4 20.00000
DATE 2042 7 20.00000
DATE 2042 10 20.00000
DATE 2043 1 20.00000
DATE 2043 4 20.00000
DATE 2043 7 20.00000
DATE 2043 10 20.00000
DATE 2044 1 20.00000
DATE 2044 4 20.00000
DATE 2044 7 20.00000
DATE 2044 10 20.00000
DATE 2045 1 20.00000
DATE 2045 4 20.00000
DATE 2045 7 20.00000
DATE 2045 10 20.00000
DATE 2046 1 20.00000
DATE 2046 4 20.00000
DATE 2046 7 20.00000
DATE 2046 10 20.00000
DATE 2047 1 20.00000
```

```
DATE 2047 4 20.00000
DATE 2047 7 20.00000
DATE 2047 10 20.00000
DATE 2048 1 20.00000
DATE 2048 4 20.00000
DATE 2048 7 20.00000
DATE 2048 10 20.00000
DATE 2049 1 20.00000
DATE 2049 4 20.00000
DATE 2049 7 20.00000
DATE 2049 10 20.00000
DATE 2050 1 20.00000
STOP

**--------------------  SIMULATION STOP  ------------------
```

APPENDIX B

BASE CASE CO_2 SEQUESTRATION DATA FILE

Following in the GEM input file used for simulating the CO_2 injection in the Aruma aquifer. This is a base case data file; diffusion and local grid refinement are not modeled here. The SI units are used in all the sequestration data files in this study. The depth, permeability, and porosity data are not a part of the main data file, and are included separately. The author may be contacted if those files are required.

```
RESULTS SIMULATOR GEM 200800


** This is a base case. Henry's Law is used to model
solubility
** Diffusion and Hysteresis are not modeled here.




INUNIT SI
WSRF WELL 1
WSRF GRID TIME
```

```
OUTSRF GRID SG SW PRES DENW DENG Z 'CO2' W 'CO2' Y 'H2O' W
'H2O'
OUTSRF WELL  PAVG GHGTHY GHGSCRIT GHGSOL GHGLIQ GHGGAS
OUTSRF RES NONE
WPRN GRID 0
OUTPRN GRID NONE
OUTPRN RES NONE
WRST 10000
INVENTORY-CO2
**$  Distance units: m
RESULTS XOFFSET      156547.0000
RESULTS YOFFSET      378337.0000
RESULTS ROTATION           0.0000  **$  (DEGREES)
RESULTS AXES-DIRECTIONS 1.0 -1.0 1.0


**--------------------- RESERVOIR DATA ---------------------


GRID CORNER 106 145 7
DI IVAR      500             500             500
500
             500             500             500
500             500
             500             500             500
500             500
             500             500             500
500             500
             500             500             500
500             500
             500             500             500
500             500
             500             500             500
500             500
             500             500             500
500             500
             500             500             500
500             500
             500             500             500
500             500
             500             500             500
500             500
             500             500             500
500             500
```

```
             500             500             500
500             500
             500             500             500
500             500
             500             500             500
500             500
             500             500             500
500             500
             500             500             500
500             500
             500             500             500
500             500
             500             500             500
500             500
             500             500             500
500             500
             500             500             500
500             500
             500             500
DJ JVAR      500             500             500
500
             500             500             500
500             500
             500             500             500
500             500
             500             500             500
500             500
             500             500             500
500             500
             500             500             500
500             500
             500             500             500
500             500
             500             500             500
500             500
             500             500             500
500             500
             500             500             500
500             500
             500             500             500
500             500
             500             500             500
500             500
             500             500             500
500             500
```

```
             500             500             500
500             500
             500             500             500
500             500
             500             500             500
500             500
             500             500             500
500             500
             500             500             500
500             500
             500             500             500
500             500
             500             500             500
500             500
             500             500             500
500             500
             500             500             500
500             500
             500             500             500
500             500
             500             500             500
500             500
             500             500             500
500             500
             500             500             500
500             500
             500             500             500
500             500
             500             500             500
500             500
             500             500             500
500             500
             500
ZCORN
 INCLUDE "ZCORN.IN"
**$ Property: NULL Blocks  Max: 1  Min: 1
**$  0 = null block, 1 = active block
NULL CON            1

*MOD

    1:1        41:41        1:7     = 0
   78:78        1:1         1:7     = 0
    1:32        1:24        1:7     = 0
   27:53        1:13        1:7     = 0
```

22:43	10:18	1:7	= 0
31:48	9:16	1:7	= 0
1:15	26:33	1:7	= 0
1:25	25:28	1:7	= 0
1:6	33:38	1:7	= 0
1:10	30:36	1:7	= 0
1:2	38:39	1:7	= 0
3:4	39:39	1:7	= 0
11:23	29:29	1:7	= 0
10:18	27:31	1:7	= 0
18:20	29:30	1:7	= 0
56:66	1:7	1:7	= 0
54:76	1:3	1:7	= 0
50:59	2:9	1:7	= 0
26:28	25:26	1:7	= 0
33:37	19:21	1:7	= 0
38:39	20:20	1:7	= 0
38:41	19:19	1:7	= 0
11:11	34:34	1:7	= 0
12:12	34:34	1:7	= 0
1:1	40:40	1:7	= 0
33:34	22:22	1:7	= 0
54:56	10:10	1:7	= 0
49:50	14:14	1:7	= 0
44:44	17:17	1:7	= 0
105:105	64:64	1:7	= 0
87:106	1:20	1:7	= 0
96:106	19:41	1:7	= 0
91:97	18:29	1:7	= 0
88:91	18:24	1:7	= 0
82:88	1:9	1:7	= 0
80:81	2:4	1:7	= 0
93:97	29:34	1:7	= 0
90:90	25:27	1:7	= 0
101:106	42:52	1:7	= 0
98:106	34:46	1:7	= 0
104:106	52:58	1:7	= 0
102:106	51:55	1:7	= 0
105:106	57:62	1:7	= 0
85:85	10:12	1:7	= 0
86:86	9:14	1:7	= 0
82:82	8:9	1:7	= 1
75:76	2:3	1:7	= 1
79:82	1:1	1:7	= 0
106:106	64:89	1:7	= 0

106:106	63:63	1:7	= 0
105:105	63:63	1:7	= 0
87:104	119:145	1:7	= 0
100:106	121:142	1:7	= 0
98:105	106:117	1:7	= 0
100:106	113:122	1:7	= 0
98:105	135:143	1:7	= 0
101:103	140:145	1:7	= 0
104:105	142:145	1:7	= 0
77:88	135:144	1:7	= 0
68:79	139:145	1:7	= 0
64:73	142:145	1:7	= 0
91:105	114:123	1:7	= 0
79:90	130:138	1:7	= 0
2:23	124:145	1:7	= 0
1:4	126:144	1:7	= 0
2:5	60:98	1:7	= 0
1:2	50:63	1:7	= 0
6:9	71:89	1:7	= 0
2:4	106:129	1:7	= 0
1:2	63:124	1:7	= 0
3:7	111:126	1:7	= 0
23:35	134:145	1:7	= 0
77:77	123:123	1:7	= 0
82:102	118:122	1:7	= 0
106:106	108:119	1:7	= 0
103:106	99:114	1:7	= 0
100:100	102:102	1:7	= 0
100:104	103:106	1:7	= 0
106:106	143:145	1:7	= 0
80:93	143:145	1:7	= 0
82:87	123:130	1:7	= 0
76:84	129:136	1:7	= 0
70:81	134:144	1:7	= 0
63:69	140:145	1:7	= 0
48:48	143:143	1:7	= 0
55:65	140:145	1:7	= 0
62:75	134:140	1:7	= 0
68:81	129:134	1:7	= 0
77:84	124:131	1:7	= 0
79:84	121:126	1:7	= 0
59:61	137:139	1:7	= 0
65:67	131:133	1:7	= 0
72:76	126:128	1:7	= 0
35:57	144:145	1:7	= 0

```
   75:76      124:126       1:7     = 0
   87:90      115:117       1:7     = 0
   92:97      109:113       1:7     = 0
   92:94      109:111       1:7     = 1
    5:15      114:125       1:7     = 1
    1:15      114:127       1:7     = 0
   18:28      129:133       1:7     = 0
   12:18      120:124       1:7     = 0
   34:40      139:145       1:7     = 0
   38:44      141:143       1:7     = 0
   28:30      131:133       1:7     = 0
   13:15      114:115       1:7     = 1
**$ Property: Porosity  Max: 0.268061  Min: 0.0574038
POR ALL
 INCLUDE "POR.IN"
**$ Property: Permeability I (md)   Max: 4177.73  Min: 0.01
PERMI ALL
 INCLUDE "PERMI.IN"
PERMJ EQUALSI
PERMK EQUALSI * 0.1
**$ Property: Pinchout Array  Max: 1  Min: 1
**$  0 = pinched block, 1 = active block
PINCHOUTARRAY CON           1
PRPOR 4130
CPOR 4.38e-07


**---------------- FLUID COMPONENT DATA ------------------


MODEL PR
NC 3 3
COMPNAME 'CO2' 'C1' 'H2O'
HCFLAG 0 0 0
VISCOR PEDERSEN
MIXVC 1
VISCOEFF 0.291 1.4 0.0005747 4.265 1.0579
MW 4.4010000E+01 1.6043000E+01 1.8015000E+01
AC 0.225 0.008 0.344
PCRIT 7.2800000E+01 4.5400000E+01 2.1760000E+02
VCRIT 9.4000000E-02 9.9000000E-02 5.6000000E-02
TCRIT 3.0420000E+02 1.9060000E+02 6.4730000E+02
PCHOR 78 77 52
SG 0.818 0.3 1
TB -78.45 -161.45 100
```

```
OMEGA 0.457236 0.457236 0.457236
OMEGB 0.0777961 0.0777961 0.0777961
VSHIFT 0 0 0
HEATING_VALUES 0 890773 0
VISVC 9.4000000E-02 9.9000000E-02 5.6000000E-02

BIN
1.0300000E-01
2.0000000E-01 4.9070000E-01

TRES 46.1111
PHASEID GAS
PSAT -1
DENW 1036.3
CW 4.45E-07
REFPW 5882
VISW 0.61
SOLUBILITY HENRY
DERIVATIVEMETHOD NUMERALL
H2O_INCLUDED
HENRY-CORR-CO2
TRACE-COMP 2
SATWCUTOFF 0.0
SWR-H2OVAP 0.0
OGW_FLASH ON
METHOD-OGW 1
NC-AQUEOUS 1
COMPNAME-AQUEOUS 'NaCl'
AQFILL OFF
SALINITY PPMVOL 5000
SALINITY-CALC OFF
AQUEOUS-DENSITY ROWE-CHOU
AQUEOUS-VISCOSITY KESTIN




**-------------------- ROCK FLUID -------------------------

ROCKFLUID
RPT 1
SWT
**$         Sw          krw         krow
```

```
        0.25           0    0.741513
       0.259  0.00100683    0.721249
       0.268  0.00180539    0.704854
       0.295   0.0038533    0.641721
       0.322   0.0079916    0.581367
       0.349   0.0128232    0.501012
       0.376   0.0193238    0.421985
     0.40092   0.0294565    0.363937
       0.421   0.0387603    0.319328
       0.448    0.051718    0.259998
       0.475    0.070279    0.207043
       0.502    0.093775    0.164473
       0.529     0.11933    0.123684
       0.556    0.149558   0.0883395
       0.583    0.186321   0.0615307
        0.61    0.227836    0.039882
     0.63416    0.266466   0.0212892
       0.655    0.306498  0.00995504
     0.67532     0.35208  0.00545978
         0.7    0.408888           0
     0.71648    0.448173           0
     0.74392    0.519642           0
     0.77136    0.607685           0
      0.7988    0.695778           0
     0.82624    0.777445           0
     0.85368    0.852026           0
     0.88112     0.92274           0
     0.90856     0.98431           0
       0.936           1           0
SLT
**$          Sl           krg          krog
        0.25            1              0
      0.2602     0.951272   0.000408816
      0.2704     0.902544   0.000817632
      0.2908     0.810565    0.00265018
      0.3112     0.723454    0.00542236
      0.3316     0.642796    0.00933594
       0.352     0.567034     0.0142417
      0.3724     0.497842     0.0204728
      0.3928     0.432889      0.027559
      0.4132     0.374559     0.0360611
      0.4336     0.319843     0.0454498
       0.454     0.271738     0.0560851
      0.4744     0.226656     0.0675863
      0.4948     0.188098     0.0805607
```

```
       0.5152     0.152006    0.0941881
       0.5356     0.122259     0.109483
        0.556    0.0944639     0.125456
       0.5764    0.0727291     0.142851
       0.5968    0.0524727     0.161062
       0.6172    0.0378599     0.180665
       0.6376    0.0242972      0.20085
        0.658     0.015786     0.222925
       0.6784   0.00794832     0.245442
       0.6988   0.00430131     0.269631
       0.7192   0.00101088     0.294517
       0.7396  0.000449725     0.320785
         0.76            0     0.347774
       0.7864            0      0.38488
       0.8162            0     0.428813
        0.846            0     0.474841
       0.8758            0     0.523413
       0.9056            0      0.57472
       0.9354            0     0.628123
       0.9652            0     0.683586
        0.995            0     0.741513


**----------------- INITIAL CONDITION ---------------------

INITIAL

VERTICAL DEPTH_AVE WATER_GAS

ZGAS
.001 .999 0.0

REFPRES
  4975

REFDEPTH
  500

DWGC
  250

SWOC
  0.995
```

```
GASZONE NOOIL

**--------------------- NUMERICAL ------------------------

NUMERICAL
DTMAX 1
DTMIN 0.001
NORM PRESS 3450
MAXCHANGE GMOLAR 0.5
MAXCHANGE SATUR 0.5
CONVERGE PRESS 3.55

**---------------------- WELL DATA -----------------------

RUN
DATE 2011 1 1
**$
WELL  'DW06'
INJECTOR 'DW06'
INCOMP  SOLVENT  1.  0.
OPERATE  MAX  STG  18406.  CONT
**$          rad  geofac  wfrac  skin
GEOMETRY  K  0.0762  0.37  1.  0.
PERF  GEOA  'DW06'
**$ UBA      ff  Status  Connection
    53 84 7  1.  OPEN    FLOW-FROM  'SURFACE'
**$
WELL  'DW07'
INJECTOR 'DW07'
INCOMP  SOLVENT  1.  0.
OPERATE  MAX  STG  18406.  CONT
**$          rad  geofac  wfrac  skin
GEOMETRY  K  0.0762  0.37  1.  0.
PERF  GEOA  'DW07'
**$ UBA      ff  Status  Connection
    51 36 7  1.  OPEN    FLOW-FROM  'SURFACE'
**$
WELL  'DW08'
INJECTOR 'DW08'
INCOMP  SOLVENT  1.  0.
OPERATE  MAX  STG  18406.  CONT
**$          rad  geofac  wfrac  skin
GEOMETRY  K  0.0762  0.37  1.  0.
PERF  GEOA  'DW08'
**$ UBA       ff  Status  Connection
```

```
    50 129 7  1.  OPEN    FLOW-FROM  'SURFACE'
**$
WELL  'DW10'
INJECTOR 'DW10'
INCOMP  SOLVENT  1.  0.
OPERATE  MAX  STG  18406.  CONT
**$          rad  geofac  wfrac  skin
GEOMETRY  K  0.0762  0.37  1.  0.
PERF  GEOA  'DW10'
**$ UBA       ff  Status  Connection
    55 104 7  1.  OPEN    FLOW-FROM  'SURFACE'
**$
WELL  'DW12'
INJECTOR 'DW12'
INCOMP  SOLVENT  1.  0.
OPERATE  MAX  STG  18406.  CONT
**$          rad  geofac  wfrac  skin
GEOMETRY  K  0.0762  0.37  1.  0.
PERF  GEOA  'DW12'
**$ UBA      ff  Status  Connection
    68 66 7  1.  OPEN    FLOW-FROM  'SURFACE'
**$
WELL  'DW13'
INJECTOR 'DW13'
INCOMP  SOLVENT  1.  0.
OPERATE  MAX  STG  18406.  CONT
**$          rad  geofac  wfrac  skin
GEOMETRY  K  0.0762  0.37  1.  0.
PERF  GEOA  'DW13'
**$ UBA       ff  Status  Connection
    56 116 7  1.  OPEN    FLOW-FROM  'SURFACE'
**$
WELL  'DW14'
INJECTOR 'DW14'
INCOMP  SOLVENT  1.  0.
OPERATE  MAX  STG  18406.  CONT
**$          rad  geofac  wfrac  skin
GEOMETRY  K  0.0762  0.37  1.  0.
PERF  GEOA  'DW14'
**$ UBA      ff  Status  Connection
    20 68 7  1.  OPEN    FLOW-FROM  'SURFACE'
**$
WELL  'DW15'
INJECTOR 'DW15'
INCOMP  SOLVENT  1.  0.
```

```
OPERATE  MAX  STG  18406.  CONT
**$          rad  geofac  wfrac  skin
GEOMETRY  K  0.0762  0.37  1.  0.
PERF  GEOA  'DW15'
**$ UBA      ff  Status  Connection
    23 82 7  1.  OPEN    FLOW-FROM  'SURFACE'
DATE 2011 5  1.00000
DATE 2011 9  1.00000
DTMAX 10
DATE 2012 1  1.00000
DATE 2012 5  1.00000
DATE 2012 9  1.00000
DATE 2013 1  1.00000
DATE 2013 5  1.00000
DATE 2013 9  1.00000
DATE 2014 1  1.00000
DATE 2014 5  1.00000
DTMAX 20
DATE 2014 9  1.00000
DATE 2015 1  1.00000
DATE 2015 5  1.00000
DATE 2015 9  1.00000
DATE 2016 1  1.00000
DTMAX 30
DATE 2016 5  1.00000
DATE 2016 9  1.00000
DATE 2017 1  1.00000
DATE 2017 5  1.00000
DATE 2017 9  1.00000
DATE 2018 1  1.00000
DATE 2018 5  1.00000
DATE 2018 9  1.00000
DATE 2019 1  1.00000
DATE 2019 5  1.00000
DATE 2019 9  1.00000
DATE 2020 1  1.00000
DATE 2020 5  1.00000
DATE 2020 9  1.00000
DTMAX 40
DATE 2021 1  1.00000
DATE 2021 5  1.00000
DATE 2021 9  1.00000
DATE 2022 1  1.00000
DATE 2022 5  1.00000
DATE 2022 9  1.00000
```

```
DATE 2023 1  1.00000
DATE 2023 5  1.00000
DATE 2023 9  1.00000
DATE 2024 1  1.00000
DATE 2024 5  1.00000
DTMAX 100
DATE 2024 9  1.00000
DATE 2025 1  1.00000
DATE 2025 5  1.00000
DATE 2025 9  1.00000
DATE 2026 1  1.00000
DATE 2026 5  1.00000
DATE 2026 9  1.00000
DATE 2027 1  1.00000
DATE 2027 5  1.00000
DATE 2027 9  1.00000
DATE 2028 1  1.00000
DATE 2028 5  1.00000
DATE 2028 9  1.00000
DATE 2029 1  1.00000
DATE 2029 5  1.00000
DATE 2029 9  1.00000
DATE 2030 1  1.00000
DATE 2030 5  1.00000
DATE 2030 9  1.00000
DATE 2031 1  1.00000
DATE 2031 5  1.00000
DATE 2031 9  1.00000
DATE 2032 1  1.00000
DATE 2032 5  1.00000
DATE 2032 9  1.00000
DATE 2033 1  1.00000
DATE 2033 5  1.00000
DATE 2033 9  1.00000
DATE 2034 1  1.00000
DATE 2034 5  1.00000
DATE 2034 9  1.00000
DATE 2035 1  1.00000
DTMAX 300
DATE 2035 5  1.00000
DATE 2035 9  1.00000
DATE 2036 1  1.00000
DATE 2036 5  1.00000
DATE 2036 9  1.00000
DATE 2037 1  1.00000
```

```
DATE 2037 5  1.00000
DATE 2037 9  1.00000
DATE 2038 1  1.00000
DATE 2038 5  1.00000
DATE 2038 9  1.00000
DATE 2039 1  1.00000
DATE 2039 5  1.00000
DATE 2039 9  1.00000
DATE 2040 1  1.00000
DATE 2040 5  1.00000
DATE 2040 9  1.00000
DATE 2041 1  1.00000
SHUTIN 'DW06'
SHUTIN 'DW07'
SHUTIN 'DW08'
SHUTIN 'DW10'
SHUTIN 'DW12'
SHUTIN 'DW13'
SHUTIN 'DW14'
SHUTIN 'DW15'
DATE 2041 5  1.00000
DATE 2041 9  1.00000
DATE 2042 1  1.00000
DATE 2042 5  1.00000
DATE 2042 9  1.00000
DATE 2043 1  1.00000
DATE 2043 5  1.00000
DATE 2043 9  1.00000
DATE 2044 1  1.00000
DATE 2044 5  1.00000
DATE 2044 9  1.00000
DATE 2045 1  1.00000
DATE 2045 5  1.00000
DATE 2045 9  1.00000
DATE 2046 1  1.00000
DATE 2046 5  1.00000
DATE 2046 9  1.00000
DATE 2047 1  1.00000
DATE 2047 5  1.00000
DATE 2047 9  1.00000
DATE 2048 1  1.00000
DTMAX 1000
DATE 2048 5  1.00000
DATE 2048 9  1.00000
DATE 2049 1  1.00000
```

```
DATE 2049 5  1.00000
DATE 2049 9  1.00000
DATE 2050 1  1.00000
DATE 2050 5  1.00000
DATE 2050 9  1.00000
DATE 2051 1  1.00000
DATE 2051 5  1.00000
DATE 2051 9  1.00000
DATE 2052 1  1.00000
DATE 2052 5  1.00000
DATE 2052 9  1.00000
DATE 2053 1  1.00000
DATE 2053 5  1.00000
DATE 2053 9  1.00000
DATE 2054 1  1.00000
DATE 2054 5  1.00000
DATE 2054 9  1.00000
DATE 2055 1  1.00000
DATE 2055 5  1.00000
DATE 2055 9  1.00000
DATE 2056 1  1.00000
DATE 2056 5  1.00000
DATE 2056 9  1.00000
DATE 2057 1  1.00000
DATE 2057 5  1.00000
DATE 2057 9  1.00000
DATE 2058 1  1.00000
DATE 2058 5  1.00000
DATE 2058 9  1.00000
DATE 2059 1  1.00000
DATE 2059 5  1.00000
DATE 2059 9  1.00000
DATE 2060 1  1.00000
DATE 2060 5  1.00000
DATE 2060 9  1.00000
DATE 2061 1  1.00000
DATE 2061 5  1.00000
DATE 2061 9  1.00000
DATE 2062 1  1.00000
DATE 2062 5  1.00000
DATE 2062 9  1.00000
DATE 2063 1  1.00000
DATE 2063 5  1.00000
DATE 2063 9  1.00000
DATE 2064 1  1.00000
```

```
DATE 2064 5  1.00000
DATE 2064 9  1.00000
DATE 2065 1  1.00000
DATE 2065 5  1.00000
DATE 2065 9  1.00000
DATE 2066 1  1.00000
DATE 2066 5  1.00000
DATE 2066 9  1.00000
DATE 2067 1  1.00000
DATE 2067 5  1.00000
DATE 2067 9  1.00000
DATE 2068 1  1.00000
DATE 2068 5  1.00000
DATE 2068 9  1.00000
DATE 2069 1  1.00000
DATE 2069 5  1.00000
DATE 2069 9  1.00000
DATE 2070 1  1.00000
DATE 2070 5  1.00000
DATE 2070 9  1.00000
DATE 2071 1  1.00000
DATE 2071 5  1.00000
DATE 2071 9  1.00000
DATE 2072 1  1.00000
DATE 2072 5  1.00000
DATE 2072 9  1.00000
DATE 2073 1  1.00000
DATE 2073 5  1.00000
DATE 2073 9  1.00000
DATE 2074 1  1.00000
DATE 2074 5  1.00000
DATE 2074 9  1.00000
DATE 2075 1  1.00000
DATE 2075 5  1.00000
DATE 2075 9  1.00000
DATE 2076 1  1.00000
DATE 2076 5  1.00000
DATE 2076 9  1.00000
DATE 2077 1  1.00000
DATE 2077 5  1.00000
DATE 2077 9  1.00000
DATE 2078 1  1.00000
DATE 2078 5  1.00000
DATE 2078 9  1.00000
DATE 2079 1  1.00000
```

```
DATE 2079 5  1.00000
DATE 2079 9  1.00000
DATE 2080 1  1.00000
DATE 2080 5  1.00000
DATE 2080 9  1.00000
DATE 2081 1  1.00000
DATE 2081 5  1.00000
DATE 2081 9  1.00000
DATE 2082 1  1.00000
DATE 2082 5  1.00000
DATE 2082 9  1.00000
DATE 2083 1  1.00000
DATE 2083 5  1.00000
DATE 2083 9  1.00000
DATE 2084 1  1.00000
DATE 2084 5  1.00000
DATE 2084 9  1.00000
DATE 2085 1  1.00000
DATE 2085 5  1.00000
DATE 2085 9  1.00000
DATE 2086 1  1.00000
DATE 2086 5  1.00000
DATE 2086 9  1.00000
DATE 2087 1  1.00000
DATE 2087 5  1.00000
DATE 2087 9  1.00000
DATE 2088 1  1.00000
DATE 2088 5  1.00000
DATE 2088 9  1.00000
DATE 2089 1  1.00000
DATE 2089 5  1.00000
DATE 2089 9  1.00000
DATE 2090 1  1.00000
DATE 2090 5  1.00000
DATE 2090 9  1.00000
DATE 2091 1  1.00000
DATE 2091 5  1.00000
DATE 2091 9  1.00000
DATE 2092 1  1.00000
DATE 2092 5  1.00000
DATE 2092 9  1.00000
DATE 2093 1  1.00000
DATE 2093 5  1.00000
DATE 2093 9  1.00000
DATE 2094 1  1.00000
```

```
DATE 2094 5  1.00000
DATE 2094 9  1.00000
DATE 2095 1  1.00000
DATE 2095 5  1.00000
DATE 2095 9  1.00000
DATE 2096 1  1.00000
DATE 2096 5  1.00000
DATE 2096 9  1.00000
DATE 2097 1  1.00000
DATE 2097 5  1.00000
DATE 2097 9  1.00000
DATE 2098 1  1.00000
DATE 2098 5  1.00000
DATE 2098 9  1.00000
DATE 2099 1  1.00000
DATE 2099 5  1.00000
DATE 2099 9  1.00000
DATE 2100 1  1.00000
DATE 2100 5  1.00000
DATE 2100 9  1.00000
DATE 2101 1  1.00000
DATE 2101 5  1.00000
DATE 2101 9  1.00000
DATE 2102 1  1.00000
DATE 2102 5  1.00000
DATE 2102 9  1.00000
DATE 2103 1  1.00000
DATE 2103 5  1.00000
DATE 2103 9  1.00000
DATE 2104 1  1.00000
DATE 2104 5  1.00000
DATE 2104 9  1.00000
DATE 2105 1  1.00000
DATE 2105 5  1.00000
DATE 2105 9  1.00000
DATE 2106 1  1.00000
DATE 2106 5  1.00000
DATE 2106 9  1.00000
DATE 2107 1  1.00000
DATE 2107 5  1.00000
DATE 2107 9  1.00000
DATE 2108 1  1.00000
DATE 2108 5  1.00000
DATE 2108 9  1.00000
DATE 2109 1  1.00000
```

```
DATE 2109 5  1.00000
DATE 2109 9  1.00000
DATE 2110 1  1.00000
DATE 2110 5  1.00000
DATE 2110 9  1.00000
DATE 2111 1  1.00000
DATE 2111 5  1.00000
DATE 2111 9  1.00000
DATE 2112 1  1.00000
DATE 2112 5  1.00000
DATE 2112 9  1.00000
DATE 2113 1  1.00000
DATE 2113 5  1.00000
DATE 2113 9  1.00000
DATE 2114 1  1.00000
DATE 2114 5  1.00000
DATE 2114 9  1.00000
DATE 2115 1  1.00000
DATE 2115 5  1.00000
DATE 2115 9  1.00000
DATE 2116 1  1.00000
DATE 2116 5  1.00000
DATE 2116 9  1.00000
DATE 2117 1  1.00000
DATE 2117 5  1.00000
DATE 2117 9  1.00000
DATE 2118 1  1.00000
DATE 2118 5  1.00000
DATE 2118 9  1.00000
DATE 2119 1  1.00000
DATE 2119 5  1.00000
DATE 2119 9  1.00000
DATE 2120 1  1.00000
DATE 2120 5  1.00000
DATE 2120 9  1.00000
DATE 2121 1  1.00000
DATE 2121 5  1.00000
DATE 2121 9  1.00000
DATE 2122 1  1.00000
DATE 2122 5  1.00000
DATE 2122 9  1.00000
DATE 2123 1  1.00000
DATE 2123 5  1.00000
DATE 2123 9  1.00000
DATE 2124 1  1.00000
```

```
DATE 2124 5  1.00000
DATE 2124 9  1.00000
DATE 2125 1  1.00000
DATE 2125 5  1.00000
DATE 2125 9  1.00000
DATE 2126 1  1.00000
DATE 2126 5  1.00000
DATE 2126 9  1.00000
DATE 2127 1  1.00000
DATE 2127 5  1.00000
DATE 2127 9  1.00000
DATE 2128 1  1.00000
DATE 2128 5  1.00000
DATE 2128 9  1.00000
DATE 2129 1  1.00000
DATE 2129 5  1.00000
DATE 2129 9  1.00000
DATE 2130 1  1.00000
DATE 2130 5  1.00000
DATE 2130 9  1.00000
DATE 2131 1  1.00000
DATE 2131 5  1.00000
DATE 2131 9  1.00000
DATE 2132 1  1.00000
DATE 2132 5  1.00000
DATE 2132 9  1.00000
DATE 2133 1  1.00000
DATE 2133 5  1.00000
DATE 2133 9  1.00000
DATE 2134 1  1.00000
DATE 2134 5  1.00000
DATE 2134 9  1.00000
DATE 2135 1  1.00000
DATE 2135 5  1.00000
DATE 2135 9  1.00000
DATE 2136 1  1.00000
DATE 2136 5  1.00000
DATE 2136 9  1.00000
DATE 2137 1  1.00000
DATE 2137 5  1.00000
DATE 2137 9  1.00000
DATE 2138 1  1.00000
DATE 2138 5  1.00000
DATE 2138 9  1.00000
DATE 2139 1  1.00000
```

```
DATE 2139 5  1.00000
DATE 2139 9  1.00000
DATE 2140 1  1.00000
DATE 2140 5  1.00000
DATE 2140 9  1.00000
DATE 2141 1  1.00000
DATE 2141 5  1.00000
DATE 2141 9  1.00000
DATE 2142 1  1.00000
DATE 2142 5  1.00000
DATE 2142 9  1.00000
DATE 2143 1  1.00000
DATE 2143 5  1.00000
DATE 2143 9  1.00000
DATE 2144 1  1.00000
DATE 2144 5  1.00000
DATE 2144 9  1.00000
DATE 2145 1  1.00000
DATE 2145 5  1.00000
DATE 2145 9  1.00000
DATE 2146 1  1.00000
DATE 2146 5  1.00000
DATE 2146 9  1.00000
DATE 2147 1  1.00000
DATE 2147 5  1.00000
DATE 2147 9  1.00000
DATE 2148 1  1.00000
DATE 2148 5  1.00000
DATE 2148 9  1.00000
DATE 2149 1  1.00000
DATE 2149 5  1.00000
DATE 2149 9  1.00000
DATE 2150 1  1.00000
DATE 2150 5  1.00000
DATE 2150 9  1.00000
DATE 2151 1  1.00000
DATE 2151 5  1.00000
DATE 2151 9  1.00000
DATE 2152 1  1.00000
DATE 2152 5  1.00000
DATE 2152 9  1.00000
DATE 2153 1  1.00000
DATE 2153 5  1.00000
DATE 2153 9  1.00000
DATE 2154 1  1.00000
```

```
DATE 2154 5  1.00000
DATE 2154 9  1.00000
DATE 2155 1  1.00000
DATE 2155 5  1.00000
DATE 2155 9  1.00000
DATE 2156 1  1.00000
DATE 2156 5  1.00000
DATE 2156 9  1.00000
DATE 2157 1  1.00000
DATE 2157 5  1.00000
DATE 2157 9  1.00000
DATE 2158 1  1.00000
DATE 2158 5  1.00000
DATE 2158 9  1.00000
DATE 2159 1  1.00000
DATE 2159 5  1.00000
DATE 2159 9  1.00000
DATE 2160 1  1.00000
DATE 2160 5  1.00000
DATE 2160 9  1.00000
DATE 2161 1  1.00000
DATE 2161 5  1.00000
DATE 2161 9  1.00000
DATE 2162 1  1.00000
DATE 2162 5  1.00000
DATE 2162 9  1.00000
DATE 2163 1  1.00000
DATE 2163 5  1.00000
DATE 2163 9  1.00000
DATE 2164 1  1.00000
DATE 2164 5  1.00000
DATE 2164 9  1.00000
DATE 2165 1  1.00000
DATE 2165 5  1.00000
DATE 2165 9  1.00000
DATE 2166 1  1.00000
DATE 2166 5  1.00000
DATE 2166 9  1.00000
DATE 2167 1  1.00000
DATE 2167 5  1.00000
DATE 2167 9  1.00000
DATE 2168 1  1.00000
DATE 2168 5  1.00000
DATE 2168 9  1.00000
DATE 2169 1  1.00000
```

```
DATE 2169 5  1.00000
DATE 2169 9  1.00000
DATE 2170 1  1.00000
DATE 2170 5  1.00000
DATE 2170 9  1.00000
DATE 2171 1  1.00000
DATE 2171 5  1.00000
DATE 2171 9  1.00000
DATE 2172 1  1.00000
DATE 2172 5  1.00000
DATE 2172 9  1.00000
DATE 2173 1  1.00000
DATE 2173 5  1.00000
DATE 2173 9  1.00000
DATE 2174 1  1.00000
DATE 2174 5  1.00000
DATE 2174 9  1.00000
DATE 2175 1  1.00000
DATE 2175 5  1.00000
DATE 2175 9  1.00000
DATE 2176 1  1.00000
DATE 2176 5  1.00000
DATE 2176 9  1.00000
DATE 2177 1  1.00000
DATE 2177 5  1.00000
DATE 2177 9  1.00000
DATE 2178 1  1.00000
DATE 2178 5  1.00000
DATE 2178 9  1.00000
DATE 2179 1  1.00000
DATE 2179 5  1.00000
DATE 2179 9  1.00000
DATE 2180 1  1.00000
DATE 2180 5  1.00000
DATE 2180 9  1.00000
DATE 2181 1  1.00000
DATE 2181 5  1.00000
DATE 2181 9  1.00000
DATE 2182 1  1.00000
DATE 2182 5  1.00000
DATE 2182 9  1.00000
DATE 2183 1  1.00000
DATE 2183 5  1.00000
DATE 2183 9  1.00000
DATE 2184 1  1.00000
```

```
DATE 2184 5  1.00000
DATE 2184 9  1.00000
DATE 2185 1  1.00000
DATE 2185 5  1.00000
DATE 2185 9  1.00000
DATE 2186 1  1.00000
DATE 2186 5  1.00000
DATE 2186 9  1.00000
DATE 2187 1  1.00000
DATE 2187 5  1.00000
DATE 2187 9  1.00000
DATE 2188 1  1.00000
DATE 2188 5  1.00000
DATE 2188 9  1.00000
DATE 2189 1  1.00000
DATE 2189 5  1.00000
DATE 2189 9  1.00000
DATE 2190 1  1.00000
DATE 2190 5  1.00000
DATE 2190 9  1.00000
DATE 2191 1  1.00000
DATE 2191 5  1.00000
DATE 2191 9  1.00000
DATE 2192 1  1.00000
DATE 2192 5  1.00000
DATE 2192 9  1.00000
DATE 2193 1  1.00000
DATE 2193 5  1.00000
DATE 2193 9  1.00000
DATE 2194 1  1.00000
DATE 2194 5  1.00000
DATE 2194 9  1.00000
DATE 2195 1  1.00000
DATE 2195 5  1.00000
DATE 2195 9  1.00000
DATE 2196 1  1.00000
DATE 2196 5  1.00000
DATE 2196 9  1.00000
DATE 2197 1  1.00000
DATE 2197 5  1.00000
DATE 2197 9  1.00000
DATE 2198 1  1.00000
DATE 2198 5  1.00000
DATE 2198 9  1.00000
DATE 2199 1  1.00000
```

```
DATE 2199 5  1.00000
DATE 2199 9  1.00000
DATE 2200 1  1.00000
DATE 2200 5  1.00000
DATE 2200 9  1.00000
DATE 2201 1  1.00000
DATE 2201 5  1.00000
DATE 2201 9  1.00000
DATE 2202 1  1.00000
DATE 2202 5  1.00000
DATE 2202 9  1.00000
DATE 2203 1  1.00000
DATE 2203 5  1.00000
DATE 2203 9  1.00000
DATE 2204 1  1.00000
DATE 2204 5  1.00000
DATE 2204 9  1.00000
DATE 2205 1  1.00000
DATE 2205 5  1.00000
DATE 2205 9  1.00000
DATE 2206 1  1.00000
DATE 2206 5  1.00000
DATE 2206 9  1.00000
DATE 2207 1  1.00000
DATE 2207 5  1.00000
DATE 2207 9  1.00000
DATE 2208 1  1.00000
DATE 2208 5  1.00000
DATE 2208 9  1.00000
DATE 2209 1  1.00000
DATE 2209 5  1.00000
DATE 2209 9  1.00000
DATE 2210 1  1.00000
DATE 2210 5  1.00000
DATE 2210 9  1.00000
DATE 2211 1  1.00000
STOP
**--------------------  SIMULATION STOP  ------------------
```

VITA

Tausif Khizar Ahmed received his Bachelor of Science degree in petroleum engineering from Texas A&M University at Qatar in 2009. He entered the petroleum engineering distance learning program at Texas A&M University in September 2009. He completed his research at Texas A&M University at the Qatar campus and received his Master of Science degree in August 2011.

His research interests include CO_2 crude oil fluid characterization and CO_2 sequestration.

Mr. Ahmed may be reached at: tausif.k.ahmed@gmail.com, and:

Texas A&M University at Qatar

P O Box 23874

Education City

Doha, Qatar